INFLUENCE OF SWELL ON SHEAR STRENGTH OF EXPANSIVE SOILS

A THESIS SUBMITTED TO
THE GRADUATE SCHOOL OF NATURAL AND APPLIED SCIENCES
OF
MIDDLE EAST TECHNICAL UNIVERSITY

BY

CEREN DELİKTAŞ

IN PARTIAL FULFILMENT OF THE REQUIREMENTS
FOR
THE DEGREE OF MASTER OF SCIENCE
IN
CIVIL ENGINEERING

MARCH 2016

Approval of the thesis:

INFLUENCE OF SWELL ON SHEAR STRENGTH OF EXPANSIVE SOILS

submitted by **CEREN DELİKTAŞ** in partial fulfillment of the requirements for the degree of **Master of Science in Civil Engineering Department, Middle East Technical University** by,

Prof. Dr. Gülbin Dural Ünver _____
Dean, Graduate School of **Natural and Applied Sciences**

Prof. Dr. İsmail Özgür Yaman _____
Head of Department, **Civil Engineering**

Prof. Dr. Erdal Çokça _____
Supervisor, **Civil Engineering Dept., METU**

Examining Committee Members:

Assoc. Prof. Dr. Zeynep Gülerce _____
Civil Engineering Dept., METU

Prof. Dr. Erdal Çokça _____
Civil Engineering Dept., METU

Assoc. Prof. Dr. Cem Akgüner _____
Civil Engineering Dept., TEDU

Assist. Prof. Dr. Nejan Huvaj Sarıhan _____
Civil Engineering Dept., METU

Assist. Prof. Dr. Nabi Kartal Toker _____
Civil Engineering Dept., METU

Date: 9.3.2016

I hereby declare that all information in this document has been obtained and presented in accordance with academic rules and ethical conduct. I also declare that, as required by these rules and conduct, I have fully cited and referenced all material and results that are not original to this work.

Name, Last Name: CEREN DELİKTAŞ

Signature:

ABSTRACT

INFLUENCE OF SWELL ON SHEAR STRENGTH OF EXPANSIVE SOILS

Deliktaş, Ceren

M.S., Department of Civil Engineering

Supervisor: Prof. Dr. Erdal Çokça

March 2016, 161 pages

Behavior of swelling soils is thoroughly investigated since they cause significant hazard to structures all around the world, especially in the regions with climate of arid or semi-arid. These types of soils expand upon wetting and shrink when water is removed. Existence of water significantly alters the shear strength of swelling soils. Therefore, the objective of this study is to examine the influence of swell on the shear strength of expansive soils. For the first series of tests, an artificial expansive soil was prepared in the laboratory by mixing 15% bentonite and 85% kaolinite. Grain size distribution, specific gravity, Atterberg limits and dry density versus moisture content curve were determined. Then, to obtain swell percent and rate of swell, swell tests were conducted in special molds and unconfined compression tests were made. For the first series of tests, soil samples were sheared without allowing expansion to take place. This test was considered as the reference test. Then, specimens were sheared after they were allowed to swell in specially designed molds until vertical swell stopped, which were referred to 100% swell. In the mid-steps,

shear strength was obtained when soil sample reached to 10%, 15%, 20%, 25%, 50% and 75% of ultimate vertical swell. These eight swell and shear tests were repeated for three expansive Ankara clays having different swelling potentials since natural soil samples could be found just in Ankara. As the result of shearing tests, it was seen that when the specimen reached to ultimate swell, shear strength was reduced to approximately 90% of its initial value. Free swell index test and methylene blue test were performed to estimate the swelling potential. Besides, tests showed that a frictional stress equal to about 17-25% of swell pressure developed between the mold and specimen.

Key Words: Expansive Soil, Swelling Potential, Shear Strength, Rate of Swell

ÖZ

ŞİŞEN ZEMİNLERDE ŞİŞMENİN KAYMA MUKAVEMETİ ÜZERİNDEKİ ETKİSİ

Deliktaş, Ceren

Yüksek Lisans, İnşaat Mühendisliği Bölümü

Tez Yöneticisi: Prof. Dr. Erdal Çokça

Mart 2016, 161 sayfa

Dünyanın her yerinde, özellikle kurak ya da yarı kurak iklimlerin yaşandığı bölgelerde, yapılarda ciddi hasarlara neden olduğu için şişen zeminlerin davranışı derinlemesine araştırılmıştır. Bu tip zeminler ıslanmaya bağlı olarak şişer ve su kaybettiklerinde büzülürler. Suyun varlığı, şişen zeminlerin kayma mukavemetlerini önemli miktarda değiştirirler. Bundan dolayı, bu çalışmanın amacı, şişmenin şişen zeminlerin kayma mukavemeti üzerindeki etkisini sorgulamaktır: İlk seri deneyler için, %15 bentonit ve %85 kaolin, laboratuvarda karıştırılarak, yapay bir şişen zemin hazırlanmıştır. Numunenin dane çapı dağılımı, özgül ağırlığı, kıvam limitleri ve kuru yoğunluk-su muhtevası eğrileri belirlenmiştir. Daha sonra, şişme yüzdesi ve şişme hızını tespit etmek amacıyla, şişme deneyleri özel tasarlanan kalıplar ile ve kesme deneyleri serbest basınç aleti ile yapılmıştır. İlk seri deney olarak, zemin numunelerine, şişmenin gerçekleşmesine izin verilmeden, serbest basınç test düzeneği ile kesme kuvveti uygulanmıştır. Bu deney referans deney olarak düşünülmüştür. Daha sonra, özel tasarlanmış kalıplarda, düşey şişme duruncaya

kadar şişmesine izin verilen numunelere kesme kuvveti uygulanmıştır ve bu deney %100 şişme olarak isimlendirilmiştir. Ara basamaklarda, zemin örneği maksimum düşey şişme miktarının %10, %15, %20, %25, %50 ve %75'ine ulaştığında kayma mukavemeti elde edilmiştir. Bu sekiz şişme ve kesme deneyleri, farklı şişme potansiyellerine sahip, üç Ankara kili için tekrar edilmiştir çünkü doğal zemin numuneleri sadece Ankara'dan bulunabilmiştir. Kesme deneylerinin sonucunda, örneklerin nihai şişmeye ulaştığında, kayma mukavemetlerinin ilk değerlerinin yaklaşık %90'ına düştüğü görülmüştür. Şişme potansiyelini tahmin etmek için, serbest şişme indis deneyi ve metilen mavisi testi uygulanmıştır. Ayrıca, testler, numune ile kalıplar arasında şişme basıncının yaklaşık %17-25'ine eşit bir sürtünme gerilmesi oluştuğunu göstermiştir.

Anahtar Kelimeler: Şişen Zemin, Şişme Potansiyeli, Kayma Mukavemeti, Şişme Hızı

To my mum

ACKNOWLEDGEMENTS

Immeasurable appreciation and deepest gratitude for the help and support are extended to the following people without whom the completion of this thesis could not be possible:

Firstly, I would like to express my sincere appreciation to my supervisor, Prof. Dr. Erdal Çokça for his trust in me, continuous patience, endless support and invaluable guidance throughout this study.

I also would like to thank to geological engineer Mr. Ulaş Nacar and technicians Mr. Kamber Bilgen for their valuable advices and help as well as friendly attitude during laboratory works.

Moreover, my sincere thankfulness goes to my friends Berkan Söylemez, Yılmaz Emre Sarıçiçek, Yiğit Değer and Bengü Elcik for their suggestions, help and encouragement. Especially, help received from Yılmaz and Berkan about experimental measurements within working hours was really invaluable. In addition, I would like to express my special thanks to Amir Jalehforouzan who shares all experience, knowledge and advices about the experiments and process.

Finally, my endless thanks go to my parents, Işık and Mehmet Nedim Deliktaş and my sister Seren Deliktaş for their patience, support and encouragement throughout my life. Also, I would like to thank to my fiancé Okan Demirel for his limitless love.

TABLE OF CONTENTS

ABSTRACT V

ÖZ... VII

ACKNOWLEDGEMENTS X

TABLE OF CONTENTS XI

LIST OF TABLES XIV

LIST OF FIGURES XVI

LIST OF ABBREVATIONS XXI

CHAPTERS

1) INTRODUCTION 1

1.1. GENERAL 1

1.2. AIM OF THE STUDY 3

1.3. SCOPE OF THE STUDY 3

1.4. OUTLINE OF THESIS 4

2) LITERATURE REVIEW 5

2.1. MINERALOGICAL COMPOSITION OF CLAY 5

2.1.1. Illite Mineral 8

2.1.2. Kaolinite Mineral 9

2.1.3. Smectite Mineral 10

2.1.4. Vermiculite Mineral 11

2.1.5. Comparison of Clay Minerals' Properties 11

2.2. SWELL MECHANISM 13

2.3. CLAY STRUCTURE AND FABRIC 15

2.4. FACTORS AFFECTING SWELLING 16

3) PREVIOUS STUDIES ON THE EFFECT OF SWELLING ON CLAY'S STRENGTH 21

3.1. INTRODUCTION 21
3.2. INVESTIGATION OF PREVIOUS STUDIES 23

4) EXPERIMENTAL STUDIES 41

4.1. OBJECTIVE 41
4.2. MATERIALS 41
4.3. PROPERTIES OF SOIL SAMPLES 43
4.4. PREPARATION OF SAMPLES 52
4.5. DESIGN STAGES OF THE MOLD PROPERTIES 53
4.6. SWELL TEST PROCEDURES 58
4.6.1. Compaction of Samples 58
4.6.2. Swell Tests 62
4.7. UNCONFINED COMPRESSION TEST PROCEDURES 66
4.7.1. Unconfined Compression Test Result for Sample A 69
4.7.2. Unconfined Compression Test Result for Sample B 75
4.7.3. Unconfined Compression Test Result for Sample O 81
4.7.4. Unconfined Compression Test Result for Sample E 87
4.8. FREE SWELL INDEX TEST 92
4.8.1. Test Procedure 92
4.8.2. Test Results 93
4.9. METHYLENE BLUE TEST 96
4.9.1. Test Procedure 97
4.9.2. Test Results 99
4.10. SWELL PRESSURE RELATION WITH SOIL EXPANSIVENESS 100
4.11. ESTIMATION OF FRICTIONAL STRESS 103

5) DISCUSSION OF TEST RESULTS 107

5.1. Relation between Unconfined Compressive Strength and % Swell 107
5.2. Relation between Undrained Shear Strength and % Swell 111
5.3. Relation between Undrained Elastic Modulus and % Swell 111
5.4. Comparison of Undrained Elastic Modulus with Literature 114
5.5. Relation between Time of Swell and % Swell 116
5.6. Relation between Degree of Saturation and % Swell 118
5.7. Relation between Liquidity Index and % Swell 121
5.8. Evaluation of Material Ability to Absorb Energy for the Measured Stress-Strain Values up to Peak Point 123
5.9. Estimation of Unconfined Compressive Strength 124
6) CONCLUSIONS 127
RECOMMENDATIONS FOR FUTURE RESEARCH 130
REFERENCES 131
APPENDICES
A) PROPERTIES OF MATERIAL USED TO MAKING MOLDS 139
B) TYPICAL PHOTOS OF SPECIMENS AT FAILURE 141
C) CALCULATION OF UNDRAINED SHEAR STRENGH 145
D) INFLUENCE OF SWELL RATIO ON NET ULTIMATE BEARING CAPACITY 147
E) INFLUENCE OF SWELL RATIO ON IMMEDIATE SETTLEMENT 151
F) INFLUENCE OF SWELL RATIO ON SLOPE STABILITY 155
G) INFLUENCE OF SWELL RATIO ON PILE LENGTH 159

LIST OF TABLES

TABLES

Table 2.1. Index properties and characteristics of clay minerals (Grim, 1968; Lambe&Whitmann, 1969) 12
Table 2.2. Factors that influence elemental swelling behavior of soils (Nelson and Miller, 1992)..... 17
Table 2.3. Factors affecting heave due to swelling soils at the field scale..... 19
Table 3.1. Variation of shear strength parameters and suction values with water content (After Tilgen, 2003)..... 29
Table 3.2. Shear strength parameters' variation with water content and swelling (After Domitrovic and Kovacevic, 2013) 36
Table 3.3. Previous studies made by other researches 39
Table 4.1. General information about samples 42
Table 4.2. Standard test methods for soil specimen identification..... 44
Table 4.3. Summary for index properties of soil samples with grain size percent, soil type and activity values 47
Table 4.4. Soil classification according to swelling potential after Chen (1983) and Seed et. al. (1962)..... 48
Table 4.5. Comparison of experimental w_{opt} value with the one got from Eqn 4.1 ... 52
Table 4.6. Water contents chosen at which samples were prepared 53
Table 4.7. Dry densities reached after static compaction..... 58
Table 4.8. Needed time to reach ultimate swell for each soil samples 62
Table 4.9. Summary of unconfined compression test result for Sample A..... 74
Table 4.10. Summary of unconfined compression test result for Sample B 80
Table 4.11. Summary of unconfined compression test result for Sample O..... 86
Table 4.12. Summary of unconfined compression test result for Sample E 91
Table 4.13. Expansivity potential of soil with respect to FSI (Sridharan and Prakash, 2000)..... 95

Table 4.14. Classification of soil swelling according to MFSI (Sridharan and Prakash, 2000) 96
Table 4.15. Calculation steps of frictional stress and comparison of frictional stress with swell pressure at 0% and 100% of swell 105
Table 5.1. Typical Young's Modulus values of soils in MPa (Kezdi, 1974 and Prat et al., 1995) 115
Table 5.2. Undrained elastic modulus with respect to % swell 116
Table 5.3. Liquidity index values of samples with respect to % swell 121
Table 5.4. Consistency of cohesive soils according to liquidity index (Ranjan and Rao, 2005) 122
Table 5.5. Absorbed energy values of soil samples up to peak points, which were obtained from stress-strain curves 124
Table A.1. Material properties of molds 139
Table C.1. Calculation steps of undrained shear strength for Sample B at 0% of swell 146
Table D.1. Change in net foundation pressure with variation of swell ratio for Sample A 149
Table E.1. Values of I_s (Birand et al., 2011) 152
Table E.2. Change in immediate settlement with variation of swell ratio for Sample A 153
Table F.1. Change in FS against sliding with variation of swell ratio for Sample A 156
Table G.1. Change in L with variation of swell ratio for Sample A 161

LIST OF FIGURES

FIGURES

Figure 1.1. Distribution of reported expansive soil zones (Chen, 1975) 2
Figure 2.1. Tetrahedral sheet structure - (a) silica tetrahedral sheet, (b) silica tetrahedron, (c) schematic representation of silica sheet (Lambe, 1958; Grim, 1968) 6
Figure 2.2. Octahedral sheet structure - (a) octahedral sheet, (b) octahedron, (c) schematic representation of gibbsite octahedral sheet (Lambe, 1958; Grim, 1968) 7
Figure 2.3. (a)1:1 clay mineral structure (b) 2:1 clay mineral structure (Mitchell, 1993)..... 8
Figure 2.4. Structure of illite group (Source: http://soils.ag.uidaho.edu/soil205-90/index.htm) 9
Figure 2.5. Kaolinite group structure (Source: http://soils.ag.uidaho.edu/soil205-90/index.htm) 10
Figure 2.6. Smectite mineral structure (Source: http://soils.ag.uidaho.edu/soil205-90/index.htm) 11
Figure 2.7. Presentation of diffuse double layer and force of attraction (Ammam, 2011)..... 14
Figure 2.8. Types of clay structure (Ishibashi and Hazarika, 2015) 16
Figure 3.1. Results of a series of semi confined swell test made on Georgian Bay Shale for the design of shafts and tunnels (After Lo et al., 1987)..... 23
Figure 3.2. Typical arrangement of modified semi confined swell test (After Lo and Lee, 1990)..... 25
Figure 3.3. Section view of modified semi confined swell test setup (After Lo and Lee, 1990)..... 26
Figure 3.4. Linear pressure and horizontal swell potential relation of Queenston Shale (After Lo and Lee, 1990)..... 27
Figure 3.5. Schematic drawing of hydraulic triaxial stress path setup (After Al-Mhaidib and Al-Shamrani, 2006)..... 21

Figure 3.6. Schematic drawing of hydraulic triaxial stress path setup (After Al-Mhaidib and Al-Shamrani, 2006) 32
Figure 3.7. Deviator stress versus axial strain graph for the sample that is at 14% of initial water content and under 100 kPa confining pressure (After Al-Mhaidib and Al-Shamrani, 2006) 33
Figure 3.8. Vertical displacement versus time graph for betonite samples under changing normal stresses (After Domitrovic and Kovacevic, 2013) 34
Figure 3.9. Peak strength versus normal stress and hydration times graphs (After Domitrovic and Kovacevic, 2013) 35
Figure 3.10. Apparatus for sample compaction (After Wang et al., 2014) 37
Figure 3.11. Relation between w-c and w-ϕ (After Wang et al., 2014) 38
Figure 3.12. Relation between e-c and e-ϕ (After Wang et al., 2014) 38
Figure 4.1. View of samples (1-Sample A, 2-Sample B, 3-Sample O, 4-Sample E). 43
Figure 4.2. Grain size distribution curves for all samples 45
Figure 4.3. Plasticity chart in order to determine soil type 46
Figure 4.4. Swelling potential chart proposed by Williams (1957) 49
Figure 4.5. Harvard miniature compaction test apparatus (a- Sample extruder, b-tamper, c-mould, d- collar of the mould, e- base of the mold) 50
Figure 4.6. Dry denstiy versus water content curves for all soil samples 51
Figure 4.7. 3-D view and photo of the mold with its parts 55
Figure 4.8. Drawing and sections of final molds with rod having rigid circular plates 56
Figure 4.9. Schematic drawing of the mold after sample preparation 57
Figure 4.10. Sample preparation process 59
Figure 4.11. Submerged specimen in perforated mold 63
Figure 4.12. 100 % of swell versus time graph for Sample A 64
Figure 4.13. 100 % of swell versus time graph for Sample B 65
Figure 4.14. 100 % Swell versus time graph for Sample O 65
Figure 4.15. 100 % Swell versus time graph for Sample E 66
Figure 4.16. Unconfined compression test machine view during shearing of a specimen 67

Figure 4.17. Cutting of a swelled specimen to be fitted to the height to diameter ratio in ASTM D2166 68
Figure 4.18. Unconfined compression test result for 0% of swell on Sample A 70
Figure 4.19. Unconfined compression test result for 10% of swell on Sample A 70
Figure 4.20. Unconfined compression test result for 15% of swell on Sample A 71
Figure 4.21. Unconfined compression test result for 20% of swell on Sample A 71
Figure 4.22. Unconfined compression test result for 25% of swell on Sample A 72
Figure 4.23. Unconfined compression test result for 50% of swell on Sample A 72
Figure 4.24. Unconfined compression test result for 75% of swell on Sample A 73
Figure 4.25. Unconfined compression test result for 100% of swell on Sample A ... 73
Figure 4.26. Unconfined compression test result for 0% of swell on Sample B 75
Figure 4.27. Unconfined compression test result for 10% of swell on Sample B 76
Figure 4.28. Unconfined compression test result for 15% of swell on Sample B 76
Figure 4.29. Unconfined compression test result for 20% of swell on Sample B 77
Figure 4.30. Unconfined compression test result for 25% of swell on Sample B 77
Figure 4.31. Unconfined compression test result for 50% of swell on Sample B 78
Figure 4.32. Unconfined compression test result for 75% of swell on Sample B 78
Figure 4.33. Unconfined compression test result for 100% of swell on Sample B ... 79
Figure 4.34. Unconfined compression test result for 0% of swell on Sample O 81
Figure 4.35. Unconfined compression test result for 10% of swell on Sample O 82
Figure 4.36. Unconfined compression test result for 15% of swell on Sample O 82
Figure 4.37. Unconfined compression test result for 20% of swell on Sample O 83
Figure 4.38. Unconfined compression test result for 25% of swell on Sample O 83
Figure 4.39. Unconfined compression test result for 50% of swell on Sample O 84
Figure 4.40. Unconfined compression test result for 75% of swell on Sample O 84
Figure 4.41. Unconfined compression test result for 100% of swell on Sample O ... 85
Figure 4.42. Unconfined compression test result for 0% of swell on Sample E..... 87
Figure 4.43. Unconfined compression test result for 15% of swell on Sample E..... 88
Figure 4.44. Unconfined compression test result for 20% of swell on Sample E..... 88
Figure 4.45. Unconfined compression test result for 25% of swell on Sample E..... 89
Figure 4.46. Unconfined compression test result for 50% of swell on Sample E..... 89

Figure 4.47. Unconfined compression test result for 75% swell 90
Figure 4.48. Unconfined compression test result for 100% swell 90
Figure 4.49. Free swell index test at resting stage 93
Figure 4.50. Comparison of free swell index values of samples 94
Figure 4.51. Summary of methylene blue test procedure 98
Figure 4.52. Comparison of methylene blue values of samples 99
Figure 4.53. Swell pressure test setup 101
Figure 4.54. Plastic rods used for specimen compaction in swell pressure test..... 101
Figure 4.55. Comparison of swell pressure values of samples 102
Figure 4.56. (a) Sketch of test setup to determine frictional force, (b) Photo of test setup to find frictional force 104
Figure 5.1. Unconfined compressive strength versus % swell for Sample A 108
Figure 5.2. Unconfined compressive strength versus % swell for Sample B 108
Figure 5.3. Unconfined compressive strength versus % swell for Sample O 109
Figure 5.4. Unconfined compressive strength versus % swell for Sample E 109
Figure 5.5. Experimental normalized $\log q_u$ values with regression equation..... 110
Figure 5.6. Comparison of experimental and predicted normalized $\log q_u$ values ... 111
Figure 5.7. Undrained elastic modulus versus % swell for Sample A 112
Figure 5.8. Undrained elastic modulus versus % swell for Sample B 112
Figure 5.9. Undrained elastic modulus versus % swell for Sample O 113
Figure 5.10. Undrained elastic modulus versus % swell for Sample E 113
Figure 5.11: Time of swell versus % swell for all samples 117
Figure 5.12. Degree of saturation versus % swell for Sample A 119
Figure 5.13. Degree of saturation versus % swell for Sample B 119
Figure 5.14. Degree of saturation versus % swell for Sample O 120
Figure 5.15. Degree of saturation versus % swell for Sample E..... 120
Figure 5.16. Comparison of normalized q_u values obtained from experiments and regression analysis 125
Figure B.1. Photo of 15% of swell test for Specimen A at the failure…..... 141
Figure B.2. Photo of reference test for Specimen B at the failure……..…..... 142
Figure B.3. Photo of reference test for Specimen O at the failure……..……142

Figure B.4. Photo of 20% of swell test for Specimen E at the failure…….143

Figure D.1. Bearing capacity factors for foundations in clay (Φ=0) (After Skempton, 1951)…….148

Figure D.2. Relation between q_{nf} and % swell for Sample A……..…….....…….149

Figure E.1. Relation between S_i and % swell for Sample A……153

Figure F.1. Change in FS aganist sliding with variation of swell ratio for Sample A ……...…….156

Figure F.2. Relation between FS and % swell for Sample A …….157

Figure G.1. Forces acting on a pile in swelling soi……..……..….……159

LIST OF ABBREVATIONS

Al	Aluminum
ASTM	American Society for Testing and Materials
A	Corrected area
$A_{net,side}$	Net lateral surface area
a_w	Normalized water area
A_0	Initial cross sectional area
$Al_2 (OH)_6$	Aluminium hydroxide
B_r	Width of the foundation
BS	British Standards
c’	Cohesion
Ca	Calcium
CEC	Cation exchange capacity
CH	Clay with high plasticity
CL	Clays with low-medium plasticity
C_p	Proving ring constant
c_u	Undrained shear strength
d	Diameter of perforation in the mold
D	Initial sample diameter
d_p	Pile diameter
e	Void ratio
e_f	Final void ratio
ec	Unit electronic charge
E_u	Undrained elastic modulus
Eqn.	Equation
f’	Sample dry weight in MB test
$F_{applied}$	Applied force

F_f	Friction force equal to the applied force
FS	Factor of safety
FSI	Free swell index
F_u	Uplift force on pile
G_s	Specific gravity
H	Slope height
H_0	Initial sample height
H_2O	Water molecule
IS	Indian Standard Methods of Tests for Soils
I_s	Shape factor
k	Boltzmann's constant
L	Depth to foundation level
LL	Liquid limit
LI	Liquidity index
MB	Methylene blue
MBV	Methylene blue value
meq	Miliequivalent
Mg	Magnesium
$Mg_3 (OH)_6$	Magnesium hydroxide
ML	Silt with slight plasticity
MSFI	Modified free swell index
Na	Sodium
N_c	Dimensionless bearing capacity factor
N_s	Stability coefficient depending on slope angle
NF	The Association Française de Normalization (AFNOR)
OH	Organic clays of medium to high plasticity
OL	Organic silts of low plasticity
OMC	Optimum moisture content
P	Axial load
PI	Plasticity index
PL	Plastic limit

P_S	Swell pressure
q_n	Net foundation pressure
Q_d	Allowable load from the superstructure
q_{nf}	Net ultimate bearing capacity
q_u	Unconfined compressive strength
R^2	Coefficient of determination
SL	Shrinkage limit
Si	Silicon
S_i	Immediate settlement determined using Elastic Theory
SiO_4	Silicon tetraoxide
%S	Swell potential
Sr	Degree of saturation
t	Diffuse double layer thickness
T	Absolute temperature
t_{xx}	Time of swell corresponding to given swell percent
u_a	Air pressure
u_w	Pore water pressure
v	Cation valence
V_{cc}	Volume of methylene blue solution injected to the sample solution
V_d	Soil specimen volume read from the graduated cylinder filled with distilled water in free swell test
V_k	Soil specimen volume read from the graduated cylinder filled with kerosene in free swell test
w	Water content
W_f	Resisting forces
w_{opt}	Optimum moisture content
Z_a	Depth of active zone
α	Adhesion factor
β	Uplift factor
ɣ	Unit weight of soil

δ_1	Strain dial gauge reading
δ_2	Proving ring dial gauge reading
ΔH	Height difference in the sample length
ε	Strain
ε_c	Dielectric constant of medium
ε_p	Swelling potential
η	Electrolyte concentration
ν	Poisson's ratio
ρ_d	Dry density
ρ_{dmax}	Maximum dry density
σ	Compressive stress
σ_f	Frictional stress
σ_t	Total normal stress
σ'_n	Effective normal stress
τ	Shear strength
Φ'	Internal friction angle
Φ^b	Angle of shearing resistance with respect to matric suction
χ	Effective stress parameter

CHAPTER 1

INTRODUCTION

1.1. General

Soils that swell when moisture content is increased and shrink when moisture content is decreased are called “expansive soils”. Donaldson (1969) categorized swelling soils into two groups according to their parent materials. Basic igneous rocks with the feldspar and pyroxene minerals, which have chemically broken down in order to form swelling clay minerals, constitute one of the groups (e.g. the basalts of the Deccan Plateau in India). The other group is the sedimentary rocks containing montmorillonite (e.g. limestone and marls in Israel). Figure 1.1 shows the spatial distribution of reported expansive soils (Chen, 1975). When Figure 1.1 is examined, it is realized that expansive soils mostly exist in the regions where annual precipitation is less than evapotranspiration. The common trait of these zones is their arid or semi-arid climate.

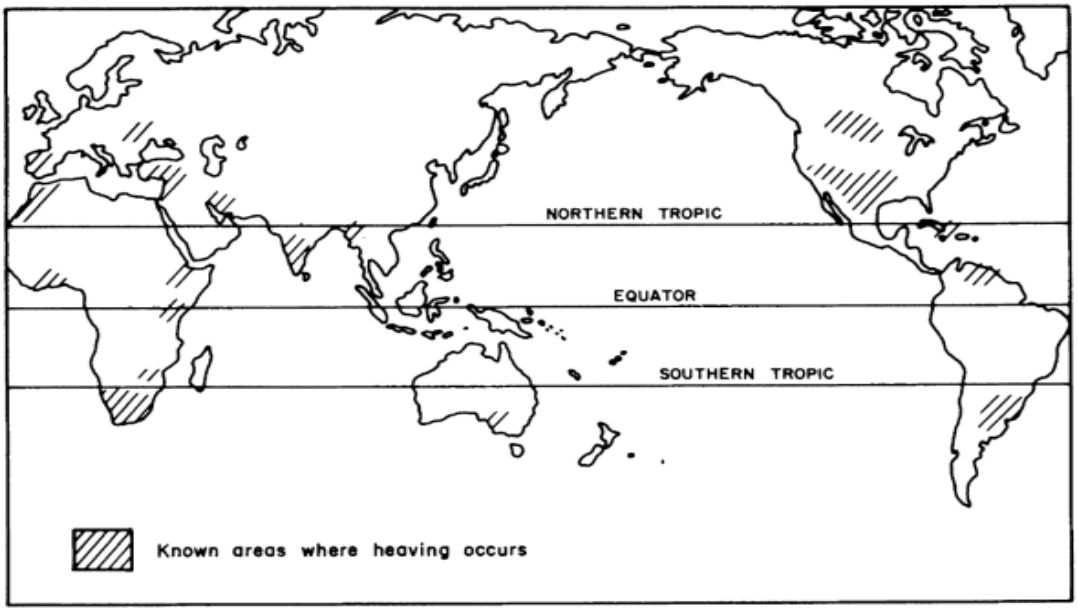

Figure 1.1. Distribution of reported expansive soil zones (Chen, 1975)

As soils swell with the addition of water, they exert uplift force to the foundations resulting in differential movement and distress in structural frame. As reported in Wyoming Multi-Hazard Mitigation Plan, USA (2011), damage due to swelling soils to buildings, roads, pipelines and other structures costs $2.3 billion, which is more than twice the damage caused by combined natural disasters such as earthquakes, floods, hurricanes and tornadoes.

Although expansive soils had been the source of many problems, they were not known by geotechnical engineers until the end of 1930. The swelling soil problem reported by Chen (1975) was first recognized by the U.S. Bureau of Reclamation in 1938, which was in the connection with a foundation for a steel siphon. Today, there are many solutions that have been suggested by engineers for swelling soils such as adjusting foundation footing size in accordance with the design, using deep footings and piles to pass expansive zone, excavating expansive

soil, stabilization of swelling soil with lime, fly ash or cement, waterproofing (Al-Rawas and Goosen, 2006).

1.2. Aim of the Study

Influence of swelling on undrained shear strength of an expansive soil is an important subject in geotechnical engineering in the sense of foundation design, slope stability prediction and calculation of earth pressure against retaining structure, (e.g. pile in expansive clay, slope stability of expansive clay, bearing capacity of foundations on expansive clay etc., which was given in Appendix D, E, F and G). There are studies about the change in shear strength and shear strength parameters of expansive soils with the water content, swelling and suction in the available literature. However, decrease in shear strength at swell ratios below 25% of ultimate swell was not presented in previous studies. Additionally, unconfined compression test was not chosen as the way for the determination of shear strength of clay. Therefore, this study aims to investigate the influence of 0%, 10%, 15%, 20%, 25%, 50%, 75% and 100% of ultimate swell on expansive soils' undrained shear strength by using unconfined compression test.

1.3. Scope of the Study

This study involves the change in undrained shear strength of swelling soils with the amount of swell. For this aim, one artificial and three natural soil samples were used. Artificial soil sample was obtained by mixing 15% bentonite and 85% kaolinite in the laboratory while three representative Ankara clays were selected as natural soil samples. Firstly, grain size distribution, specific gravity, Atterberg limits and dry density versus moisture content curves were determined for each sample separately. Then, statically compacted samples were let to swell in specially designed molds and sheared with the unconfined compression test setup to define swell

percent and rate of swell. As the first test for each material, soil samples were sheared without allowing any swell to take place. This test was accepted as the reference test. After this test, when soil samples that are allowed to swell freely, reached ultimate vertical swelling, unconfined compression test was conducted on them. This was called 100% of swell. Next, undrained shear strength of soil samples at 10%, 15%, 20%, 25%, 50% and 75% of ultimate vertical swell could be measured. After determination of swelling capacities of the samples in the specially designed molds, free swell index test and Methylene Blue test were made to verify the obtained results. In addition, swell pressures of each soil sample were determined and compared with the frictional stresses which developed between the mold and the specimen.

1.4. Outline of Thesis

This study includes literature review part, previous studies made on shear strength of expansive soils, experimental works, discussion of test results and conclusions. In Chapter 2 including literature review part, mineralogy of clay particles, clay fabric and structure, swell mechanism and factors affecting swelling are mentioned. Chapter 3 consists of previous works on shear strength of swelling soils. Experimental works like soil sample preparation, soil properties determination, swell and shear tests, free swell index test, Methylene Blue test, swell pressure and frictional stress determination are shared in Chapter 4. Tests results are given in Chapter 5. Finally, in Chapter 6 conclusions attained at the end of testing are summarized.

CHAPTER 2

LITERATURE REVIEW

2.1. Mineralogical Composition of Clay

Soil particles are classified as clay-sized if effective diameter of its particles is equal to or less than 2 microns (μm). Since only particle diameter is not enough for a true categorization of clay, clay mineralogy gains importance. First time, Grim (1968) gave a classification of clay minerals in his book, Clay Mineralogy, to show nomenclature and differences between them (Murray, 2007). Based on layer type, interlayer material and octahedral character, Guggenheim et al. (2006) proposed another grouping for clay minerals. A simple categorization can be made depending on composition and arrangement of octahedral and tetrahedral sheets, which are basic units of atomic structures in clay minerals. According to this classification, clay minerals can be grouped under four main headings: illite group, kaolinite group, smectite group and vermiculite group (Ismadji et al., 2015).

Octahedral sheet which is one of the basic units is consisting of aluminum, iron or magnesium atoms surrounded by closely packed oxygen and hydroxyls in octahedral form. In octahedral coordination, hydrated form of alumina is named as gibbsite [Al_2 (OH) $_6$] that is electrically neutral. On the other hand, magnesium hydroxide in octahedral form is called brucite [Mg_3 (OH) $_6$].

The other structural unit, named as tetrahedral sheet, is composed of silica (SiO_4), which consist of an atom and four equidistant oxygens or possibly hydroxyls around it in tetrahedron geometry configuration (Murray, 2007). Silica sheet has a

net negative charge imbalance (Craig, 2004). Below Figures 2.1 and 2.2. show the sketch of these building blocks.

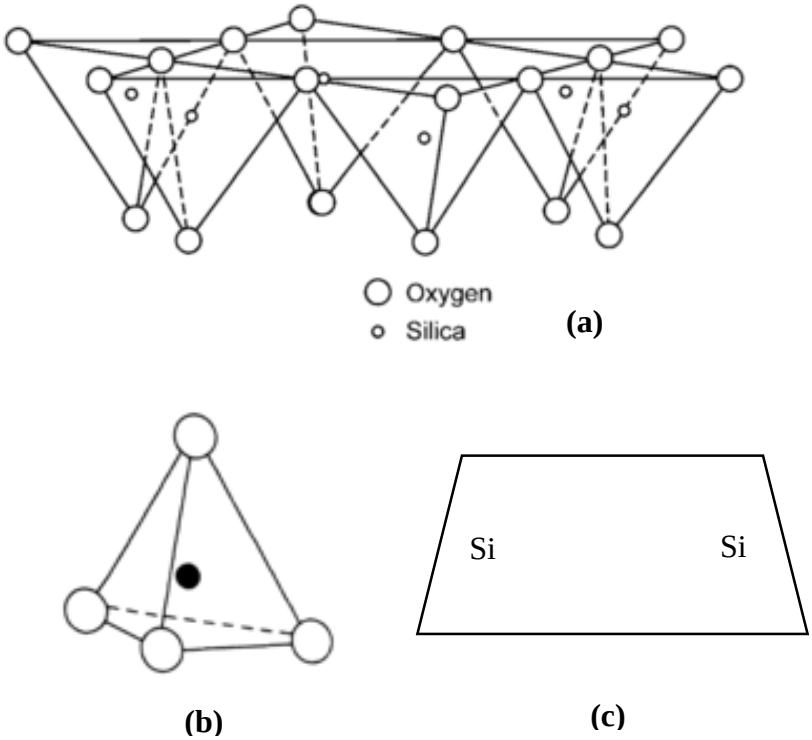

Figure 2.1. Tetrahedral sheet structure - (a) silica tetrahedral sheet, (b) silica tetrahedron, (c) schematic representation of silica sheet (Lambe, 1958; Grim, 1968)

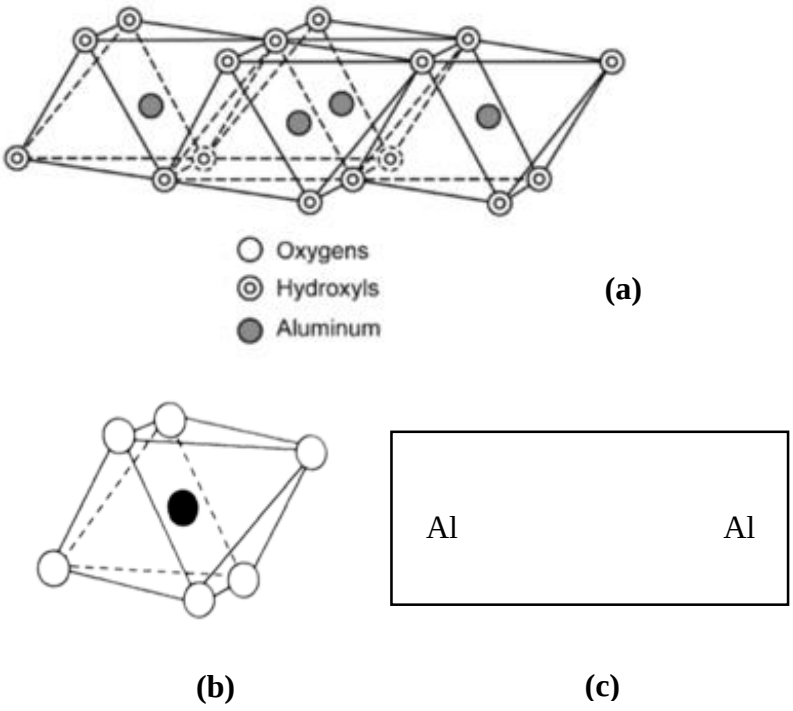

Figure 2.2. Octahedral sheet structure - (a) octahedral sheet, (b) octahedron, (c) schematic representation of gibbsite octahedral sheet (Lambe, 1958; Grim, 1968)

According to combination of octahedral and tetrahedral sheets, clay mineral structure can be divided into two groups as 1:1 and 2:1 structure (EGU, 2014). In 1:1 clay mineral, one tetrahedral sheet is attached to one octahedral sheet while two octahedral sheets with one tetrahedral sheet result in 2:1 clay mineral (Mitchell, 1993). Figure 2.3 schematically shows 1:1 and 2:1 structure of clay minerals.

(a) **(b)**

Figure 2.3. (a)1:1 clay mineral structure (b) 2:1 clay mineral structure (Mitchell, 1993)

2.1.1. Illite Mineral

Silica-gibbsite-silica sandwich forms the structure of illite. Oxygens at the tips are common for silica tetrahedra and gibbsite octahedral sheet. Replacement of a cation in the mineral structure with another cation of lower electrovalence is defined as isomorphic substitution by Terzaghi (Karl et al., 1996). For illite, isomorphic substitution of aluminum with silicon in tetrahedral sheet concludes in negative charges on the surface. Potassium, sometimes calcium and magnesium ions between 2:1 layers balance this negative charge as shown in Figure 2.4. These interlayer cations prevent water enter into the clay structure; therefore, illite clays are non-expansive (Ismadji et al., 2015).

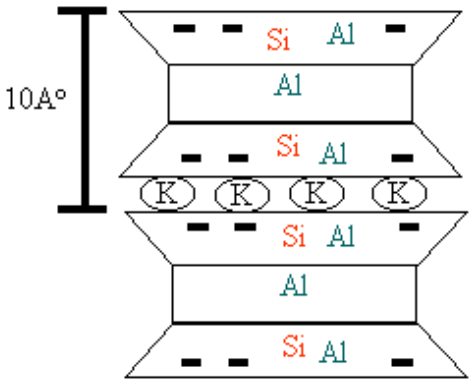

Figure 2.4. Structure of illite group (Source: http://soils.ag.uidaho.edu/soil205-90/index.htm)

2.1.2. Kaolinite Mineral

Basic structure of kaolinite mineral consists of a single sheet of gibbsite and a single sheet of tetrahedral silica. It is a 1:1 clay mineral. Oxygens existed in the tip of tetrahedron are shared by two structural blocks, gibbsite and silica. Unit layers of kaolinite are stacked one above the other with hydrogen bonding (Murray, 2007) as shown in Figure 2.5. Hydrogen bonding leads to very low expansion capacity of kaolinite.

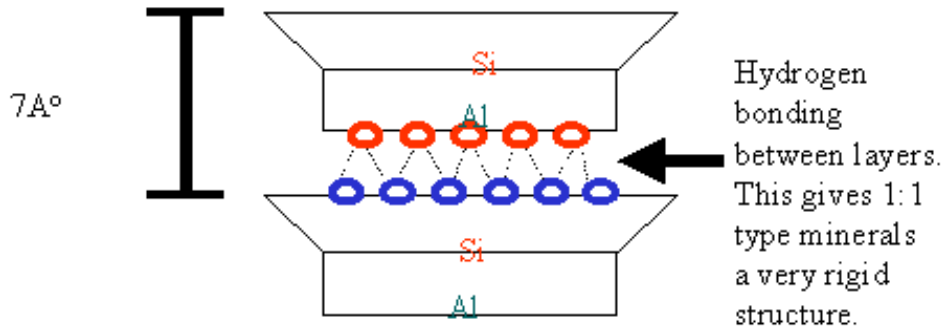

Figure 2.5. Kaolinite group structure (Source: http://soils.ag.uidaho.edu/soil205-90/index.htm)

2.1.3. Smectite Mineral

Smectite mineral has 2:1 layer in which octahedral sheet between two silica tetrahedral sheets as indicated in Figure 2.6. Smectite minerals are bonded to each other with Van der Waals forces. Water molecules and exchangeable cations such as sodium, calcium and magnesium present at interlayer spacing in order to balance the charge deficiencies (Murray, 2007). Since bonds formed by Van der Waals forces can be easily separated with polar liquids and water, smectite mineral shows very high swelling property (Lal, 2006). The most abundant smectite type is calcium montmorillonite.

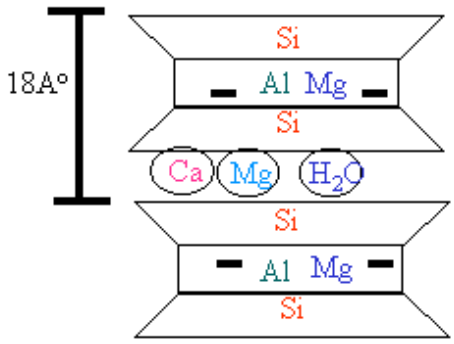

Figure 2.6. Smectite mineral structure (Source: http://soils.ag.uidaho.edu/soil205-90/index.htm)

2.1.4. Vermiculite Mineral

Structure of vermiculite mineral is similar to illlite's mineral pattern. The only difference between these two minerals is the interlayer bonding material. In vermiculite mineral, potassium, which stacks the illite mineral layers, is replaced with hydrated magnesium. The reason behind potassium loss is weathering. Since unit block structure of vermiculate is very parallel to illite, it also has limited swelling capacity (Walker, 1949).

2.1.5. Comparison of Clay Minerals' Properties

Table 2.1 presents the properties of clay minerals. Cation exchange capacity (CEC) is defined as the mineral ability to absorb an external cation.

Table 2.1. Index properties and characteristics of clay minerals (Grim, 1968; Lambe&Whitmann, 1969)

Clay Mineral	**CEC meq/ 100 g**	**Specific Gravity**	**Specific Surface m^2/g**	**LL %**	**PL %**	**Swell Potential**
Illite	3-15	2.6-2.68	10-20	30-60	25-35	Low
Sodium (Na)				53	21	
Calcium (Ca)				38	11	
Kaolinite	10-40	2.6-3.0	65-100	60-120	35-60	Medium
Na				61	34	
Ca				90	40	
Montmorillonite	80-150	2.35-2.7	700-840	100-900	50-100	High
Na				700	97	
Ca				177	63	

When Table 2.1 is examined, a direct proportion between swelling capacity and CEC, specific surface, LL and PL is observed. In this manner, illite mineral which has the lowest CEC, specific surface, liquid limit and plastic limit values swells in the lowest degree whereas montmorillonite owns the opposite characteristics.

2.2. Swell Mechanism

When the clay particle interacts with water, high concentration of cations develops near the negatively charged clay particle surface due to bipolar water molecules, release of adsorbed cations existing on the surface and release of hydrogen from the hydroxyl group (Oweis and Khera, 1998). As a result, an electrostatic force forms between negative surface and exchangeable cations (Das, 2008). The electrical interparticle force field depends on the variabilities in negative surface charges, electrochemistry of the soil-water, van der Waals forces and adsorptive forces between clay surface and water molecules. If one of these variables change, interparticle force field will also be altered. Since there is no externally applied stress to balance this change, particle spacing will change to get the system in equilibrium. This change in particle spacing as the result of disturbance of internal stress equilibrium is known as shrink/swell (Nelson and Miller, 1992).

The region of negative charges on the clay surface and balancing cations in the solution that surround clay surface is called as diffuse double (stern) layer (Das, 2008). Figure 2.7 schematically shows water molecule layers and attraction force. Water molecule layers can be divided into two parts as solid (adsorbed) water and double layer. Solid water is strongly held by particle as a very thin layer around it, which is marked as “b “in Figure 2.7. Less attractive forces and liquid water form double layer, which is responsible for the plasticity of clay (Al-Rawas and Goosen, 2006). Double layer is indicated in Figure 2.7 by “c”. The region is termed as diffuse because the further from the surface, attractive forces decreases with the inverse square of distance as stating in Figure 2.7.

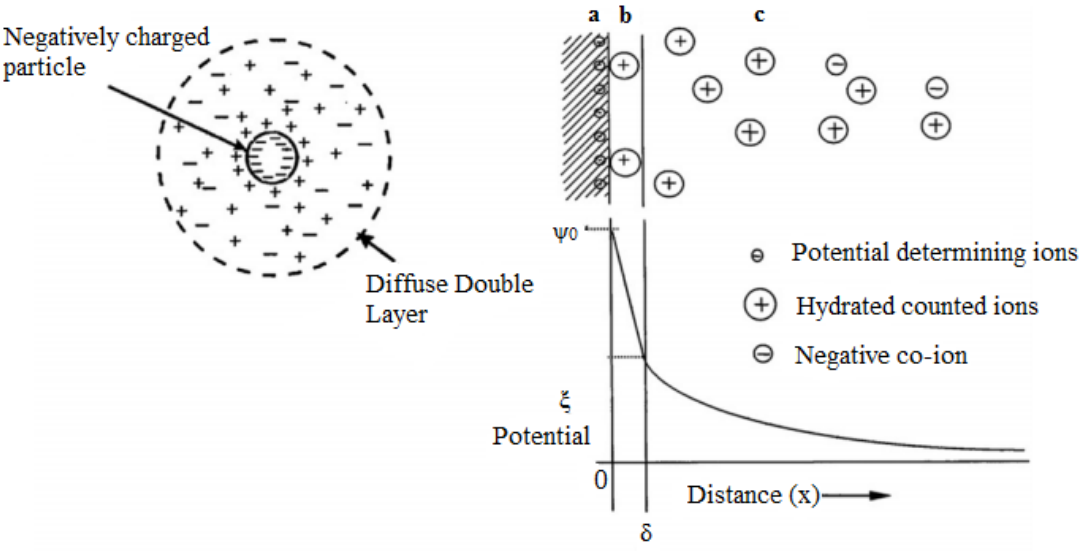

Figure 2.7. Presentation of diffuse double layer and force of attraction (Ammam, 2011)

Gouy-Chapman gives a theoretical expression in Eqn 2.1 for diffuse double layer thickness: t which can be considered as the radius in Figure 2.7.

$$t=\sqrt{\frac{\varepsilon_c * k * T}{8*\pi*\eta*ec^2*v^2}} \quad \text{..... Eqn 2.1}$$

As can be investigated from Eqn 2.1, diffuse double layer thickness depends on the medium dielectric constant (ε_c), Boltzmann's constant (k), absolute temperature (T), electrolyte concentration (η), unit electronic charge (ec) and cation valence (v). Diffuse double layer thickness is important for evaluating swelling capacity since interparticle spacing and permeability of soil increase as this thickness decreases; thus, water can easily penetrate to result in interparticle expansion.

Patel et al (2007) stated that clays swell in two ways: surface hydration and osmotic swelling. Surface hydration occurs where a layer of water molecules is

adsorbed on crystal surfaces by hydrogen bonding. Successive layers of these water molecules increase spacing with a quasi-crystalline alignment. On the other hand, when water osmotically moves between the unit layers in the clay mineral from higher concentration to the lower side in the surrounding water, overall volume increases. This phenomenon is called osmotic swelling. Volume increase due to osmotic swelling is larger than that is caused by surface hydration. A few clays such as sodium montmorillonite, a kind of smectite, undergo osmotic swell whereas surface hydration occurs in all types of clays.

2.3. Clay Structure and Fabric

Holtz and Kovacs (1981) stated that only geometrical arrangement of particles is referred as soil fabric. The structure of soil means combined effect of fabrics and interparticle forces.

When clay particles interact with water, they will repel each other and form an interparticle spacing due to negatively charged clay surface and cations existing in double layer of adjacent particles. Thickness of diffuse double layer leads to increase in magnitude of repulsive forces; therefore, parameters changing diffuse double layer thickness also alter repulsive forces.

In addition to repulsive forces, there are Van der Waals forces between approaching clay particles, regardless of the fluid between the particles.

If the net effect of repulsive and attractive forces is attractive, two particles move each other and attached, which is named as flocculation. If repulsive forces are dominant, two particles move away from each other, which is termed as dispersion. Dispersed particles have face-to-face contact while flocculated ones get in touch edge-to-face owning to their dominant force (Lambe and Whitman, 1969). Clay fabric types can be visualized from below Figure 2.8.

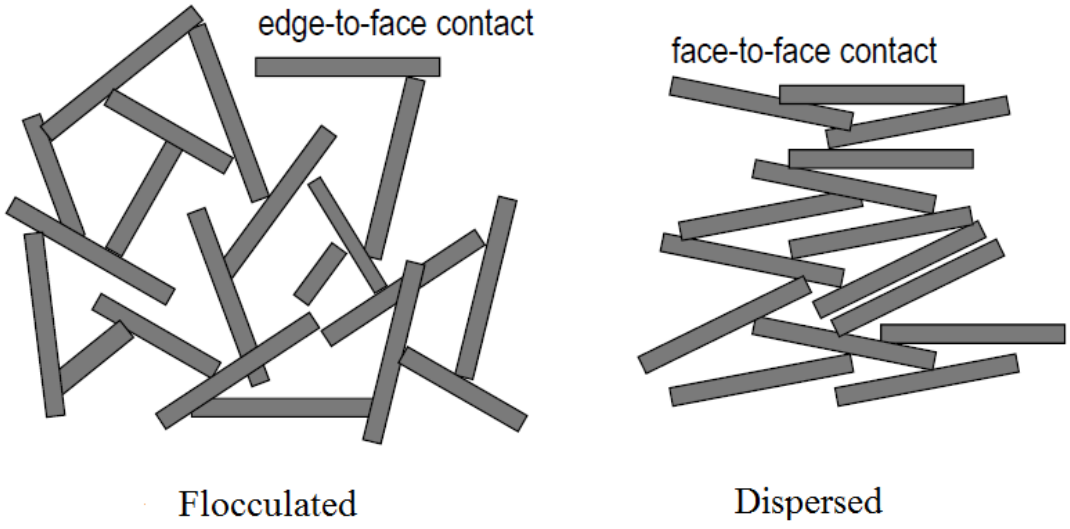

Figure 2.8. Types of clay structure (Ishibashi and Hazarika, 2015)

2.4. Factors Affecting Swelling

Swelling of clays is a complex mechanism which is affected by many factors such as present amount and type of clay minerals, internal structure, exchangeable ions and electrolyte content of aqueous phase. The elementary affecting elements can be investigated in three groups as environmental factors, soil properties and state of stress, which is given in Table 2.2. Also, Table 2.3. shows the factors affecting heave caused by expansive soils at the field (Nelson and Miller, 1992).

Table 2.2. Factors that influence elemental swelling behavior of soils (Nelson and Miller, 1992)

FACTOR		EXPLANATION
SOIL CHARACTERICTICS	Mineral Composition	Clays which contains montmorillonite, vermiculite and some mixed layer minerals own larger volume changes than the ones whose mineralogy is consists of illite and kaolinite minerals.
	Soil- Water Chemistry	One of the main roles in swelling belongs to cations. Increase in cation concentration and valence results in less expansiveness.
	Plasticity	High liquid limit and plasticity over a wide range of moisture content cause high swelling potential.
	Soil Structure and Fabric	Cemented particles and dispersed structure reduce swell. Compaction at higher water content or remolding change fabric and structure. Additionally, kneading compaction has shown to cause soil samples with lower swell potential than statically compacted soils at lower moisture contents. The reason of this situation is creating dispersed structure of soil with kneading compaction.
	Dry Density	Higher densities mean closer particle spacings and greater repulsive forces between particles, which causes higher swelling potential.

Table 2.2. (continued)

ENVIRONMENTAL CONDITIONS	Initial Moisture Content	An expansive soil with lower moisture content has higher affinity for water and suction than the one at higher moisture content.
	Permeability	Higher permeability of soil especially due to cracks and fissures let water mitigate faster. This induces higher rate of swell.

STATE OF STRESS	Loading	The amount of swell for a given moisture content depends on magnitude of surcharge load. In order to balance interparticle repulsive forces and reduce swell, an external load is applied.
	Soil Suction	Soil suction is represented by negative pore pressure in unsaturated soils. Pore size and shape, surface tension, saturation, gravity, electrochemical properties of soil and water relates soil suction.

Table 2.3. Factors affecting heave due to swelling soils at the field scale

FACTOR	EXPLANATION
Climate	Variation and amount of precipitation have influence on the moisture presence and depth of seasonal moisture fluctuation. Most of expansive soils are seen to locate in places whose climates are arid or semiarid.
Groundwater	While shallow water tables act as a source providing continuous moisture, fluctuating water tables cause different amount of moisture at different times.
Drainage and Manmade Water Sources	Water coming from the surface in a way such as leaky plumbing or ponding around a poorly graded soil can be the reason for water transportation to a deeper zone.
Vegetation	Plants consume moisture from the soil by making transpiration and photosynthesis. This leads to alteration of moisture content in areas where vegetation varies.
Temperature	Diffusion of moisture to cooler areas beneath building and pavements is provided by increasing temperature.
Soil Profile	Expected movement is considerably affected by the location and thickness of potentially expansive layers. If expansive clays extend from the surface to the depth of active zone, greatest movement will occur. If nonexpansive material or bedrock at a shallow depth overlie on swelling soil, this will result in less movement.

CHAPTER 3

PREVIOUS STUDIES ON THE EFFECT OF SWELLING ON CLAY'S STRENGTH

3.1. Introduction

In the available literature, there are many studies about the influence of water content or suction change on shear strength of expansive soils. As the soil swells, its water content and degree of saturation increases while the suction decreases.

Shear strength of saturated soils have been commonly predicted with Terzaghi's (1925;1943) effective stress principle together with Coulumb's shear strength equation, which were given in Eqn. 3.1 and 3.2 respectively.

$\sigma_t = \sigma' + u_w$……...……...…….Eqn. 3.1

$\tau = c' + \sigma' * \tan\Phi'$……..…….Eqn. 3.2

where

σ_t= Total normal stress

σ'_n= Effective stress

u_w= Pore water pressure

τ= Shear strength

c'= Cohesion

Φ'= Internal friction angle

In order to estimate the shear strength of partially saturated soils, Bishop (1959) proposed effective stress approach, which is given in Eqn. 3.3, while Fredlund and Morgenstern (1977) used independent stress state variables, whose expression is presented in Eqn. 3.4, by developing Coulumb's strength equation.

$\tau = c' + (\sigma_t - u_a) * \tan \Phi' - \chi * (u_a - u_w) * \tan \Phi''$ ……Eqn. 3.3

$\tau = c' + (\sigma_t - u_a) * \tan \Phi'' - (u_w - u_a) * \tan \Phi'^{b}$ ……Eqn. 3.4

where

u_a= Air pressure

χ= Effective stress parameter

Φ'^{b}= Angle of shearing resistance with respect to matric suction

$\tan\Phi'^{b} = a_w * \tan\Phi'$ where a_w is the normalized water area

Many researches have focused on the ways determining χ or $\tan\Phi'^{b}$ as the function of degree of saturation or suction. Karube et al. (1996) introduced a linear relationship of degree of saturation to determine χ value. Again, Öberg and Sällfors (1997) proposed an equation showing the degree of saturation and χ relationship. Khalili and Khabbaz (1998) presented an empirical correlation between soil suction and χ by analyzing the shear strength data in the available literature. Bao et al. proposed a relation involving the air entry and residual suction value for χ. In addition to the studies to obtain χ or a_w value, Tekinsoy et al. (2004) introduced an empirical equation showing the relation between shear strength and soil- water characteristic curve through air entry value.

In other respects, previous strength values were mostly found with the help of triaxial or direct shear test. Studies were mostly associated with the stress- swell relations instead of change in shear strength at different swell ratio.

3.2. Investigation of Previous Studies

Lo et al. (1987) performed semi confined swell tests on Georgian Bay Shale whose results are presented in Figure 3.1. These results show that swelling strains increase as applied vertical stresses decrease.

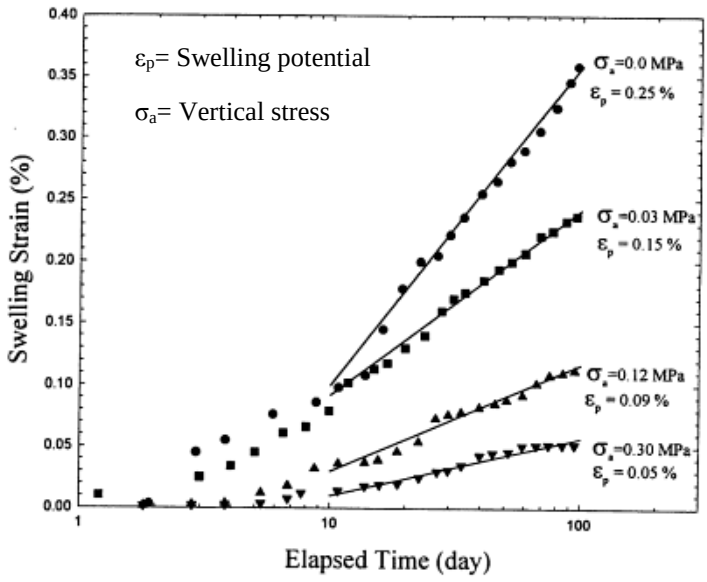

Figure 3.1. Results of a series of semi confined swell test made on Georgian Bay Shale for the design of shafts and tunnels (After Lo et al., 1987)

Lo and Lee (1990) developed semi confined swell test apparatus. A loading hanger, loading support frame, sample container, dial gauge and strain gauges mounted on cantilever beams were included in Lo and Lee's (1990) modified semi

confined swell test apparatus. A vertical load on the circular hanger was applied perpendicular and parallel to bedding planes of the sample which was submerged in water. Thus, swelling under load in different directions could be investigated. Dial gauge was designed to measure strain in the loading direction while strain gauges were utilized for lateral strains. Typical arrangement and section view of modified semi confined swell test setup is given in Figure 3.2 and 3.3 respectively. Additionally, Figure 3.4 shows that stress and swelling relation was linear according to modified semi confined swell study on Queenston Shale after Lo and Lee (1990) (Rowe, 2001).

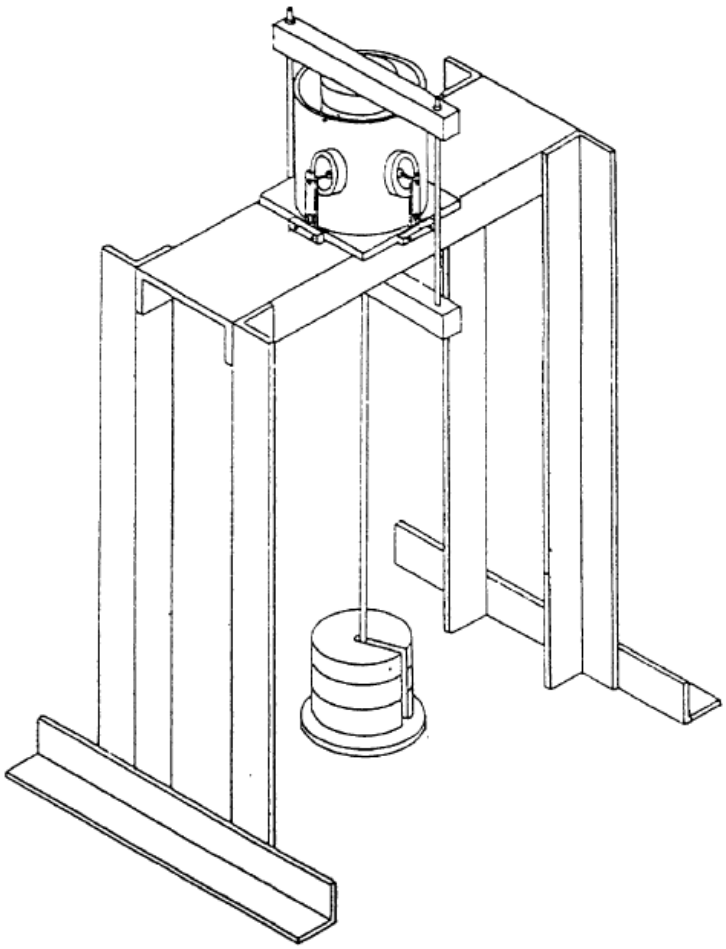

Figure 3.2. Typical arrangement of modified semi confined swell test (After Lo and Lee, 1990)

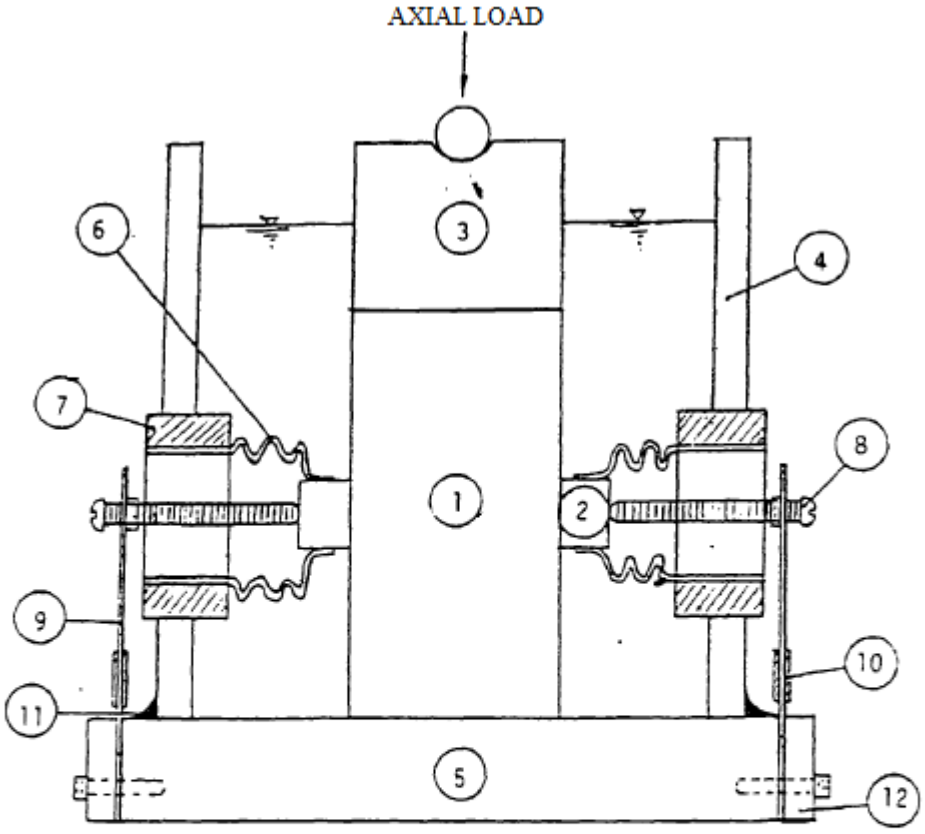

1 ROCK SAMPLE	2 GAUGE POINT
3 TOP CAP	4 PLEXI GLASS CONTAINER
5 BASE PLATE	6 RUBBER BOOT
7 BUSHING	8 ADJUSTING SCREW
9 CANTILEVER BEAM	10 STRAIN GAUGE
11 SILICONE SEAL	12 SPACER

Figure 3.3. Section view of modified semi confined swell test setup (After Lo and Lee, 1990)

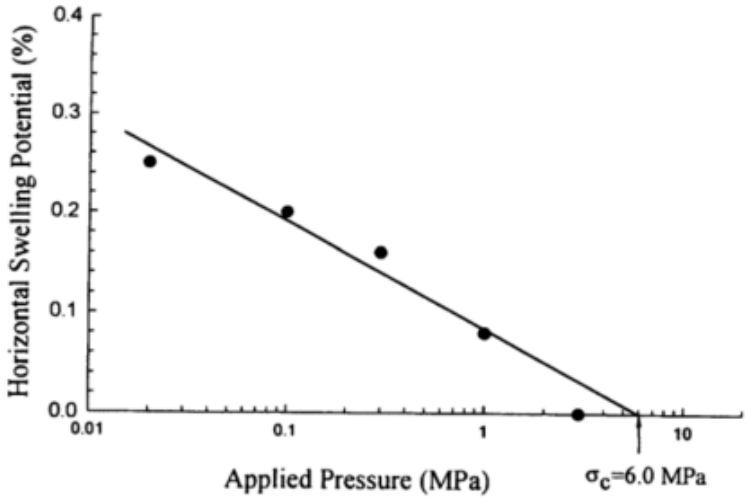

Figure 3.4. Linear pressure and horizontal swell potential relation of Queenston Shale (After Lo and Lee, 1990)

The fact that shear strength decreases as swell level rises was found by Wong (1998). Wong conducted swell and shear tests on shale specimens. For swell purpose, he used a special apparatus similar to modified semi confined swell test apparatus developed by Lo and Lee (1990) whereas samples were sheared in triaxial cell.

In order to determine shear strength parameters, Tilgen (2003) performed direct shear tests on compacted and soaked METU clays at optimum moisture content (w= 20.8%), dry side of optimum moisture content (w= 14.8%, 16.8% and 18.8%), and wet side of optimum moisture content (w= 22.8%, 24.8% and 26.8%). Besides, soil suctions, which are defined as the free energy of the soil water, were measured by filter paper method. Filter paper method depends on the equilibrium with the soil either through liquid flow or vapor flow. Once the equilibrium is set, water content of the filter paper disc is measured. After water content determination,

filter paper calibration curve is constructed or adopted to find the suction value corresponding to the water content.

Relation between water content and shear strength parameters as well as the water content and suction correlation of both compacted and soaked samples is summarized in Table 3.1. As can be seen from Table 3.1, as moisture content increased, cohesion values also increased up to OMC while angle of friction values decreased because of gained granular soil fabric. After the OMC, cohesion and angle of friction values exhibited a decreasing trend. When the results for compacted and soaked samples were compared, it was seen that cohesion and friction angle values of soaked samples were smaller than the ones obtained from compacted samples. In addition, soaked samples' cohesion and angle of friction values were almost constant at 12 kPa and 22^0 respectively. Another experimental result was the fact that total soil suction, matric soil suction and osmotic soil suction decreased with increasing water content at the dry side of OMC, which verified the direct relation between suction and shear strength.

Table 3.1. Variation of shear strength parameters and suction values with water content (After Tilgen, 2003)

Water Content of Samples (%)	**Compacted Parameters**		**Soaked Parameters**		**Total Suction as Compacted (kPa)**	**Matric Suction as Compacted (kPa)**	**Osmotic Suction as Compacted (kPa)**
	c' (kPa)	**ϕ' (^{0})**	**c' (kPa)**	**ϕ' (^{0})**			
14.8 (-6 dry side of OMC)	65	49	4	21	2365	1795	570
16.8 (-4 dry side of OMC	77	46	9	24	1707	1091	616
18.8 (-2 dry side of OMC)	81	32	18	24	1161	907	254
20.8 (OMC)	84	30	12	15	876	642	234
22..8 (+2 wet side of OMC)	56	15	9	22	530	400	130
24.8 (+4 wet side of OMC)	47	16	20	19	497	185	312
26.8 (+6 wet side of OMC)	24	19	10	21	488	291	197

Al-Mhaidib and Al-Shamrani (2006) made an experimental research about how amount of swelling affects shear strength of expansive shale samples. Specimens which had different initial moisture content, 14%, 18% and 22%, were tested under four different confining pressures, 25, 50, 100 and 150 kPa. For both shearing and swelling stages, hydraulic triaxial stress path cell which is shown in Figure 3.5 was utilized. The piston at the top of the cell moved up with swelling. A dial gauge measured vertical displacements. Once the specimens reached predetermined amount of swelling; i.e., 0, 25, 50, 75 and 100% of swell of the ultimate vertical swell, shear tests were conducted. The setup controls the axial load while keeping the strain constant and by pressurizing the lower chamber at the bottom of it.

When test results were interpreted, it was seen that swelling of shale specimens took approximately three weeks. The fact that swelling decreases with increase in initial water content was another result under same confining pressure. Figure 3.6 shows the volume change with initial water content.

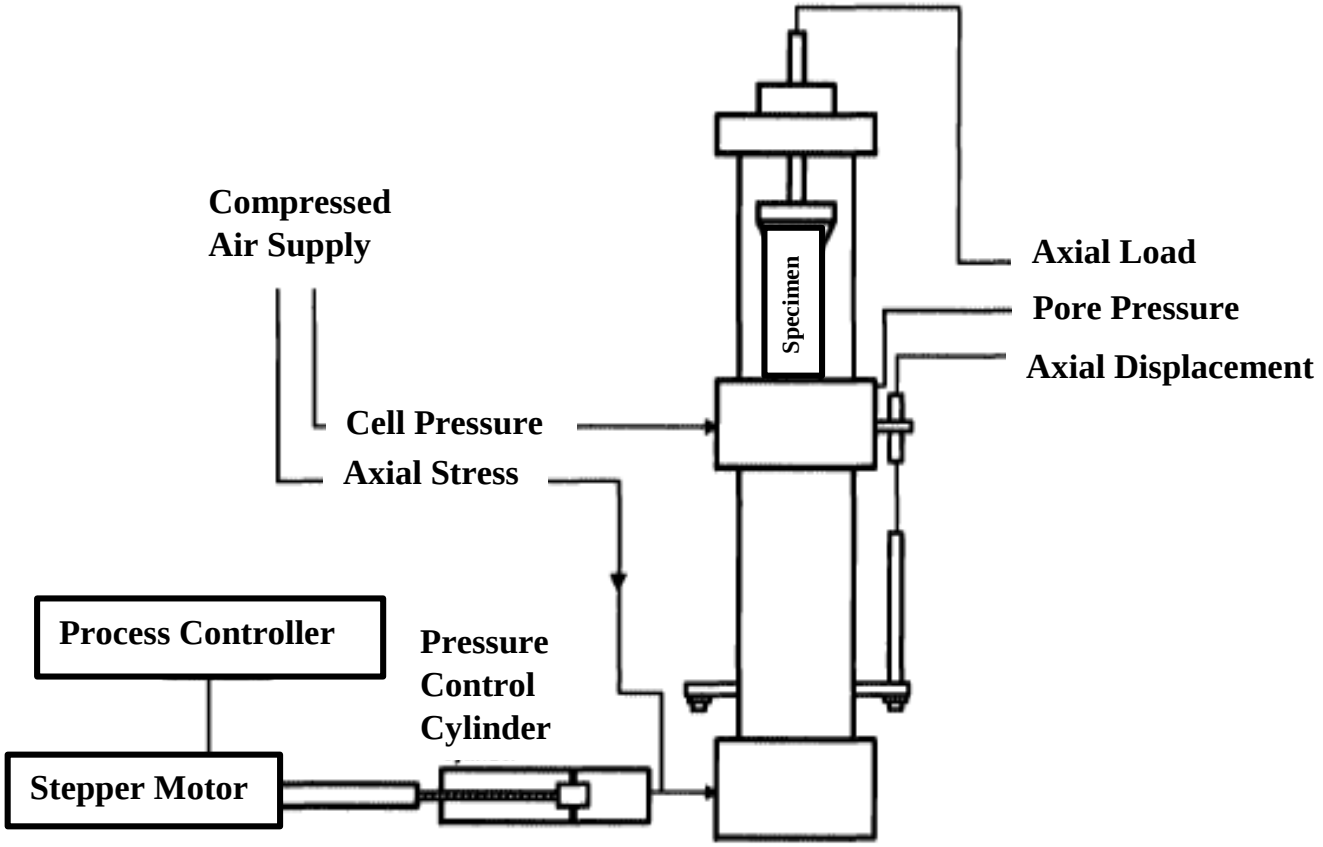

Figure 3.5. Schematic drawing of hydraulic triaxial stress path setup (After Al-Mhaidib and Al-Shamrani, 2006)

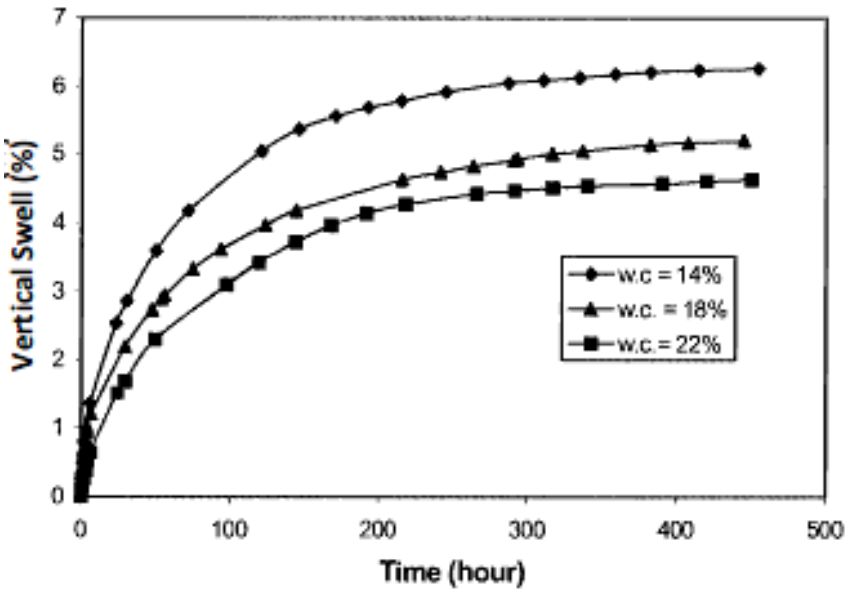

Figure 3.6. Schematic drawing of hydraulic triaxial stress path setup (After Al-Mhaidib and Al-Shamrani, 2006)

According to test results, the fact that swelling had a decreasing impact on deviator stress at the same initial water content and confining stress was proven. Figure 3.7 exemplifies the variation in deviator stress with increasing swell. Therefore, specimens sheared at a swell percent of 25% of ultimate vertical swell exhibited about one third of shear strength for samples that were prevented from swelling. On the other end of the scale, for specimens which were allowed to reach ultimate vertical swell, their shear strength values were almost 10% of non-swelled samples' shear strengths.

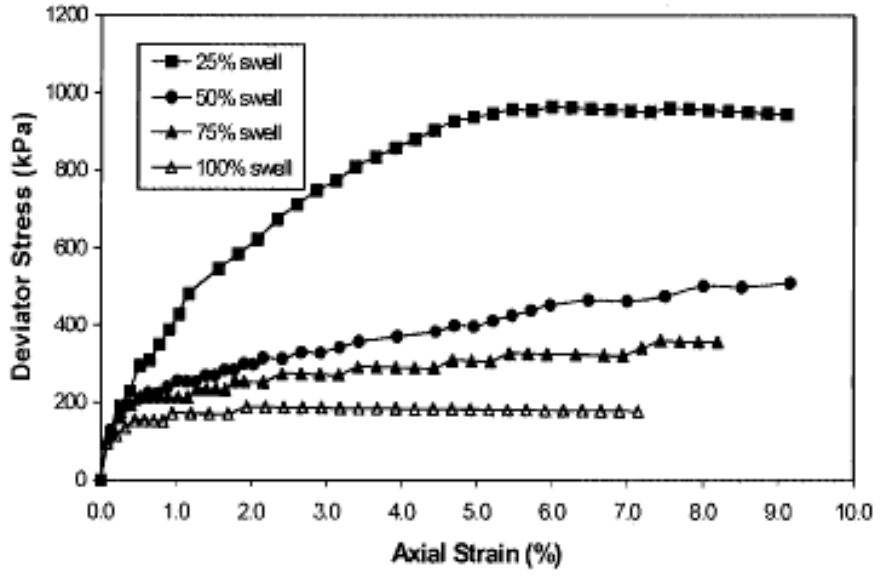

Figure 3.7. Deviator stress versus axial strain graph for the sample that is at 14% of initial water content and under 100 kPa confining pressure (After Al-Mhaidib and Al-Shamrani, 2006)

Additionally, a parameter named as shear ratio was defined by dividing strength value of swelled specimen to strength value of non-swelled specimen. Shear ratio value also reduces as samples experiences more swelling at the same water content. However, shear ratio increased as confining pressure was increased.

Domitrovic and Kovacevic (2013) studied on the correlation between shear strength and swelling properties of bentonite because of its use in Clay Geosynthetic Barriers as sealing component. The reason why bentonite exists between geosynthetic barriers is the high swelling capacity and low hydraulic conductivity. In order to quantify the role of bentonite within clay geosynthetic barrier, Volclay granular bentonite whose mineralogical composition consists of 80-85% of montmorillonite, around 5% of cristobalite, about 5% of quartz and approximately

5% of plagioclase was selected. First, swelling behavior of bentonite was determined with long term oedometer tests under three varying effective stress conditions, 50, 100 and 200 kPa. For primary swelling stage, it was seen that the specimen showing the highest level of swelling and relative vertical deformation was the one under lowest level of normal stress; i.e. under effective stress of 50 kPa. Swell test results can be seen from Figure 3.8.

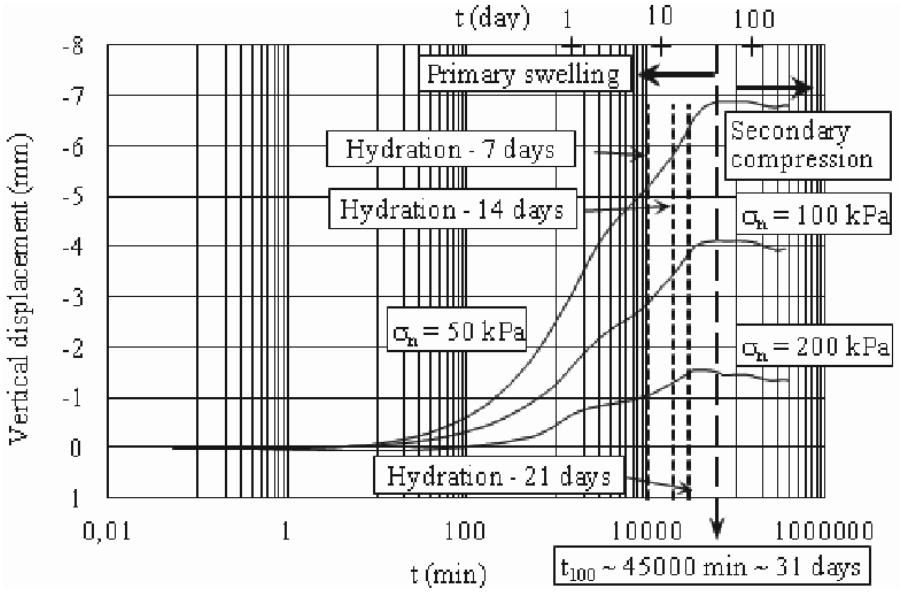

Figure 3.8. Vertical displacement versus time graph for betonite samples under changing normal stresses (After Domitrovic and Kovacevic, 2013)

As the second part, direct shear test with 60x60 mm device dimensions was conducted on granular bentonite in order to examine the influence of swelling

property on its shear strength. Specimens were tested under three different normal stress levels of 50,100 and 200 kPa with changing hydration times of 7, 14 and 21 days. After hydration times were reached, they were sheared by the same shearing rate. For both test procedures, specimens were not compacted but just flattened. Direct shear test results showed that peak and residual strength values were decreasing with reducing normal stress application and increasing hydration times; i.e. moisture content. Under 200 kPa effective stress, there was not a significant change in moisture content and shear strength with altering hydration times. Figure 3.9 explicitly shows alteration in strength with water content and effective stress.

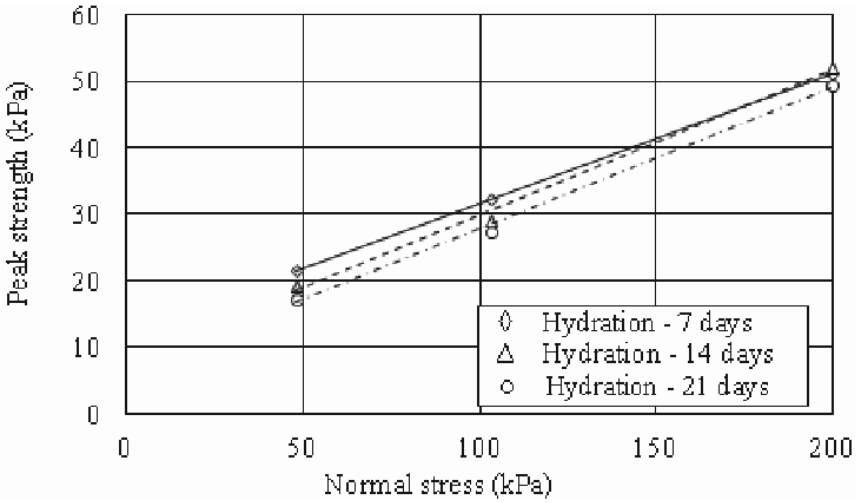

Figure 3.9. Peak strength versus normal stress and hydration times graphs (After Domitrovic and Kovacevic, 2013)

Moreover, when shear strength parameters were evaluated, peak and residual cohesion values were observed to decrease with longer hydration times while peak and residual friction angle values increased in the same moisture content change. The most dramatic variation in friction angle was visible up to 14 days of hydration. Results are given in Table 3.2.

Table 3.2. Shear strength parameters' variation with water content and swelling (After Domitrovic and Kovacevic, 2013)

Hydration Time	**Peak Parameters**		**Residual Parameters**	
	c (kPa)	**Φ (^{0})**	**c (kPa)**	**Φ (^{0})**
7 days	11.99	11.23	11.05	7.80
14 days	8.04	12.47	4.79	9.38
21 days	6.32	12.27	3.63	9.31

Wang et al. (2014) performed an experimental study on disturbed compacted unsaturated clay which was taken from the construction site in Changsha, China. Soil specimens were compacted with specially designed apparatus that is given in Figure 3.10. Ten soil specimens with e=0.6 were prepared for water content controlled tests while four soil specimens with w=16% were set for void ratio controlled experiments. Then, the shear strength parameters of samples were obtained from

strain controlled multistage direct shear test under 100, 200, 300 and 400 kPa vertical loading.

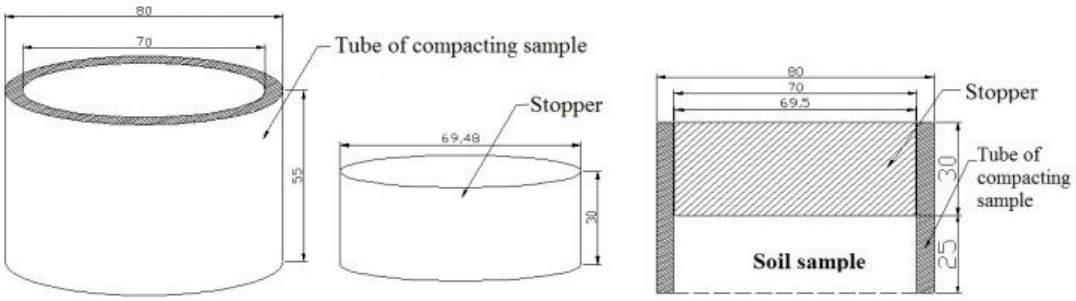

Figure 3.10. Apparatus for sample compaction (After Wang et al., 2014)

According to direct shear test results, correlation between water content and cohesion as well as the relation between water content and internal friction angle at mean void ratio of 0.6 can be examined from Figure 3.11. On the other side, Figure 3.12 shows the void ratio versus cohesion and void ratio versus angle of internal friction relations at mean water content of 15.52%. As the result, it can be said that increase in water content or void ratio had an decreasing effect on both for cohesion and internal friction angle. The reason of decrease in the cohesion could be explained as the fact that attached water caused increase in the distance between clay particles and water molecules and so thickened the hydration membrane, which resulted in the weakening of the intermolecular and electrostatic attraction forces. Moreover, due to same reasons enhancing of lubricity between clay particles induced decrease in internal friction angle.

All mentioned studies were listed below in Table 3.3:

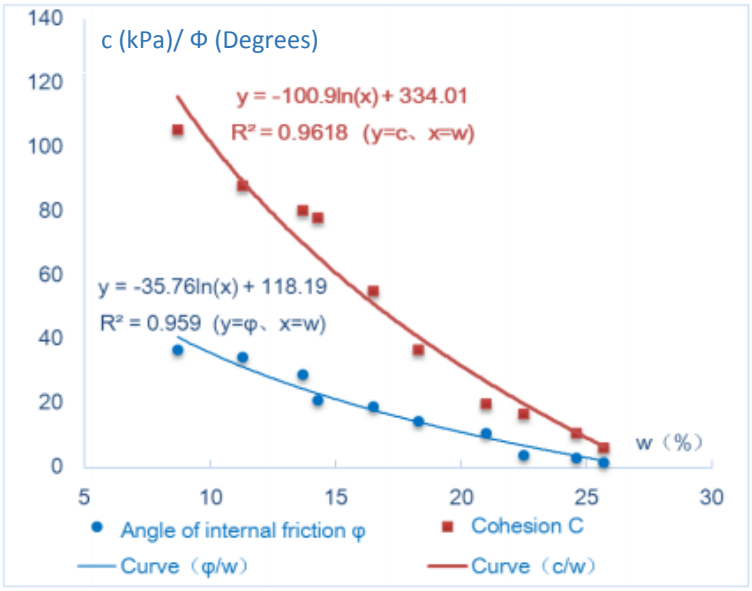

Figure 3.11. Relation between w-c and w-ϕ (After Wang et al., 2014)

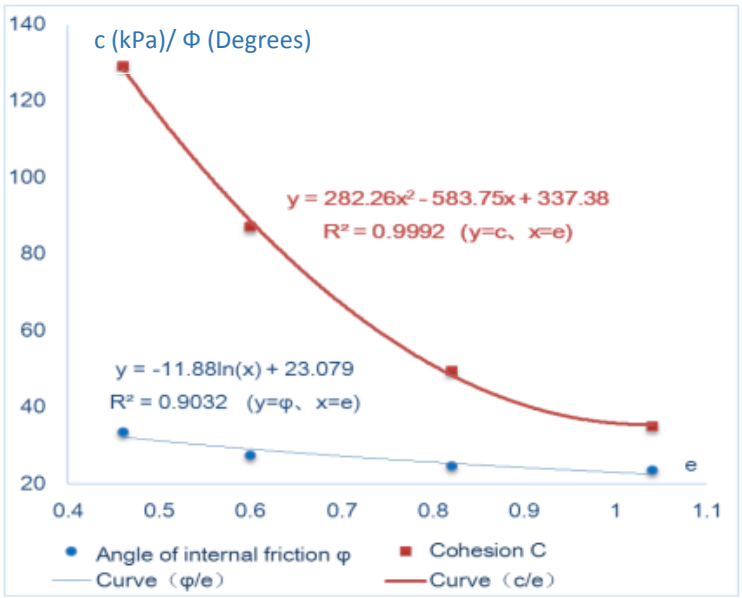

Figure 3.12. Relation between e-c and e-ϕ (After Wang et al., 2014)

Table 3.3. Previous studies made by other researches

Researcher	Swell Procedure	Shear Procedure	Conclusion
Lo K. Y. (1987)	Semi confined swell test	-	Increase in applied stress causes decrease in swelling.
Lo K. Y. and Lee Y. N. (1990)	Modified semi confined swell test	-	Decreasing in applied stress causes increase in swelling strain. Also, there is a linear relationship between stress and horizontal swelling potential.
Wong R.C.K. (1998)	Special apparatus similar to the one developed by Lo and Lee	Triaxial cell	Shear strength decreases as swelling level rises.
Tilgen H. P. (2003)	-	Direct shear test	With the increasing water content, friction angle values decrease while cohesion values increase up to OMC and from OMC both of them decreases. Values of cohesion and angle of friction for compacted samples are higher than the ones for soaked samples. Besides, soil suction increases as water content decreases at the dry side of OMC.

Table 3.3. (continued)

Al-Mhaidib A.I. and Al-Shamrani M.A. (2006)	Hydraulic triaxial stress path cell	Hydraulic triaxial stress path cell	Deviator stress and shear strength decreases with increasing swell and decreasing confining pressure.
Domitrovic D. and Kovacevic Zelic B. (2013)	Consolidometer test	Direct shear test	Shear strength and cohesion decreases with increasing swell and decreasing normal stress while friction angle shows an opposite trend.
Wang L. (2014)	-	Direct shear test	Increase in water content or void ratio has a decreasing effect on both cohesion and internal friction angle.

CHAPTER 4

EXPERIMENTAL STUDIES

4.1. Objective

The objective of this study was to investigate the change in unconfined compressive strength, undrained shear strength, undrained elastic modulus, void ratio, liquidity index and energy absorption capacity of expansive clays at swelling 0%, 10%, 15%, 20%, 25%, 50%, 75% and 100% of ultimate swell. In addition, swelling strain relation with time, swell pressure and frictional stress developed between mold and sample were determined. Expansion capacity of soil samples was also estimated with Free Swell Index Test and Methylene Blue Test.

4.2. Materials

Four samples were selected including one artificial and three natural ones in order to conduct the tests. They are listed with sampling information in Table 4.1.

Table 4.1. General information about samples

Soil Designation	**Sample Type**	**Sampling Location**	**Sampling Depth (m)**
Sample A	Artificial	Obtained by mixing 15% bentonite and 85% kaolinite. Bentonite bought from Karakaya Bentonite Inc. in Ankara and kaolinite from Kalemaden Company in Çanakkale.	-
Sample B	Natural	Bilkent Integrated Health Campus, Ankara	3-4
Sample O	Natural	Middle East Technical University Campus, Ankara	1-3
Sample E	Natural	Ege Plaza, Ankara	20-25

Furthermore, view of four samples can be seen from Figure 4.1 in order to determine their physical properties like color.

Figure 4.1. View of samples (1-Sample A, 2-Sample B, 3-Sample O, 4-Sample E)

4.3. Properties of Soil Samples

Maximum dry density, optimum water content, specific gravity, Atterberg limits; liquid limit (LL), plastic limit (PL), plasticity index (PI) and shrinkage limit (SL) values were determined in order to obtain the index properties of each sample. Additionally, hydrometer test and sieve analysis were performed for each sample. Standard test methods that were used to identify the soil samples are presented in Table 4.2.

Table 4.2. Standard test methods for soil specimen identification

Index Properties	Utilized Test Method
Optimum water content and maximum dry density	Harvard Miniature Compaction (for Sample A) Test Methods for Laboratory Compaction Characteristics of Soil Using Standard Effort (for Samples B, O and E)---ASTM D698
Specific Gravity	Test Methods for Specific Gravity of Soil Solids by Water Pycnometer (for all samples)--- ASTM D854
Sieve Analysis	Test Methods for Particle Size Distribution (Gradation) of Soils Using Sieve Analysis (for Samples B, O and E)--- ASTM D6913
Particle Sedimentation	Test Methods for Particle-Size Analysis of Soils (for all samples)--- ASTM D422
Liquid Limit, Plastic Limit and Plasticity Index	Test Methods for Liquid Limit, Plastic Limit and Plasticity Index of Soils (for all samples)--- ASTM D4318
Shrinkage Limit	Test Methods for Shrinkage Factors of Soils by the Mercury Method (for all samples)--- ASTM D427

Grain size distribution curves for all soil samples are given in Figure 4.2.

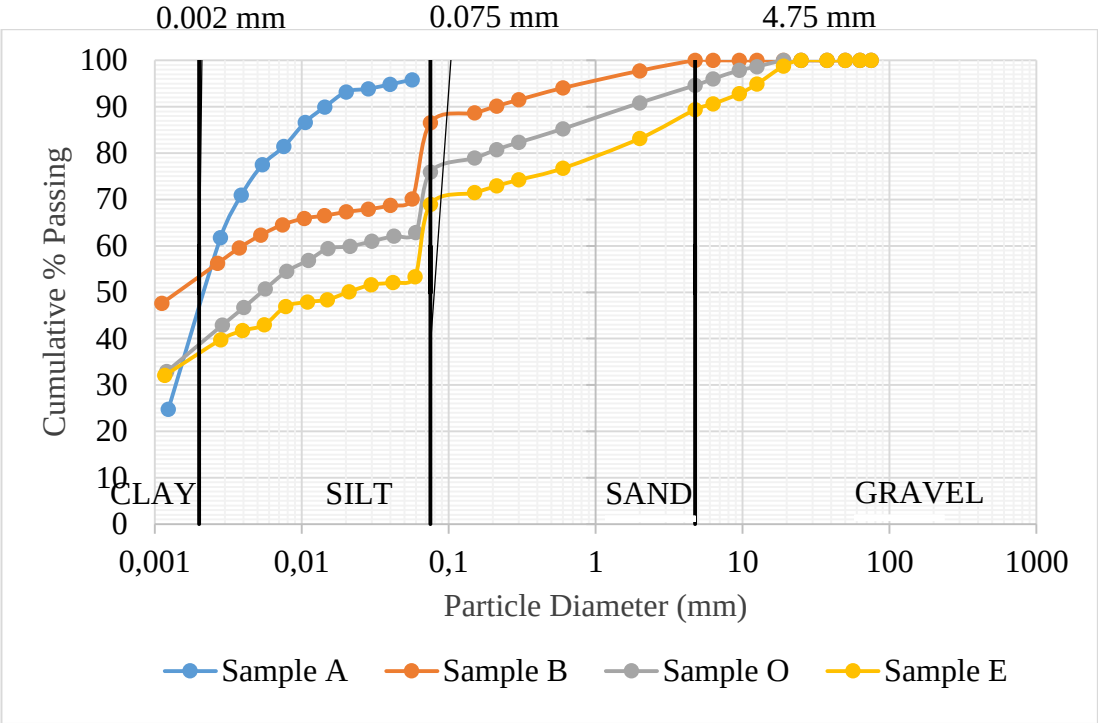

Figure 4.2. Grain size distribution curves for all samples

Liquid limit and plasticity index values of Samples A, B, O and E, which can be found in Table 4.3, were inserted in plasticity chart shown in Figure 4.3. According to the plasticity chart, all types of soils were classified as clay of high plasticity.

Moreover, Table 4.3 summarizes index properties of soil samples with grain size percent, soil type and activity values. Activity was calculated by dividing plasticity index to clay content.

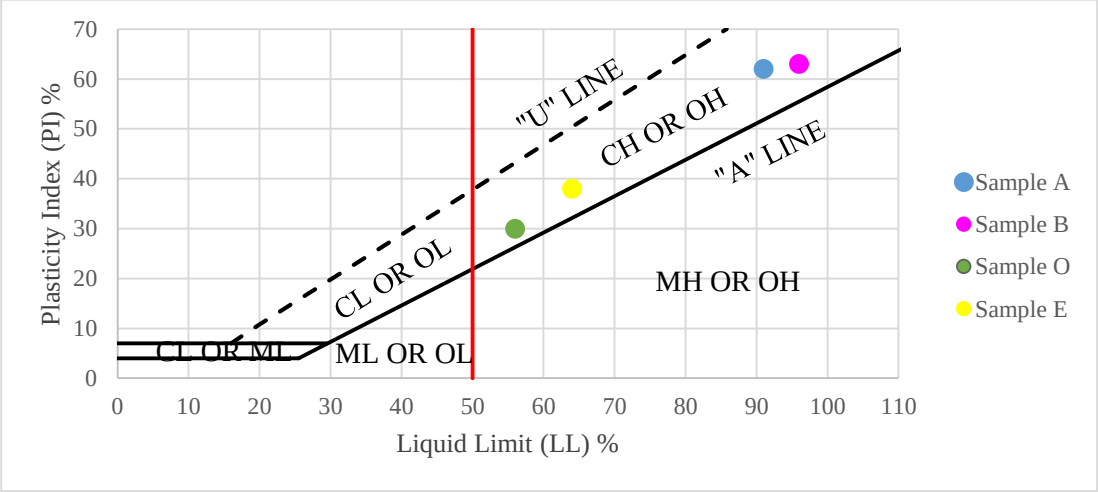

Figure 4.3. Plasticity chart in order to determine soil type

Table 4.3. Summary for index properties of soil samples with grain size percent, soil type and activity values

Sample Type	**G_s**	**LL (%)**	**PL (%)**	**PI (%)**	**SL (%)**	**Gravel Content (%)**	**Sand Content (%)**	**Silt Content (%)**	**Clay Content* (%)**	**Soil Classification**	**Activity**
Sample A	2.59	91	29	62	24	0	0	48	48	CH	1,29
Sample B	2.7	96	34	63	13	0	13,5	32,8	53,7	CH	1,17
Sample O	2.51	56	26	30	10	5,5	18,5	37	39	CH	0,77
Sample E	2.7	64	26	38	12	11	20	32	37	CH	1,03

*: Clay content of the samples was determined from Figure 4.2 by considering the last two hydrometer test readings. Therefore, they are approximate.

In order to estimate the expansion potential of the samples, literature was searched. Thus, it was seen that Chen (1983) and Seed et al. (1962) were proposed a correlation between LL and swelling potential, PI and degree of swelling respectively. Moreover, Williams (1957) found expansiveness of soil changes with clay content and PL respectively. Below Table 4.4 and Figure 4.4 can serve as a check for the swelling potential of samples.

When the methods given in Table 4.4 were compared with the information about sample properties in Table 4.3, it was seen that the swelling potential of Sample A, Sample B and Sample E could be evaluated as very high while Sample O:'s as high potential. Results on Figure 4.4 followed the same trend with methods of Chen's (1983) and Seed et al.'s (1962). Thus, all selected samples were decided to swell upon wetting.

Table 4.4. Soil classification according to swelling potential after Chen (1983) and Seed et. al. (1962)

Degree of Expansion	**Chen (1983)**	**Seed et al. (1962)**
Very High	LL> 60	PI> 35
High	40< LL ≤ 60	20< PI ≤ 35
Medium	30< LL ≤ 40	10< PI ≤ 20
Low	LL< 30	PI< 10

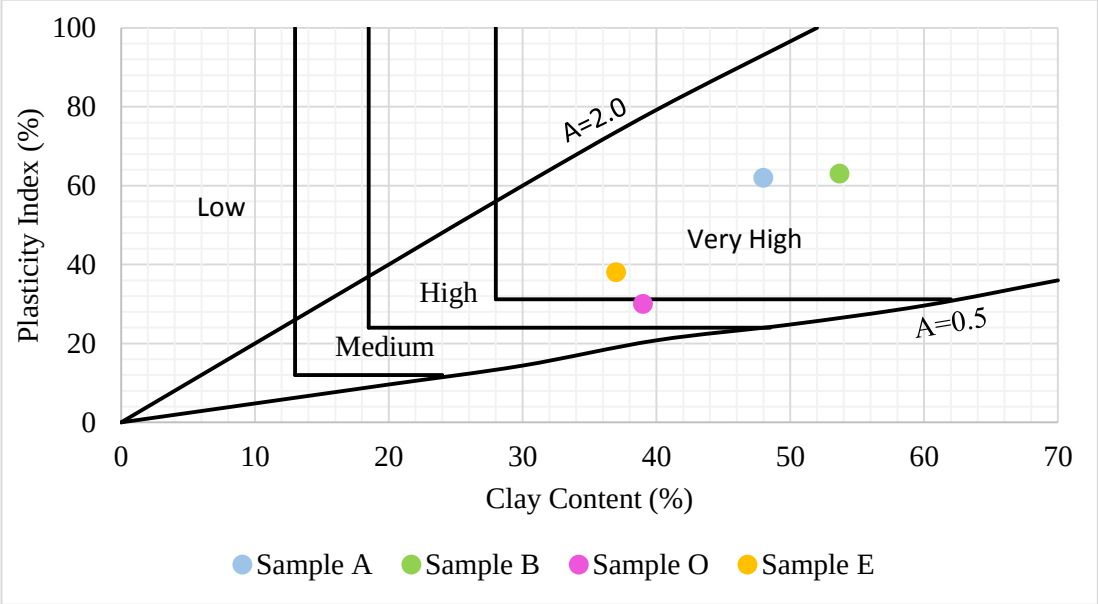

Figure 4.4. Swelling potential chart proposed by Williams (1957)

Separately, dry density versus moisture content curves were obtained by making Standard Proctor Test for natural soil samples and by applying Harvard miniature compaction test on artificial soil specimen; i.e. Sample A. The reason behind the use of Harvard miniature compaction apparatus was the difficulty in sample preparation and scarcity of sample amount.

Wilson (1950) developed Harvard miniature compaction for small amount of fine grained soils. Specimens can be produced in a short amount of time due to ease and size of the test. In addition to the determination of moisture content-density relationship, dimension of extruded specimens is suitable for testing strength, stiffness and permeability. The test is performed on the soil which is sieved through No. 4 sieve. The soil is compacted in three layers in a 0.0715 m height and 0.033 m diameter mould with a cylindrical tamping foot whose diameter is 0.0127 m. 25

tamps per layer is applied. Tamping force does not exceed the predetermined value owing to pre-set compression spring in the tamping (Wilbourn, 2007). Harvard miniature compaction test apparatus can be seen from Figure 4.5.

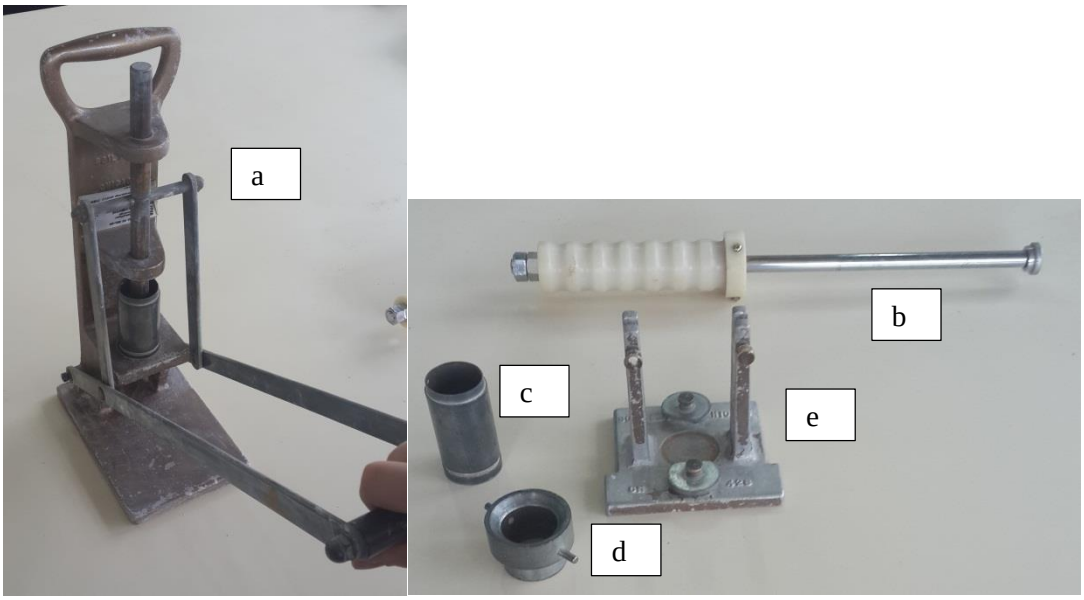

Figure 4.5. Harvard miniature compaction test apparatus (a- Sample extruder, b- tamper, c-mould, d- collar of the mould, e- base of the mold)

Dry density versus water content curves were used to determine the appropriate dry density according to desired water content in sample preparation stage. Curves are stated in Figure 4.6.

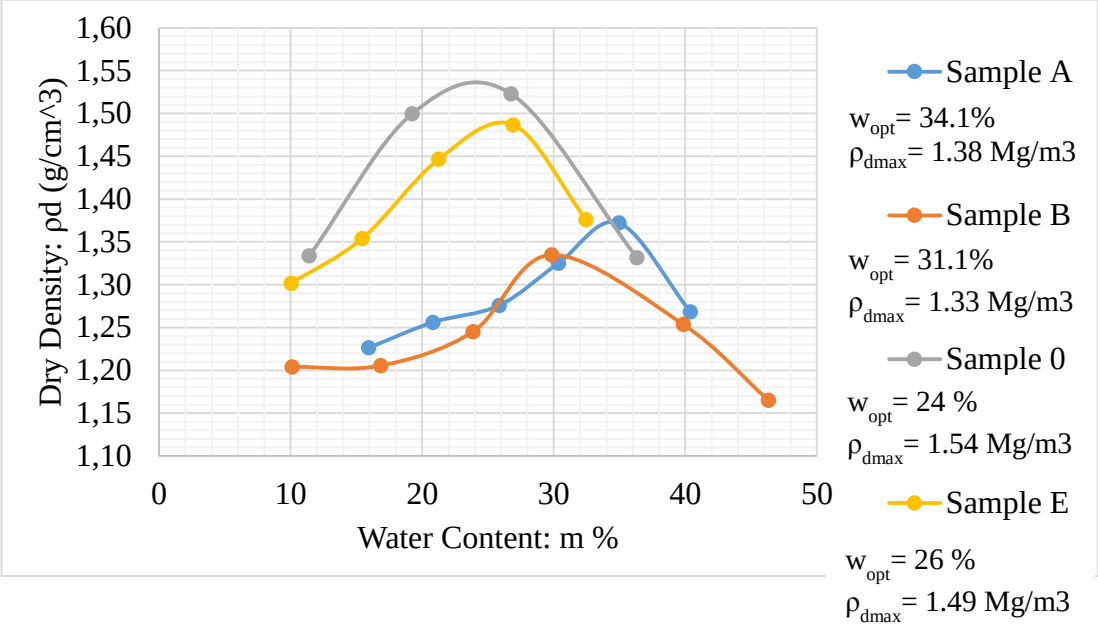

Figure 4.6. Dry denstiy versus water content curves for all soil samples

In order to get an idea about how accurate results were acquired from the tests, relationships in literature between Atterberg limits and optimum water content were searched. In this way, following parameters for fine grained soils were related each other in Eqn 4.1 proposed in US. Navy Design Manual (1962).

w_{opt} (std)= 6.77+0.43*LL-0.21*PI ……..Eqn 4.1

"std" means values obtained from Standard Laboratory Compaction Test. Therefore, the optimum moisture content value for Sample A could not be obtained with the relationship given in Eqn. 4.1 since it was found with Harvard Miniature Compaction Test.

Experimental results were compared in Table 4.5 with the ones obtained from Eqn 4.1. When Table 4.5 is examined, it is seen that both results are very similar to each other.

Table 4.5. Comparison of experimental w_{opt} value with the one got from Eqn 4.1

Sample Type	**Experimental w_{opt} %**	**w_{opt} from Eqn 4.1 %**
Sample B	31.1	34.8
Sample O	24	24.6
Sample E	26	26.3

4.4. Preparation of Samples

Specimen preparation for this study started with drying in oven at 105 ^{0}C. All soil specimens were oven-dried for approximately 24 hours. For Sample A, bentonite and kaolinite were mixed in proportions of 15% and 85% respectively. Then, all samples were pulverized into powder with a wooden hammer and sieved through No. 40 sieve individually. Sieved samples were again sieved two more times through No. 40 sieve to ensure the uniformity. After sieving, they were mixed with water to reach the water contents given in Table 4.6. Water contents given in Table 4.6 was determined such that they could be equal to approximately 5% below the PL value by considering the workability of the sample. Due to workability problems, water content of Sample B could not be determined according to this principle.

Table 4.6. Water contents chosen at which samples were prepared

Sample Type	Water Content at Which Samples were Prepared (%)
Sample A	24
Sample B	25
Sample O	20
Sample E	19

In order to maintain a uniform water distribution in soil sample mass by curing, specimens were stored air tight bags in the humid room at a room temperature of about 24 ^{0}C for 6 to 36 hours.

4.5. Design Stages of the Mold Properties

At the very beginning of swelling tests, full length slotted metal molds, which were inspired from standard penetration test sampler, were tried whether it works or not. Before trial test, metallic molds were thought to be useful for easy remove of sample from the mold once its inner surface was greased. However, when trial test was made, it was seen that high plastic clayey soil sample particles were stuck on to the mold's inner surface and time needed for water penetration just from top and bottom was excessively long. In response, existence of perforation at the mold surface was decided to be implemented for shorter swelling time but again there was a problem. Perforating a metallic surface was a really difficult job. Therefore, plastic was chosen as the material of mold with the ease of perforating but adhesion and so

loss of sample due to volumetric swell through perforations was still a problem. In order to eliminate this issue, filter paper was decided to be used. It was stuck with a self-adhesive tape at the top and bottom of mold in order to prevent filter paper from moving into the sample during static compaction. Finding a plastic pipe with diameter of 36 mm, which was determined at the beginning of study, was the single issue waiting for solution at this point. As a solution, plastic billet, whose material properties can be found in Appendix A, was shaped as a pipe with the help of a lathe. Bottom of the molds was attached with screw threads to avoid sample swell to this direction and so its loss. Moreover, there was a seat for porous stone at this part. In addition to these, a rod having a porous stone at the contact with soil sample was developed in order to facilitate the touch of dial gauge contact point to soil sample top. Mold length was designed as 0.14 m to account for the increase in length with expansiveness. Molds had a total of 154 perforations whose diameters were 0.00225 m. Additionally, rod with rigid circular plates has a length of 0.166 m. Final shape of molds can be seen from Figure 4.7 and its engineering drawing and sections are presented in Figure 4.8. Figure 4.9 shows the schematic drawing of the mold after sample preparation.

Perforated molds were utilized for 10%, 15%, 20%, 25%, 50%, 75% and 100% of swell. On the other hand, a mold without holes was employed for 0% of swell, which was called reference test. The reason behind the use of mold without perforations was no need for water entry and so swelling stage in the reference test. Samples were prepared at water contents given in Table 4.6 and then they were directly sheared without allowing them to swell.

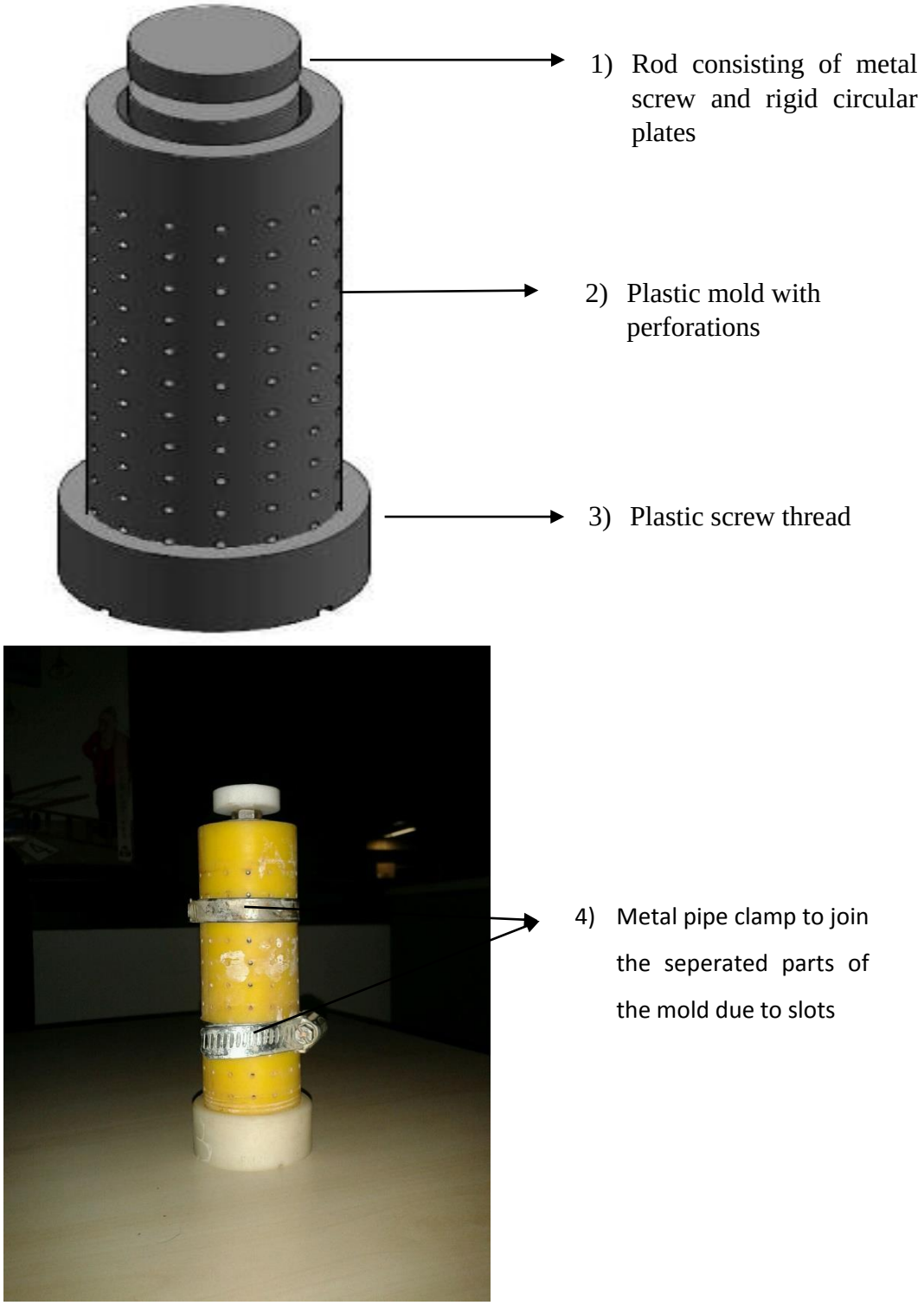

Figure 4.7. 3-D view and photo of the mold with its parts

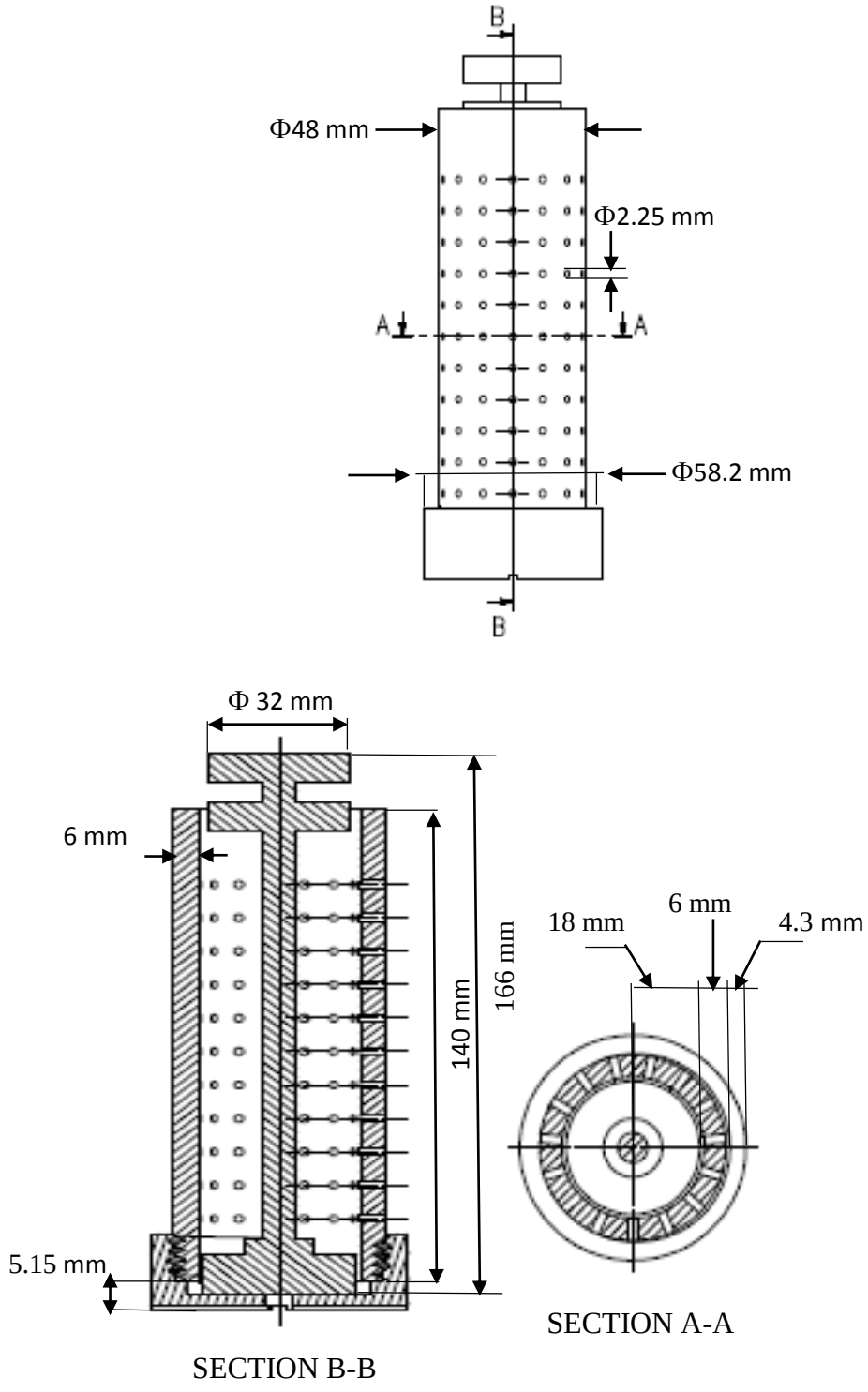

Figure 4.8. Drawing and sections of final molds with rod having rigid circular plates

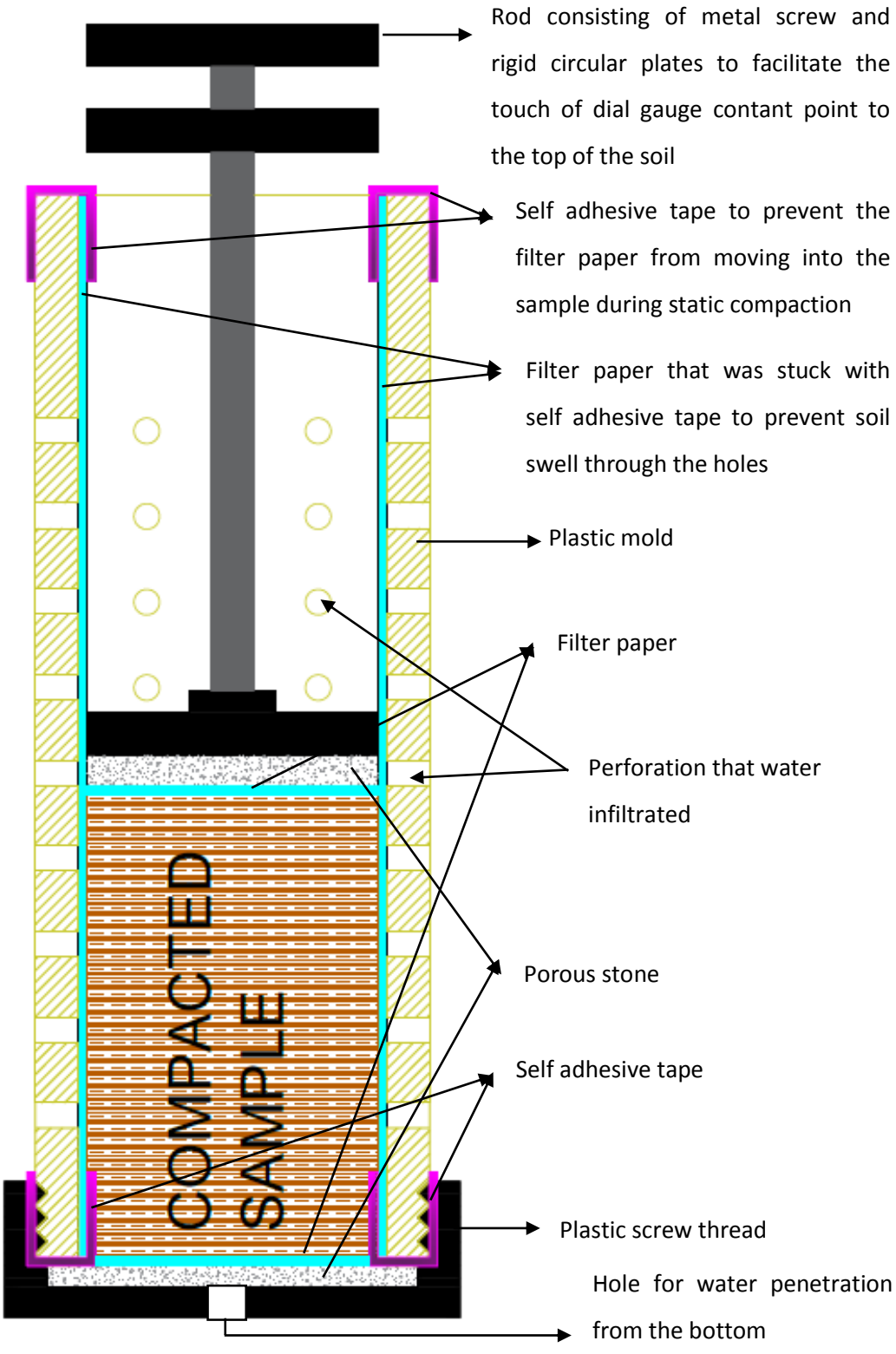

Figure 4.9. Schematic drawing of the mold after sample preparation

4.6. Swell Test Procedures

4.6.1. Compaction of Samples

Soil specimens that were prepared as described in Section 4.4 were directly compacted into the molds. Before compaction, dry densities which were listed in Table 4.7 corresponding to the selected water contents were found by using the curves obtained from standard proctor test for Sample B, O and E and from Harvard miniature compaction test for Sample A.

Table 4.7. Dry densities reached after static compaction

Sample Type	**Dry Density Corresponding to Water Contents in Table 4.6 (Mg/m^3)**
Sample A	1.27
Sample B	1.26
Sample O	1.51
Sample E	1.41

Bulk weight of sample whose length and diameter would be 0.072 and 0.036 m respectively was calculated according to Eqn 4.2:

Bulk weight=Volume of sample*Determined dry density ……..……...Eqn 4.2

Static compaction was performed in three steps after calculation of bulk weight. In each step, sample was poured to the mold and compacted into it so that poured sample would be weighted as 1/3 of its bulk weight. This process took about 5 minutes. Process including sample preparation and static compaction can be seen from Figure 4.10.

1) After samples were dried in oven at 105 ^{0}C, they were pulverized with the help of a wood hammer.

2) They were sieved through No. 40 sieve for at least 3 times to ensure the uniformity.

Figure 4.10. Sample preparation process

3) Calculated bulk weight according to Eqn. 4.2 and water content given in Table 4.6 were weighted.

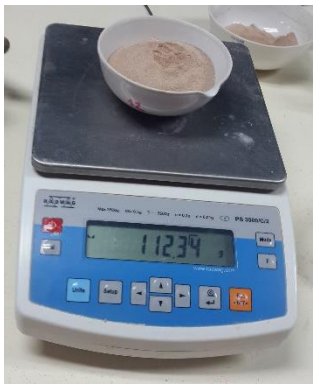

4) Weighted amount of sample and water were mixed and waited in humid room for 6- 36 hours.

5) Calculated bulk weight of sample was divided into three equal amount for static compaction.

6) Filter paper was stuck with a self-adhesive tape at the top and bottom of perforated molds. Also, circular filter papers were put on porous stones.

Figure 4.10. (continued)

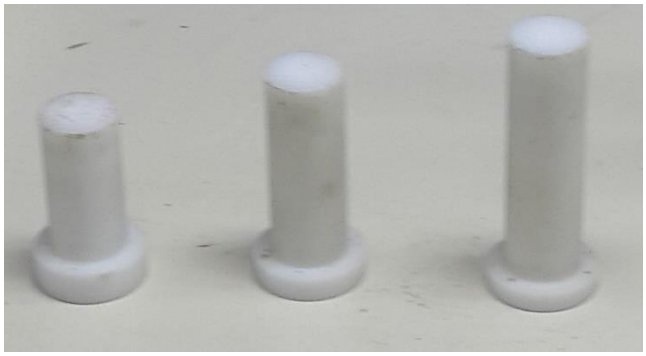

7) Samples were compacted with the help of plastic rods whose length was 0.068 m, 0.092 m and 0.116 m fitting to the compacted soil sample heights.

8) Hydraulic jack was used for static compaction. Compaction including three steps took approximately 5 minutes.

9) As distinct from perforated molds, samples were moved from the molds without perforations with the help of a metal sample extractor.

Figure 4.10. (continued)

4.6.2. Swell Tests

Swell tests were conducted on the samples in the same molds as in the case of compaction. These tests were made in accordance with ASTM D 4546 in which the requirement of at least 1 kPa pressure application is indicated. Designed rod with rigid circular plates was sufficient for this rule since the weight of about 112 g applied a pressure of approximately 1.1 kPa.

In the first test, samples were submerged, which is presented in Figure 4.11, until vertical swell stopped; in other words, vertical swell reached 100%. Dial gauge readings were taken whose sensitivity was 0.01. If last two dial gauge readings were identical in 12 hours, 100% of swell tests were ended. Needed time to reach ultimate swell is given in Table 4.8.

Table 4.8. Needed time to reach ultimate swell for each soil samples

Sample Type	**Needed Time to Reach Ultimate Swell (days)**
Sample A	12.9
Sample B	10.8
Sample O	2.8
Sample E	1.1

In order to take this test, which determined the ultimate swell, as a starting step for the tests measuring 10%, 15%, 20%, 25%, 50% and 75% of ultimate vertical swell, percent swell versus time graphs were plotted. Swell percentage in these graphs was determined by using below formula:

Axial swell (%)=(ΔH/H0)*100…….....Eqn 4.3

where

ΔH= Height difference in the sample length

H_0= Initial sample height; in this case it was always 0.072 m

Figure 4.11. Submerged specimen in perforated mold

Swell percent versus time graphs for all specimens up to 3 days were given in Figures 4.12, 4.13, 4.14 and 4.15. Each test was repeated in a second mold to verify repeatability.

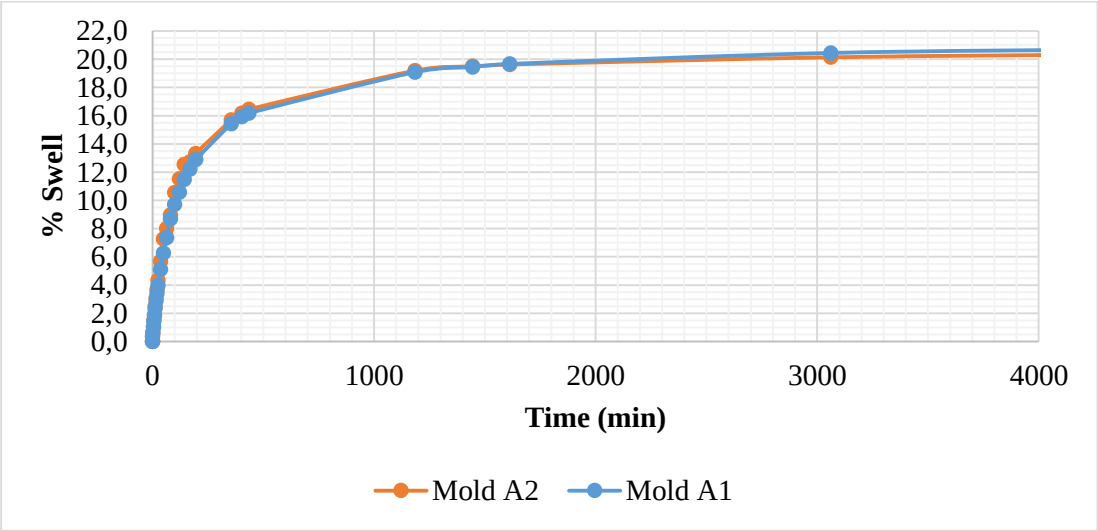

Figure 4.12. 100 % of swell versus time graph for Sample A

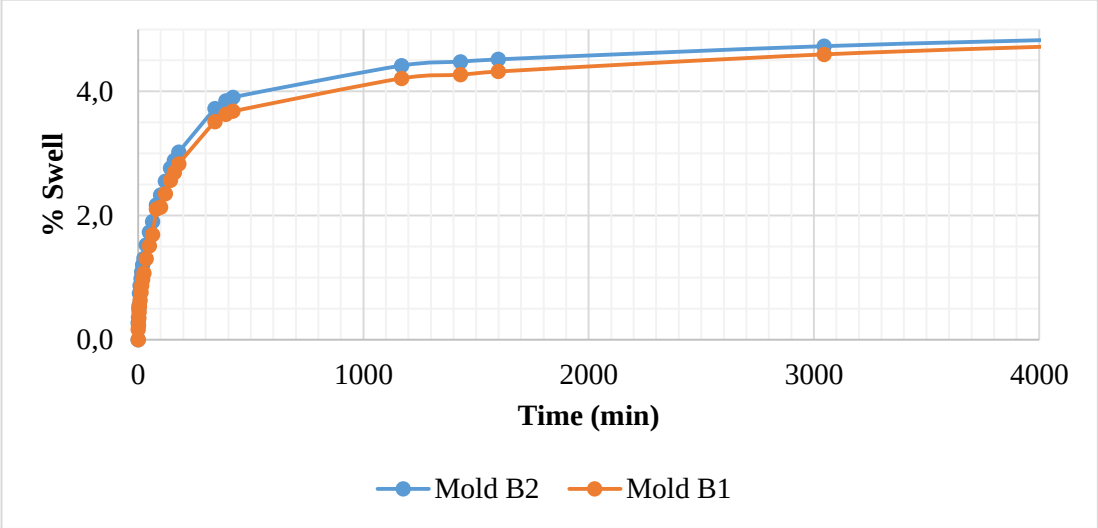

Figure 4.13. 100 % of swell versus time graph for Sample B

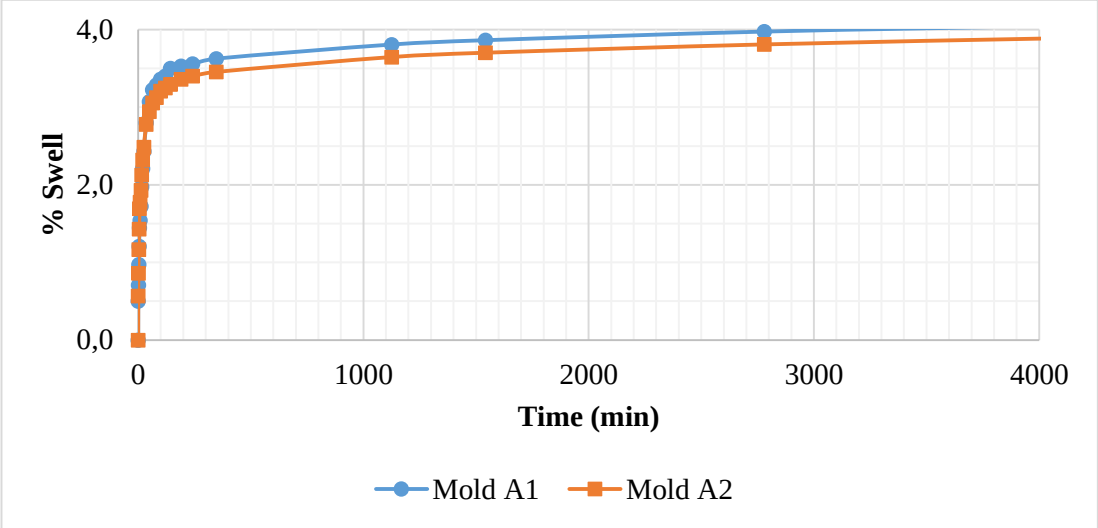

Figure 4.14. 100 % Swell versus time graph for Sample O

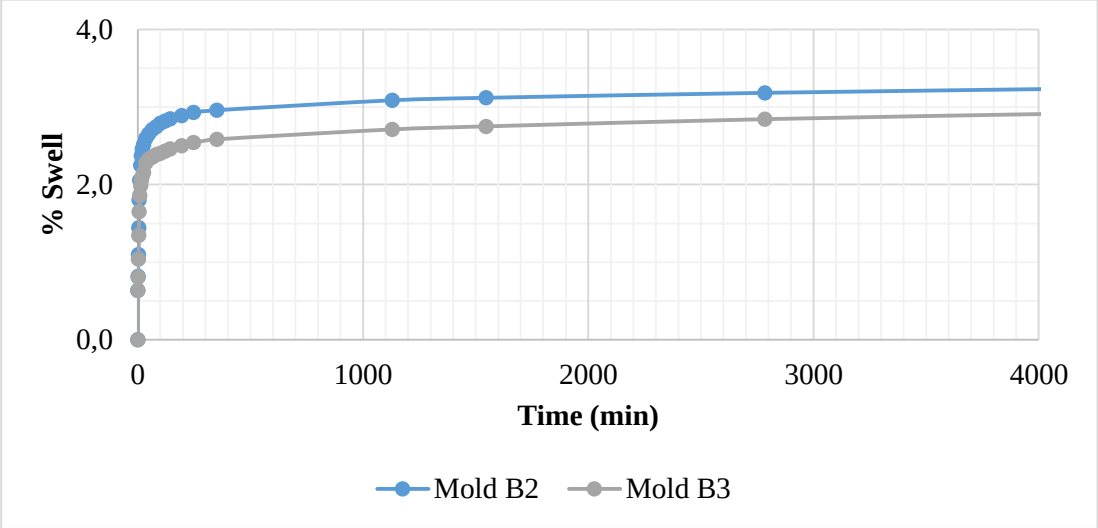

Figure 4.15. 100 % Swell versus time graph for Sample E

Figures 4.12, 4.13, 4.14 and 4.15 showed that the swelling potential of soil specimens are as follows in ascending order: Sample A> Sample B> Sample O> Sample E. Measured ultimate swell potential for Sample A, Sample B, Sample O and Sample E was found as 21.15%, 6.24%, 4.67% and 3.37% respectively. Then, corresponding swell percent for 10%, 15%, 20%, 25%, 50% and 75% swell of ultimate swell were calculated with proportion in the Figures 4.12, 4.13, 4.14 and 4.15. By using Eqn 4.3 and knowing swell percent, difference in height: ΔH was determined. Thus, the fact that the test would be ended in which reading of dial gauge was explored.

4.7. Unconfined Compression Test Procedures

Unconfined compression tests were made in accordance with the standard, ASTM D2166, in the laboratory environment under strain controlled loading.

Unconfined compression test machine during shearing process of a specimen can be seen in Figure 4.16.

Figure 4.16. Unconfined compression test machine view during shearing of a specimen

When statically compacted specimens were prepared at water contents stated in Table 4.6, they were sheared in unconfined compression test machine without allowing them to swell. These tests for 0% of swell of each sample were accepted as the reference test. Samples reaching the swell of 10%, 15%, 20%, 25%, 50% and 75% of ultimate swell as well as the specimens swelling to a ratio of 100% were cut from the top with the help of a mold which can be seen in Figure 4.17. Due to the length of cutting mold, whose length and diameter was 0.072 m and 0.036 m respectively, height to diameter ratio of 2- 2.5 written in ASTM D2166 was ensured.

All specimens were sheared at a strain rate of 0.7 mm/min. The maximum test duration was about 15 minutes.

Figure 4.17. Cutting of a swelled specimen to be fitted to the height to diameter ratio in ASTM D2166

According to ASTM D2166, unconfined compressive strength, q_u is accepted as the maximum load attained per unit area or load per unit area at 15% axial strain, whichever is secured first. For some samples at different swell ratios; for example, for Sample A at the swell ratio of 50%, 75% and 100%, point corresponding to 15% axial strain was taken as unconfined compressive strength because maximum load value was not read before it. Some specimen photos at failure was given in Appendix B. As can be seen from the photos, specimens had parallel base planes.

For each sample type and swell step; i.e. 0%, 10%, 15%, 20%, 25%, 50%, 75%, 100% of swell, stress-strain curves were obtained from unconfined compression test. In addition to these curves, undrained shear strength, unconfined compressive stress and undrained elastic modulus were stated in the following Sections 4.7.1, 4.7.2., 4.7.3. and 4.7.4. Briaud (2001) stated that one can obtain a modulus from a stress-strain curve for the case where confining pressure is zero such as unconfined compression test on clay or typical concrete cylinder test. Based on this statement, undrained elastic modulus was calculated with secant method by drawing a line from the origin to the point at 1/2 of unconfined compressive strength.

4.7.1. Unconfined Compression Test Result for Sample A

Stress- strain curves with undrained elastic modulus lines were given in Figures 4.18, 4.19, 4.20, 4.21, 4.22, 4.23, 4.24 and 4.25. Table 4.9 also shows clearly the results of curves; in other words, undrained shear strength, water content and undrained elastic modulus at 0%, 10%, 15%, 20%, 25%, 50%, 75% and 100% swell ratios.

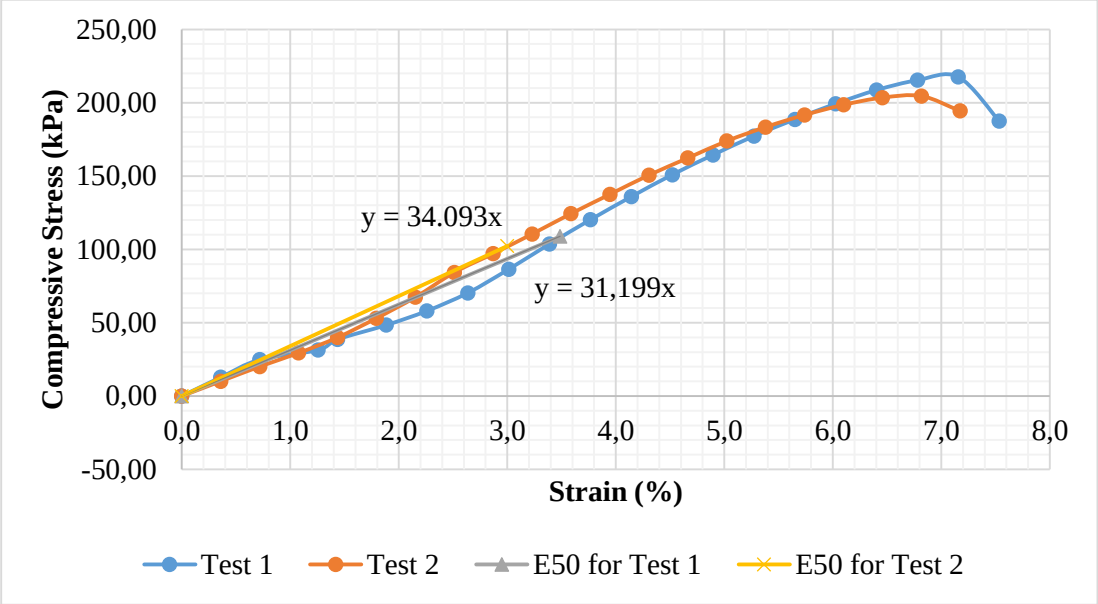

Figure 4.18. Unconfined compression test result for 0% of swell on Sample A

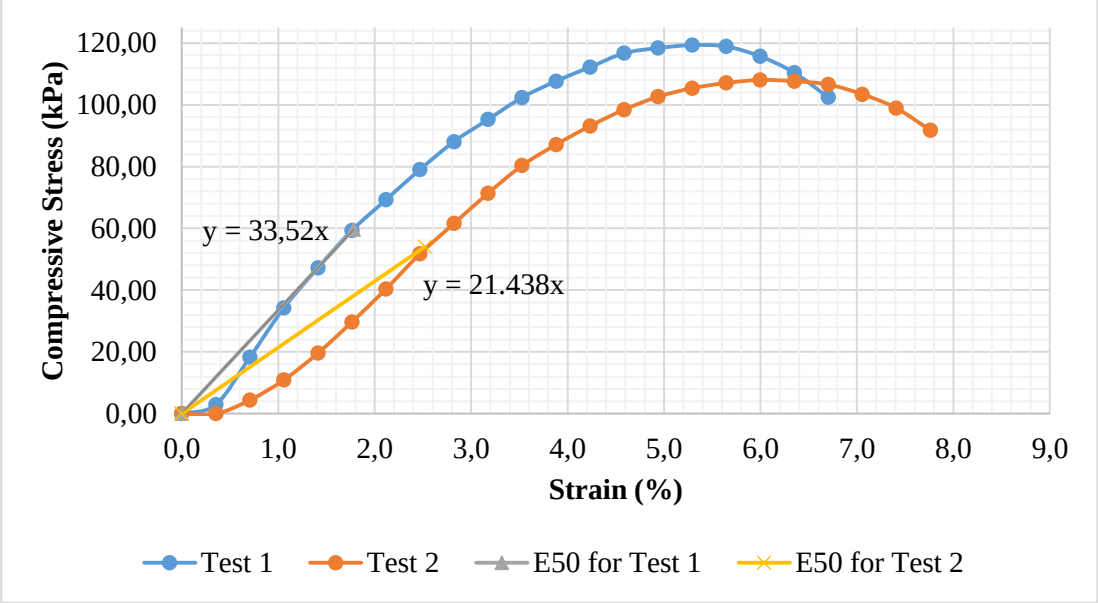

Figure 4.19. Unconfined compression test result for 10% of swell on Sample A

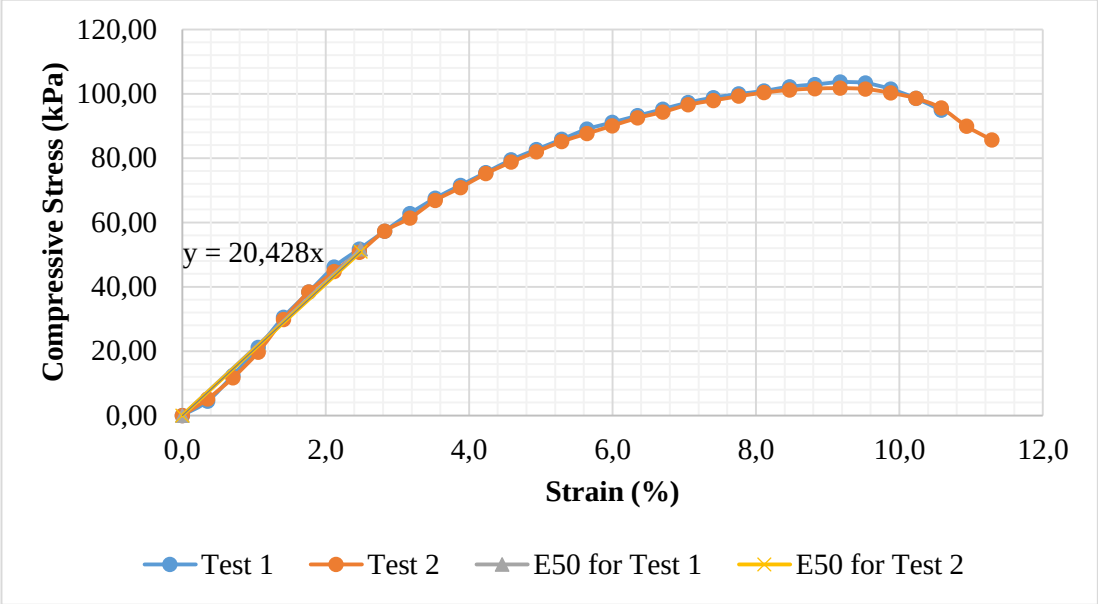

Figure 4.20. Unconfined compression test result for 15% of swell on Sample A

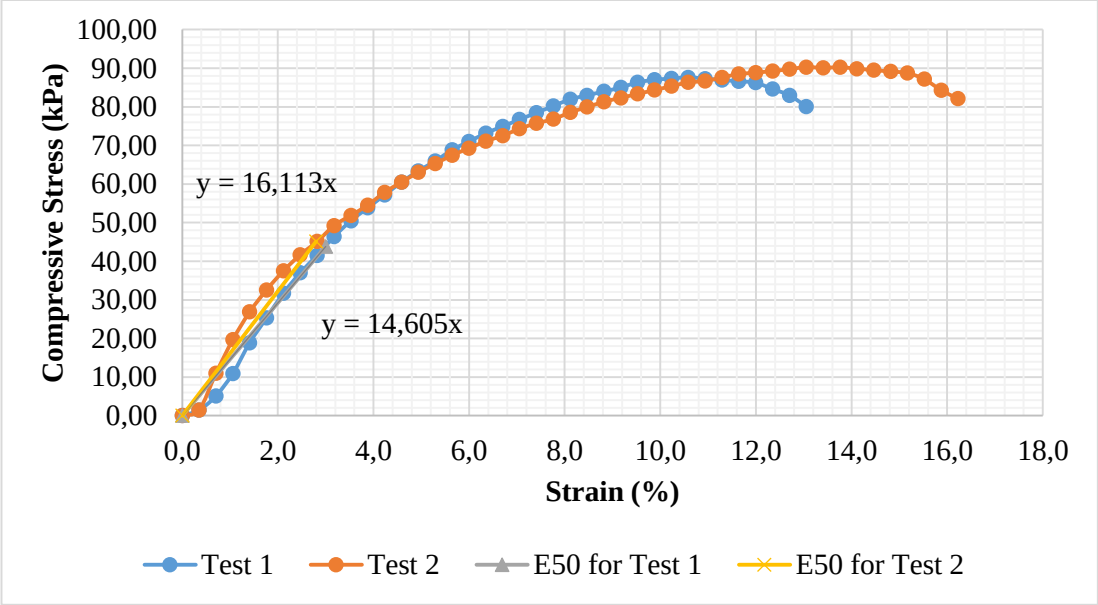

Figure 4.21. Unconfined compression test result for 20% of swell on Sample A

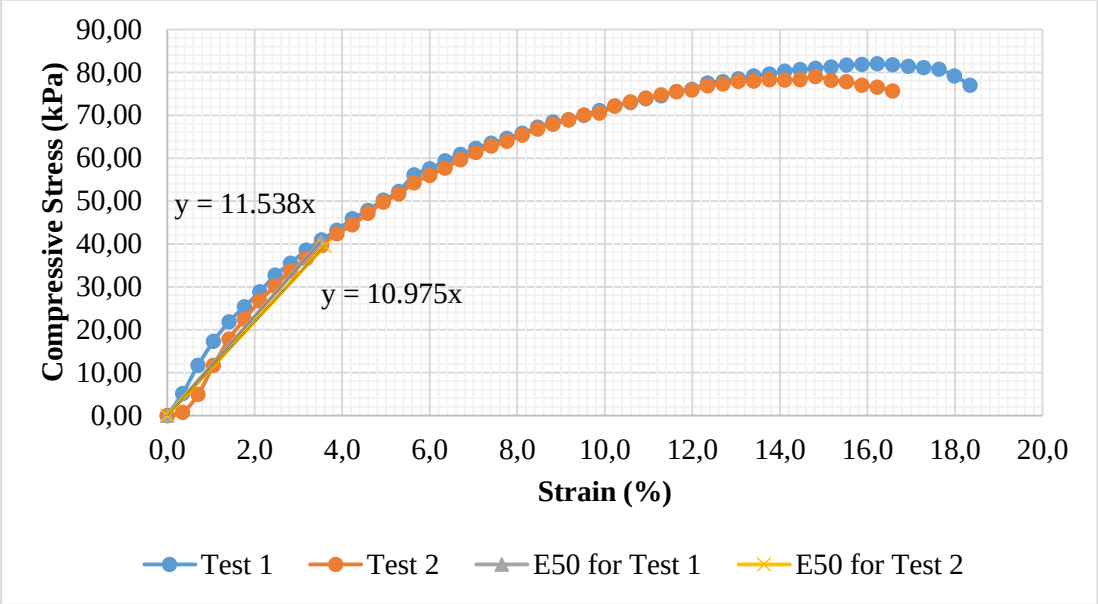

Figure 4.22. Unconfined compression test result for 25% of swell on Sample A

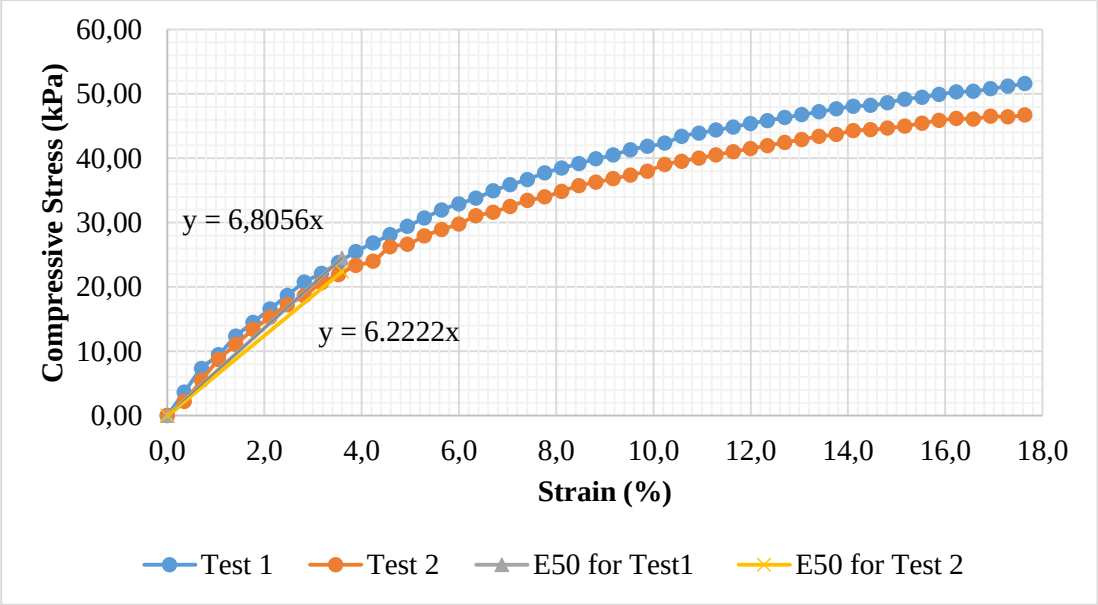

Figure 4.23. Unconfined compression test result for 50% of swell on Sample A

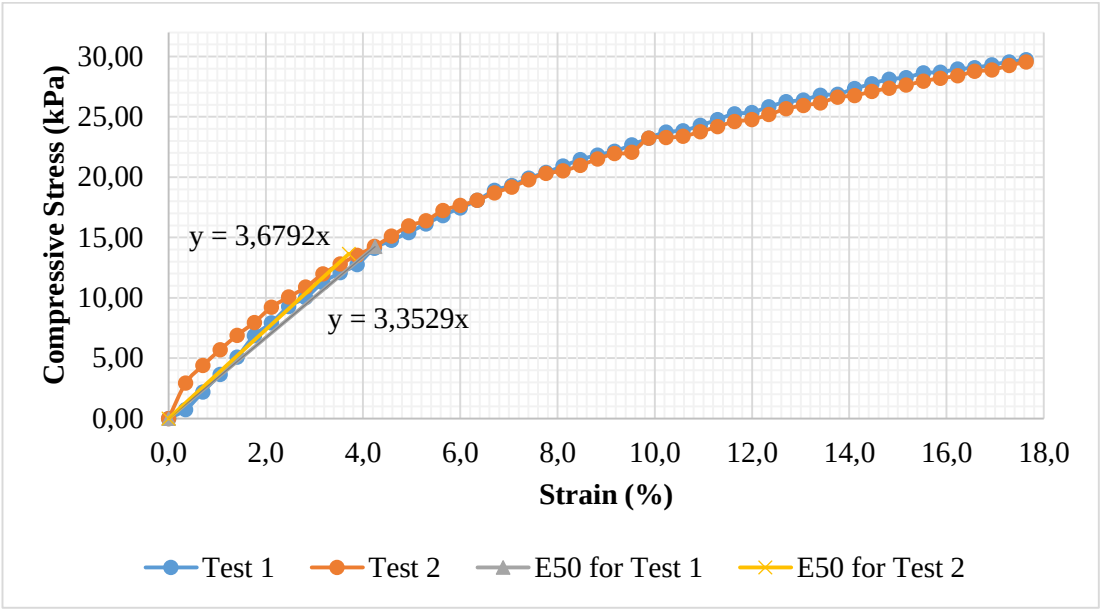

Figure 4.24. Unconfined compression test result for 75% of swell on Sample A

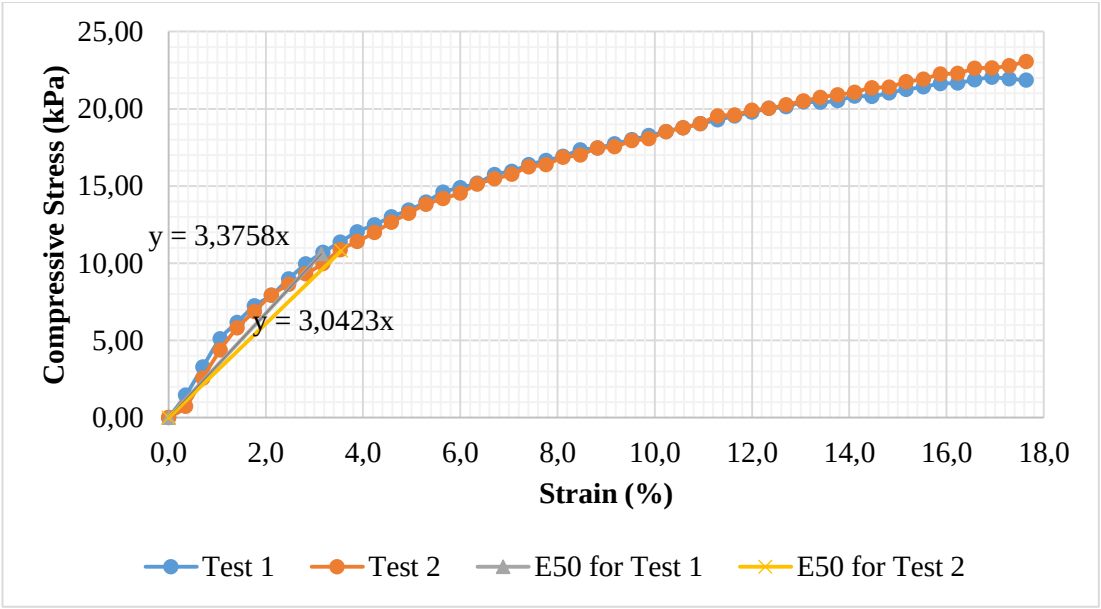

Figure 4.25. Unconfined compression test result for 100% of swell on Sample A

Table 4.9. Summary of unconfined compression test result for Sample A

%Swell	c_u (kPa)	Reduction in c_u* (%) $(c_{u,0\%} - c_{u,\ \text{given}\ \%})/c_{u,0\%}$	w %	Reduction in w (%) $(w_{0\%} - w_{\text{given}\ \%})/w_{0\%}$	E_u (kPa)	Reduction in E_u** (%) $(E_{u,0\%} - E_{u,\ \text{given}\ \%})/E_{u,0\%}$
0	105.5	0.0	23.9	0	3265	0.0
10	56.8	46.1	33.8	41	2748	15.8
15	51.3	51.4	36.7	53	2060	36.9
20	44.5	57.9	39.1	63	1535	53.0
25	40.0	62.1	41.1	71	1126	65.5
50	23.5	77.8	46.8	95	651	80.0
75	14.0	86.8	50.2	109	353	89.2
100	10.7	89.9	53.8	124	321	90.2

Water content at which sample is prepared:w_0	=	24

*: Reduction in unconfined compressive strength was same with the one for undrained shear strength.

**: Undrained elastic modulus values were determined with secant method from stress-strain curves.

4.7.2. Unconfined Compression Test Result for Sample B

Stress- strain curves with undrained elastic modulus lines were given in Figures 4.26, 4.27, 4.28, 4.29, 4.30, 4.31, 4.32 and 4.33. Table 4.10 also shows clearly the results of curves; in other words, undrained shear strength, water content and undrained elastic modulus at aforementioned swell ratios.

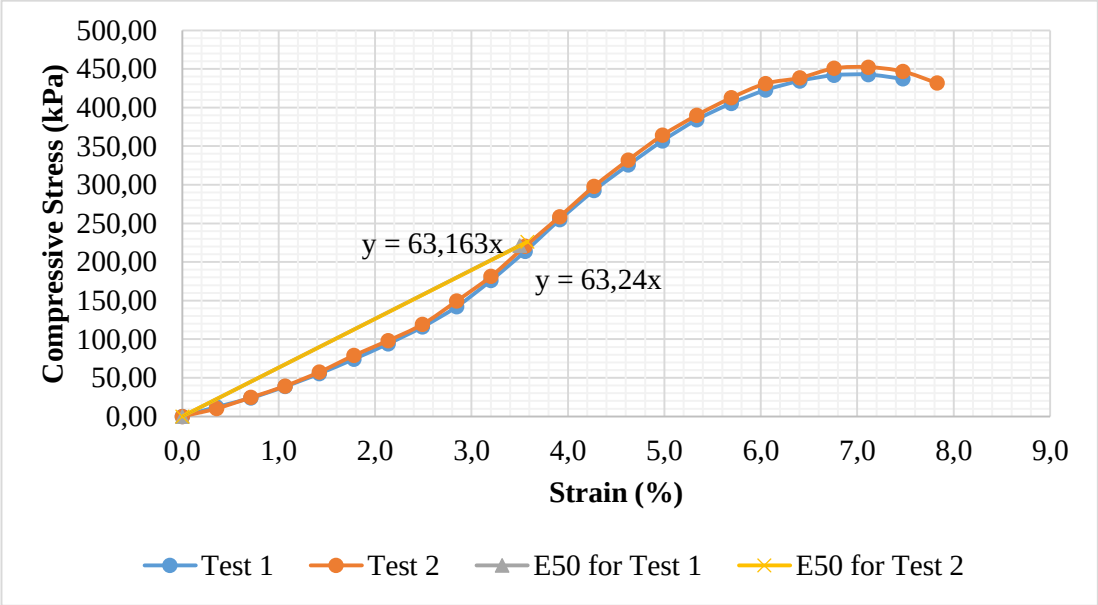

Figure 4.26. Unconfined compression test result for 0% of swell on Sample B

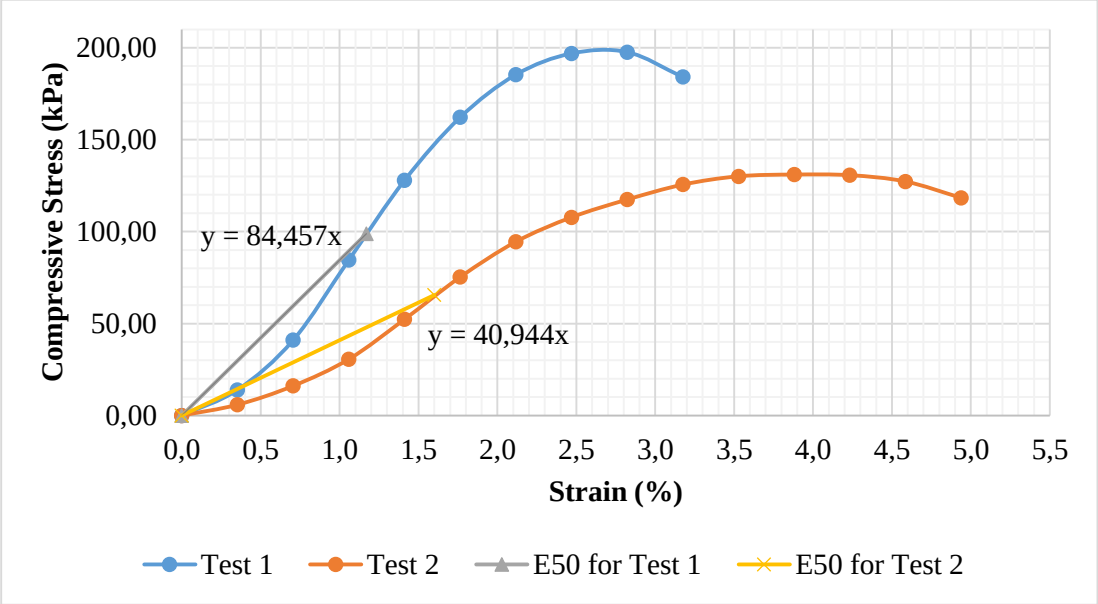

Figure 4.27. Unconfined compression test result for 10% of swell on Sample B

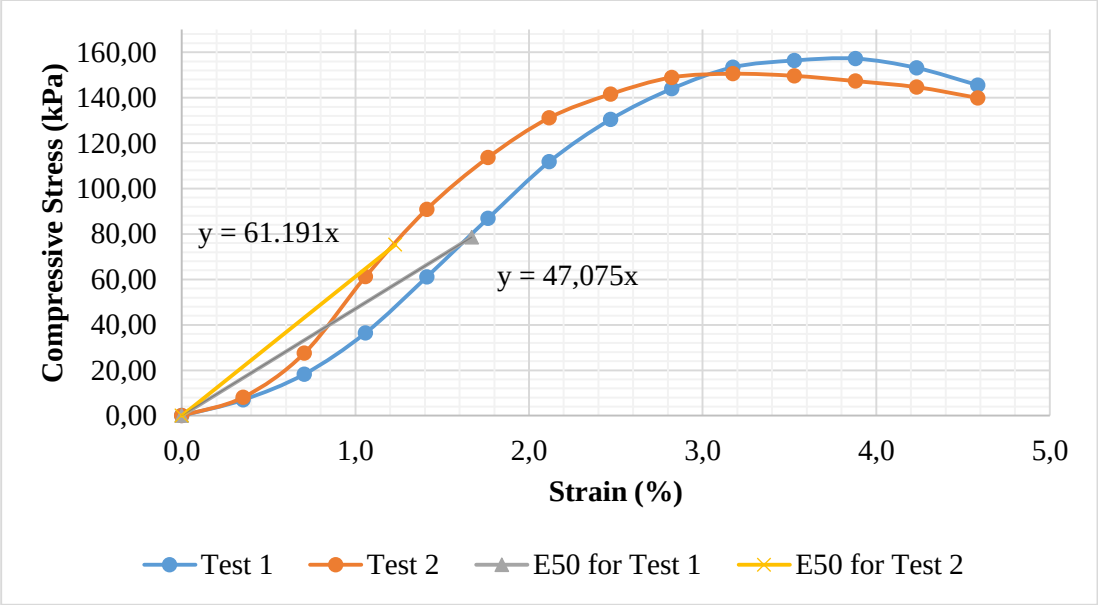

Figure 4.28. Unconfined compression test result for 15% of swell on Sample B

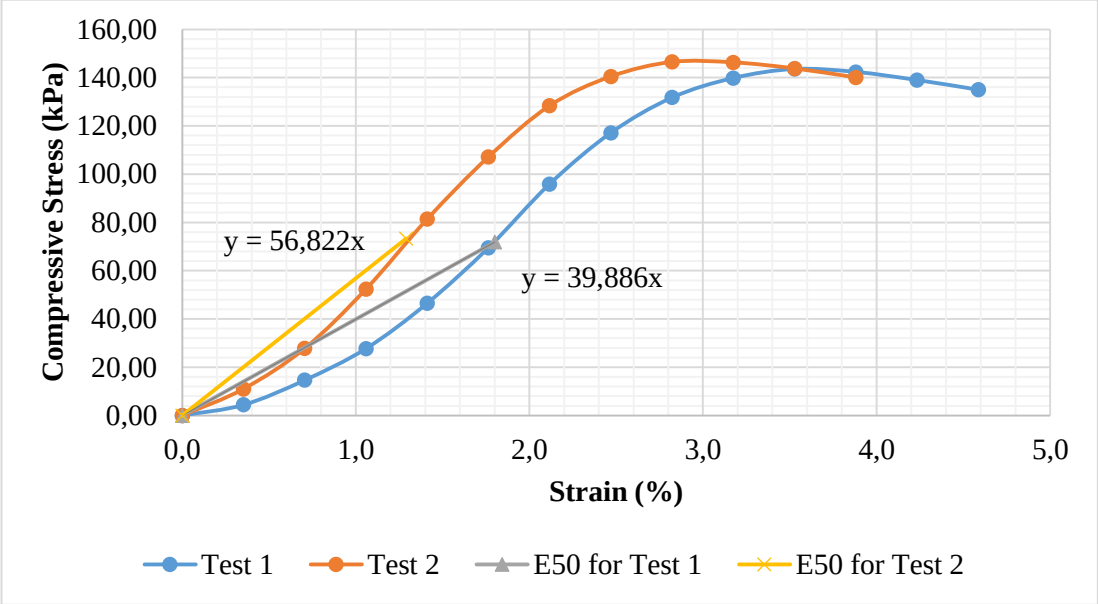

Figure 4.29. Unconfined compression test result for 20% of swell on Sample B

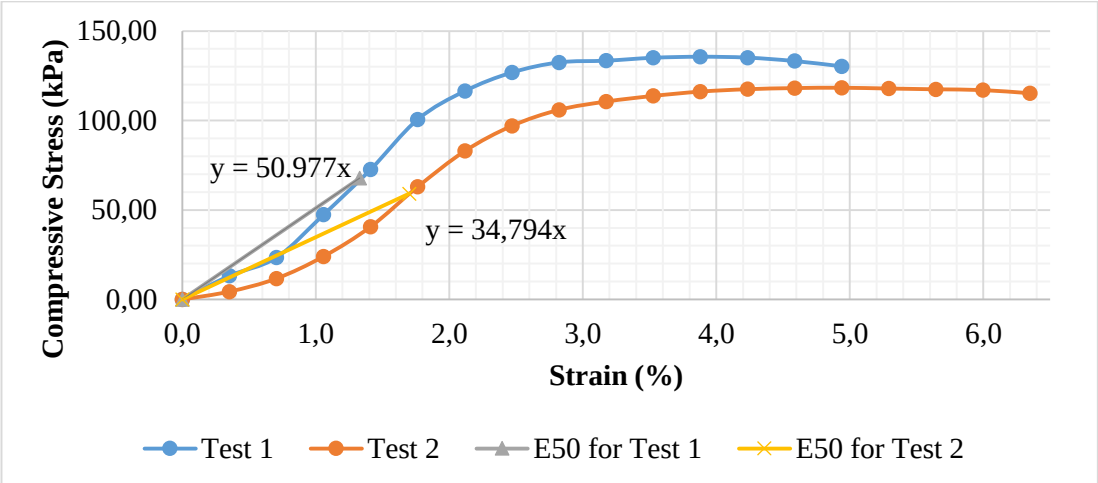

Figure 4.30. Unconfined compression test result for 25% of swell on Sample B

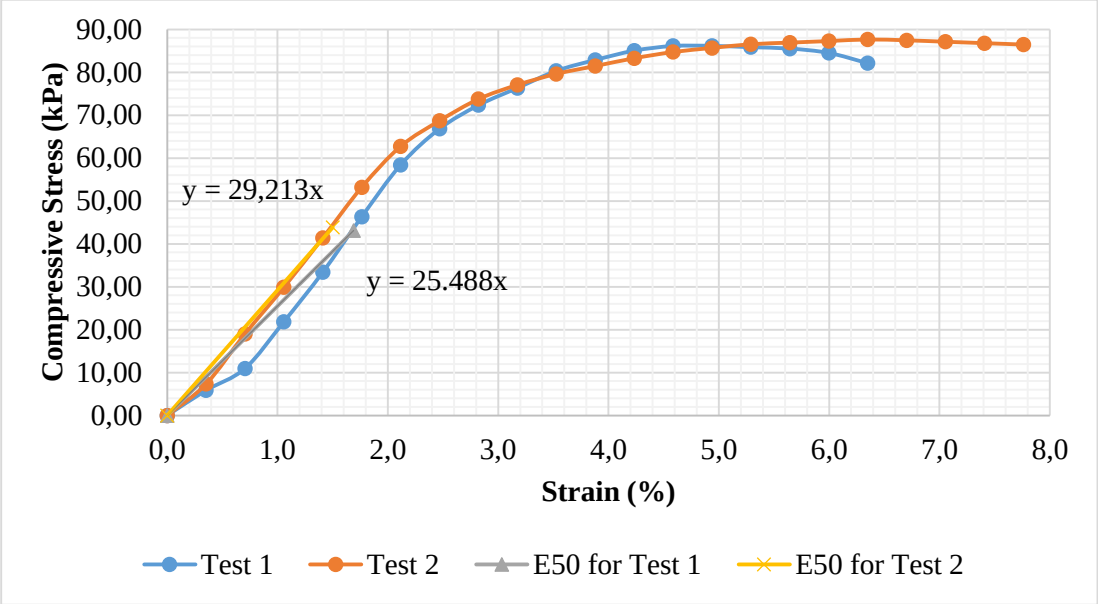

Figure 4.31. Unconfined compression test result for 50% of swell on Sample B

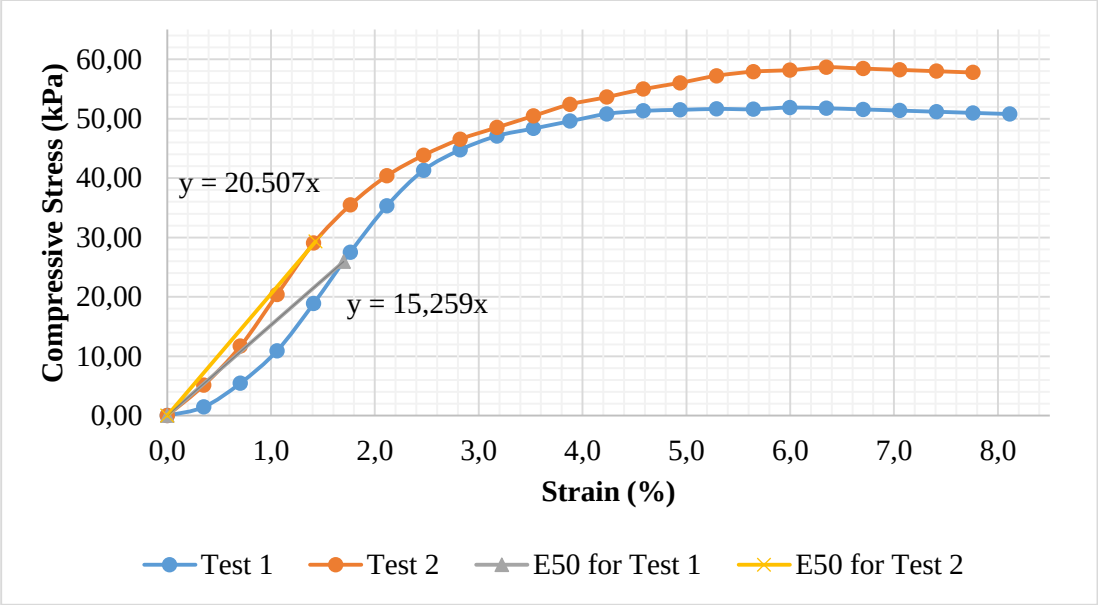

Figure 4.32. Unconfined compression test result for 75% of swell on Sample B

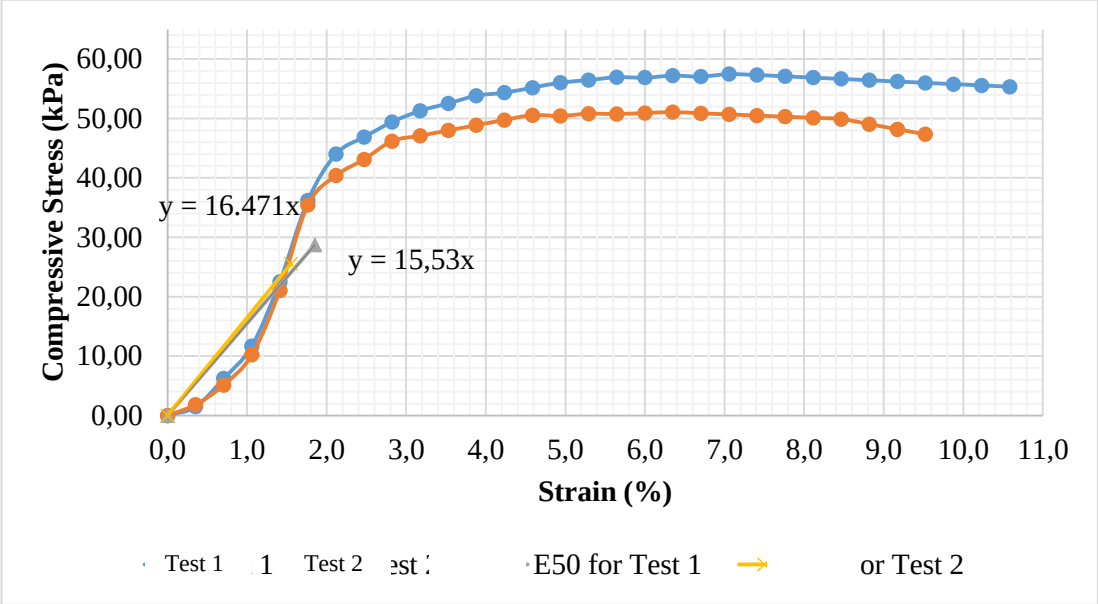

Figure 4.33. Unconfined compression test result for 100% of swell on Sample B

Table 4.10. Summary of unconfined compression test result for Sample B

%Swell	c_u (kPa)	Reduction in c_u* (%) $(c_{u,0\%} - c_{u,\ given\ \%})/c_{u,0\%}$	w %	Reduction in w (%) $(w_{0\%} - w_{given\ \%})/$	E_u (kPa)	Reduction in E_u** (%) $(E_{u,0\%} - E_{u,\ given\ \%})/E_{u,0\%}$
0	223.7	0.0	25.3	1	6320	0.0
10	82.2	63.3	33.8	35	6269	0.8
15	76.9	65.6	36.2	45	5414	14.3
20	72.5	67.6	36.9	48	4836	23.5
25	63.5	71.6	37.1	49	4290	32.1
50	43.4	80.6	40.5	62	2732	56.8
75	27.6	87.6	48.3	93	1786	71.7
100	27.1	87.9	48.7	95	1598	74.7

Water content at which sample is prepared:w_0	=	25

*: Reduction in unconfined compressive strength was same with the one for undrained shear strength.

**: Undrained elastic modulus values were determined with secant method from stress-strain curves.

4.7.3. Unconfined Compression Test Result for Sample O

Stress- strain curves with undrained elastic modulus lines were given in Figures 4.34, 4.35, 4.36, 4.37, 4.38, 4.39, 4.40 and 4.41. Table 4.11 also explicitly puts the results of curves; in other words, undrained shear strength, water content and undrained elastic modulus at aforementioned swell ratios.

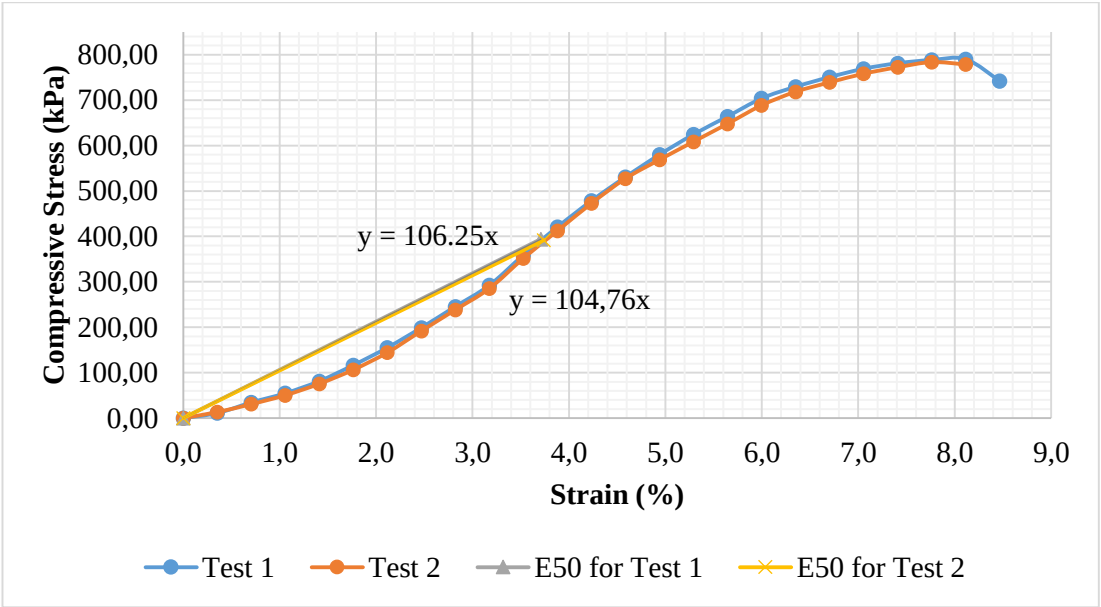

Figure 4.34. Unconfined compression test result for 0% of swell on Sample O

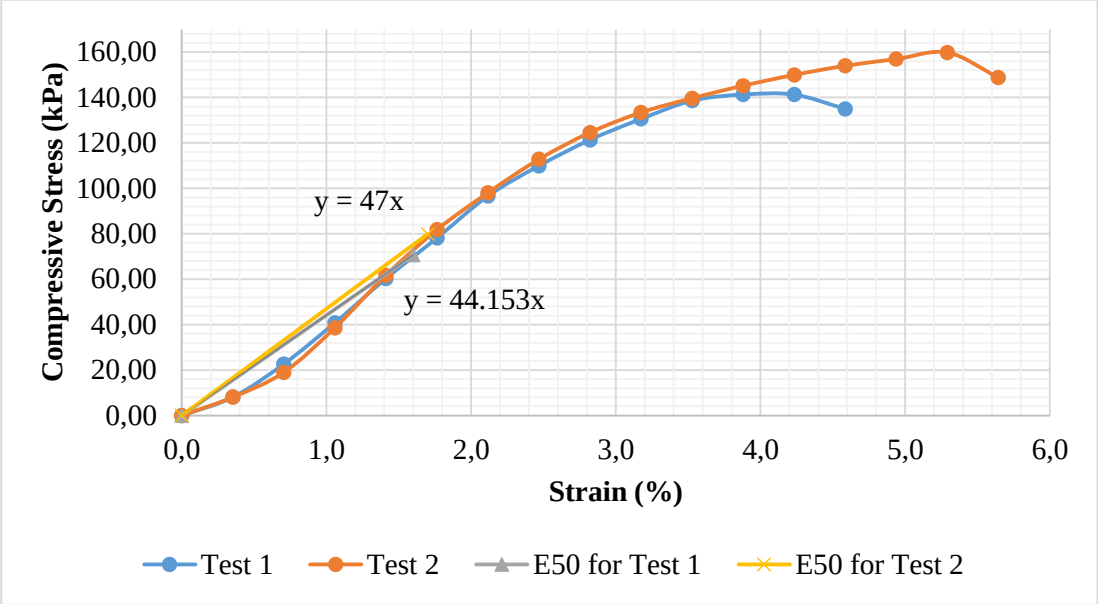

Figure 4.35. Unconfined compression test result for 10% of swell on Sample O

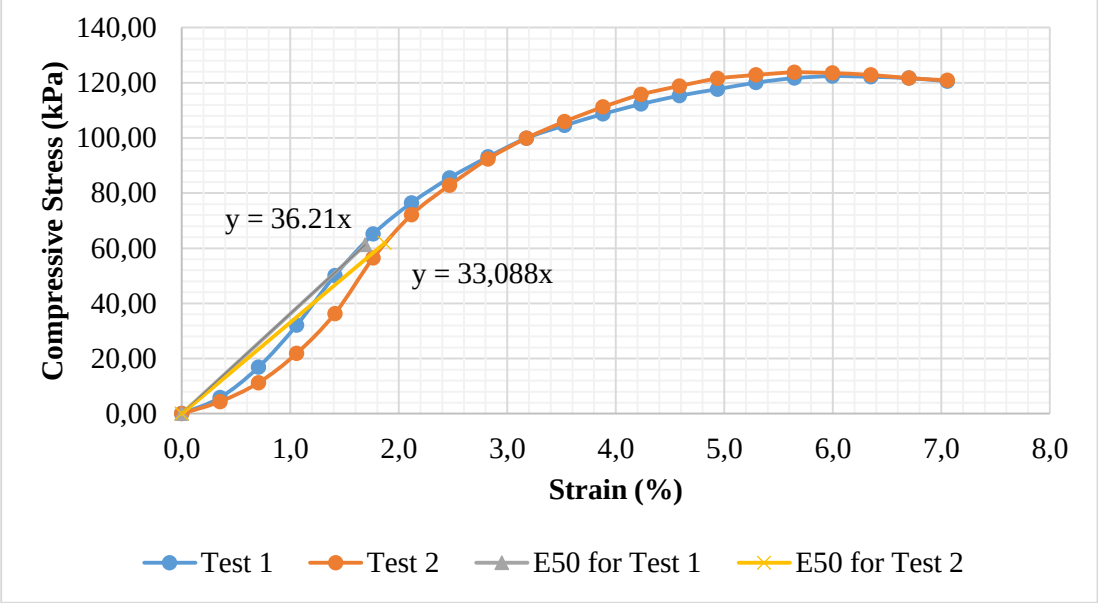

Figure 4.36. Unconfined compression test result for 15% of swell on Sample O

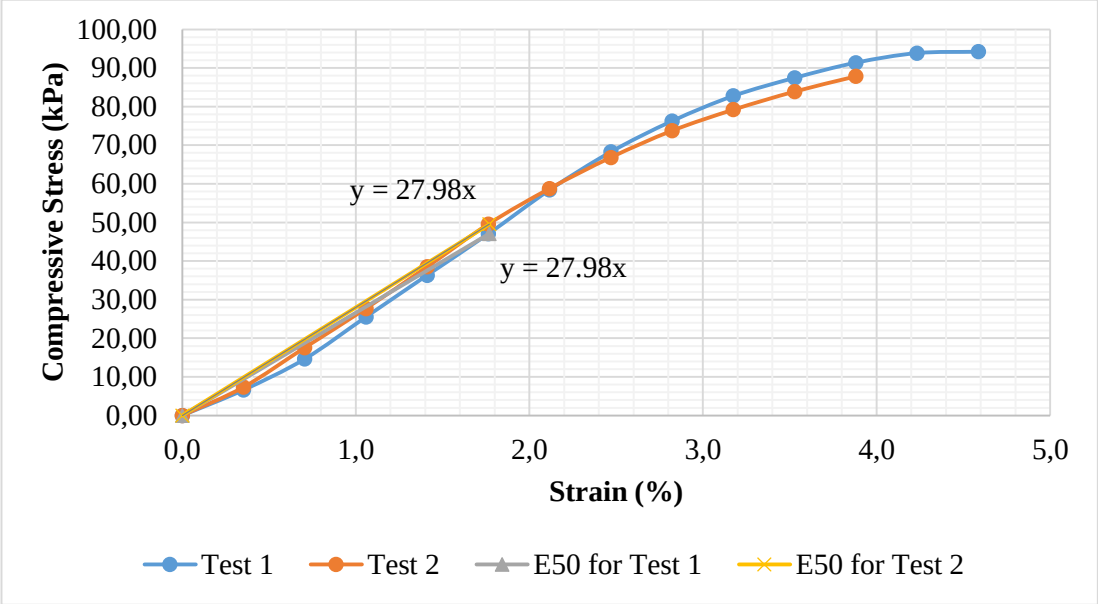

Figure 4.37. Unconfined compression test result for 20% of swell on Sample O

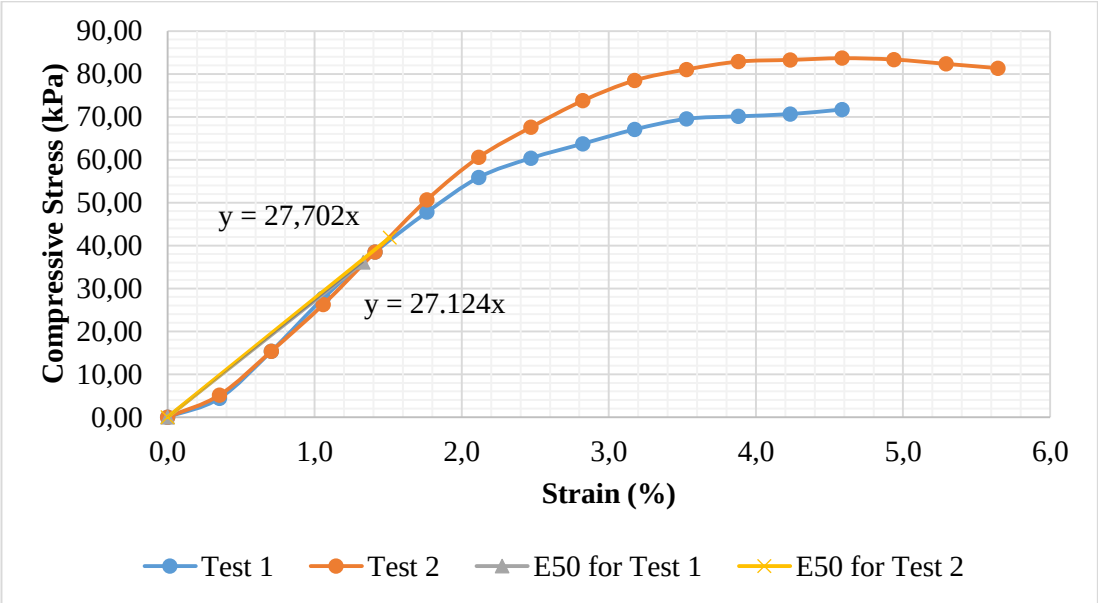

Figure 4.38. Unconfined compression test result for 25% of swell on Sample O

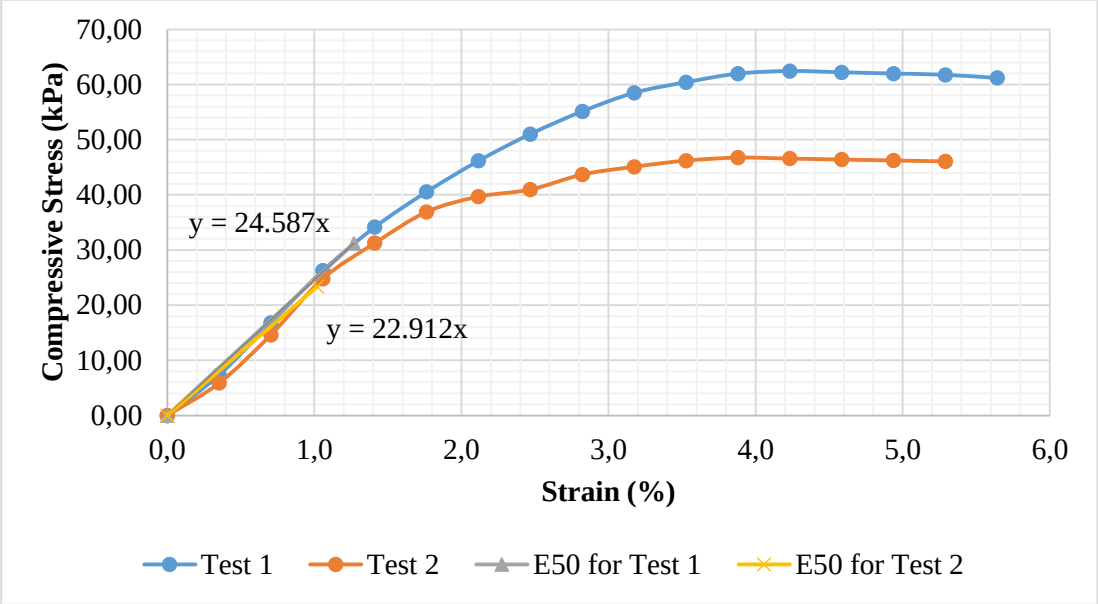

Figure 4.39. Unconfined compression test result for 50% of swell on Sample O

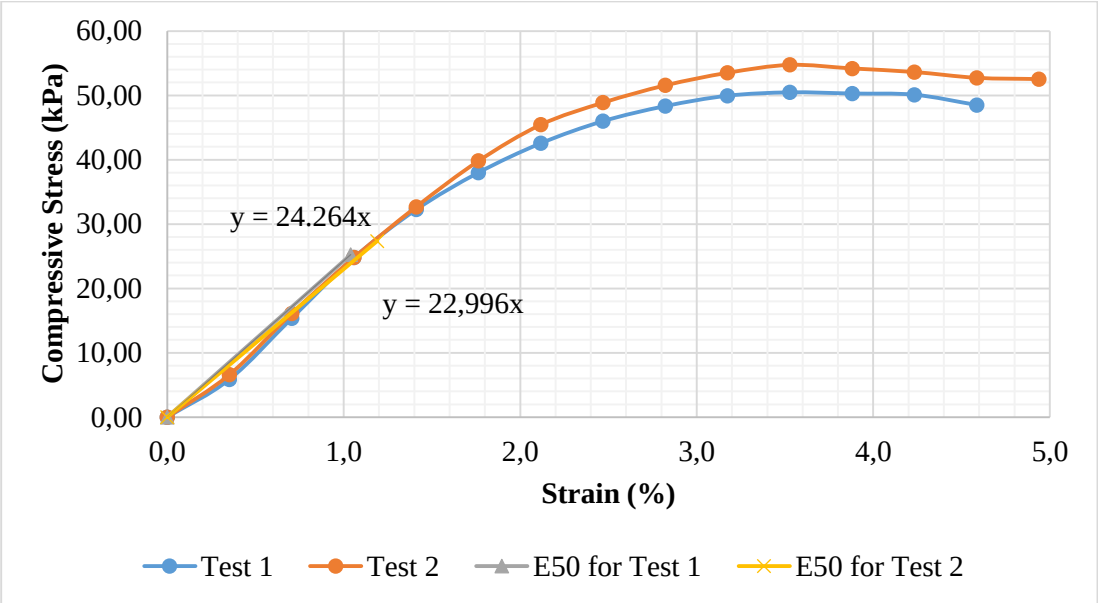

Figure 4.40. Unconfined compression test result for 75% of swell on Sample O

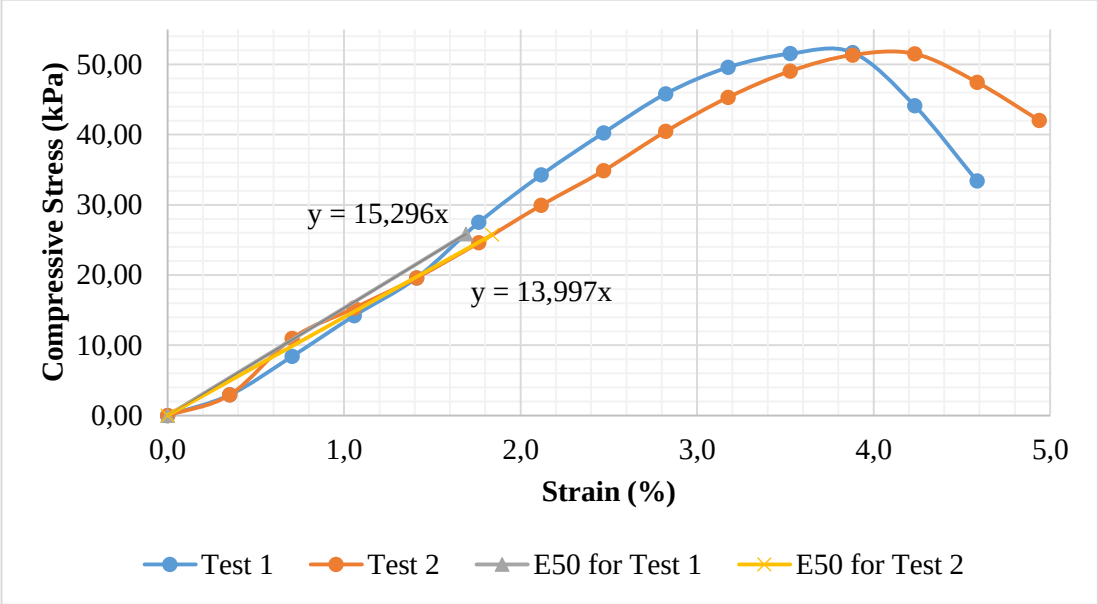

Figure 4.41. Unconfined compression test result for 100% of swell on Sample O

Table 4.11. Summary of unconfined compression test result for Sample O

%Swell	c_u (kPa)	Reduction in c_u* (%) $(c_{u,0\%} - c_{u,\ \text{given}\ \%})/c_{u,0\%}$	w %	Reduction in w (%) $(w_{0\%} - w_{\text{given}\ \%})/$v	E_u* (kPa)	Reduction in E_u** (%) $(E_{u,0\%} - E_{u,\ \text{given}\ \%})/E_{u,0\%}$
0	393.0	0.0	20.6	3	10551	0.0
10	75.3	80.8	26.0	30	4559	56.8
15	61.5	84.3	26.2	31	3466	67.2
20	48.3	87.7	28.4	42	2729	74.1
25	39.0	90.1	28.7	44	2741	74.0
50	27.3	93.1	31.6	58	2375	77.5
75	26.3	93.3	33.4	67	2363	77.6
100	25.8	93.4	34.3	72	1467	86.1

Water content at which sample is prepared:w_0	=	20

*: Reduction in unconfined compressive strength was same with the one for undrained shear strength.

**: Undrained elastic modulus values were determined with secant method from stress-strain curves.

4.7.4. Unconfined Compression Test Result for Sample E

Stress- strain curves with undrained elastic modulus lines were given in Figures 4.42, 4.43, 4.44, 4.45, 4.46, 4.47, 4.48 and 4.49. Table 4.12 also explicitly puts the results of curves; in other words, undrained shear strength, water content and undrained elastic modulus at forementioned swell ratios except for 10% due to faster swell rates.

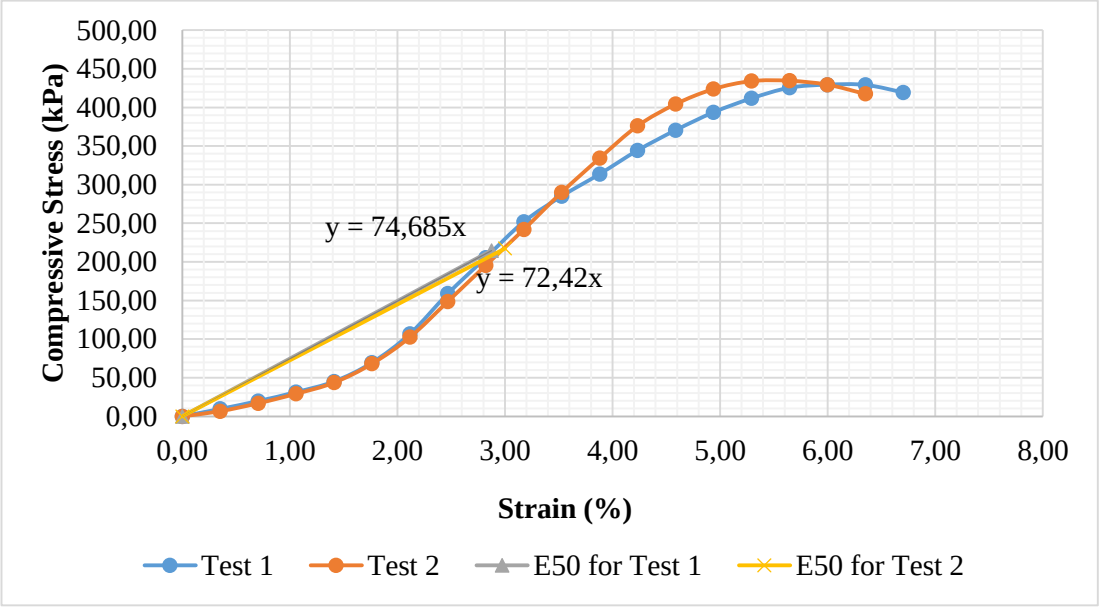

Figure 4.42. Unconfined compression test result for 0% of swell on Sample E

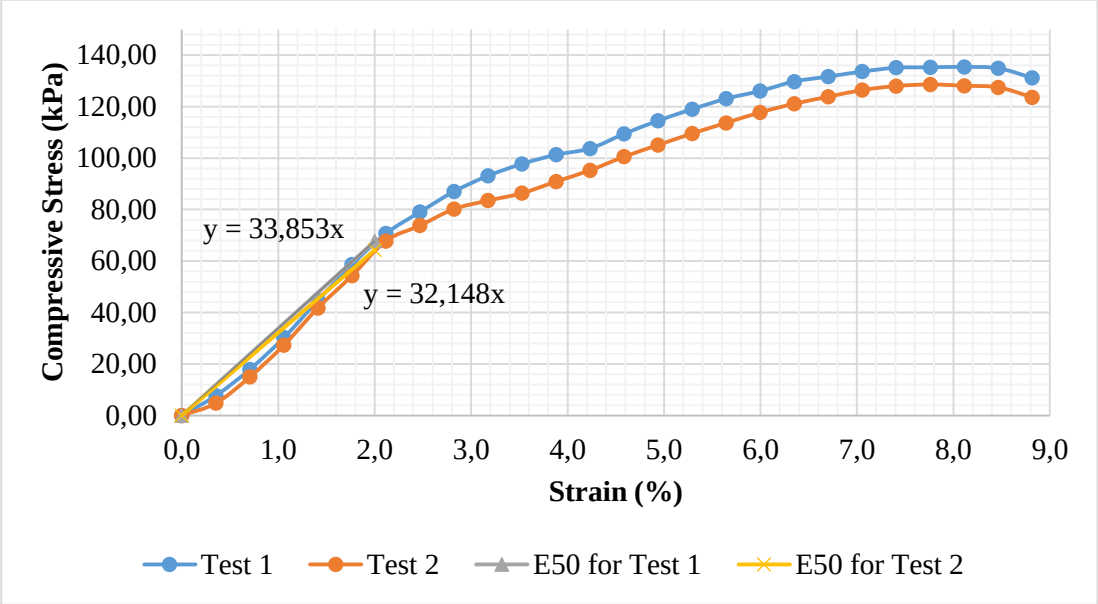

Figure 4.43. Unconfined compression test result for 15% of swell on Sample E

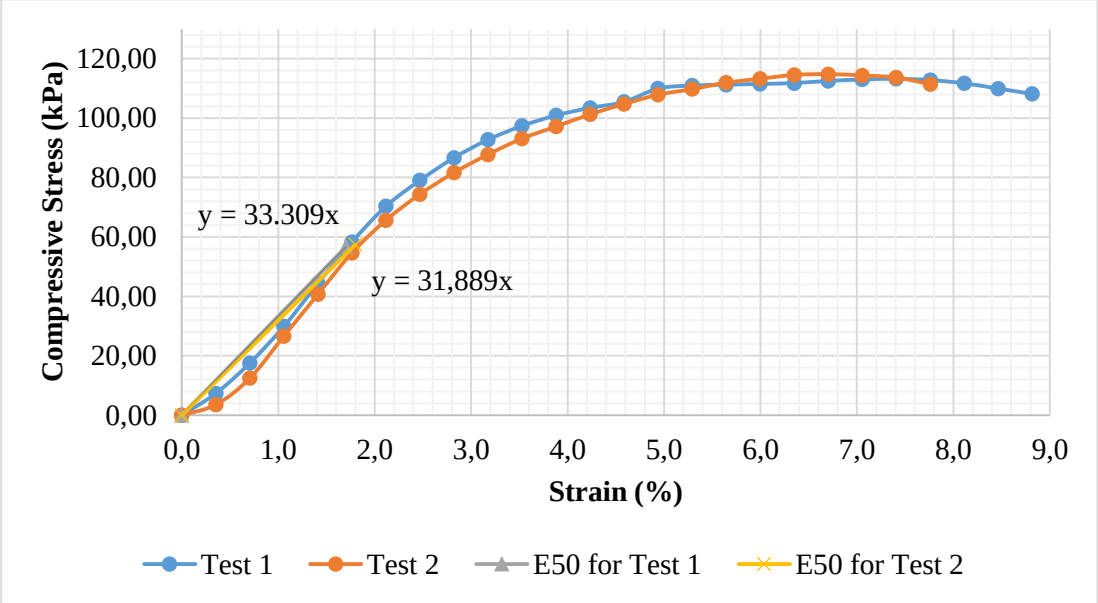

Figure 4.44. Unconfined compression test result for 20% of swell on Sample E

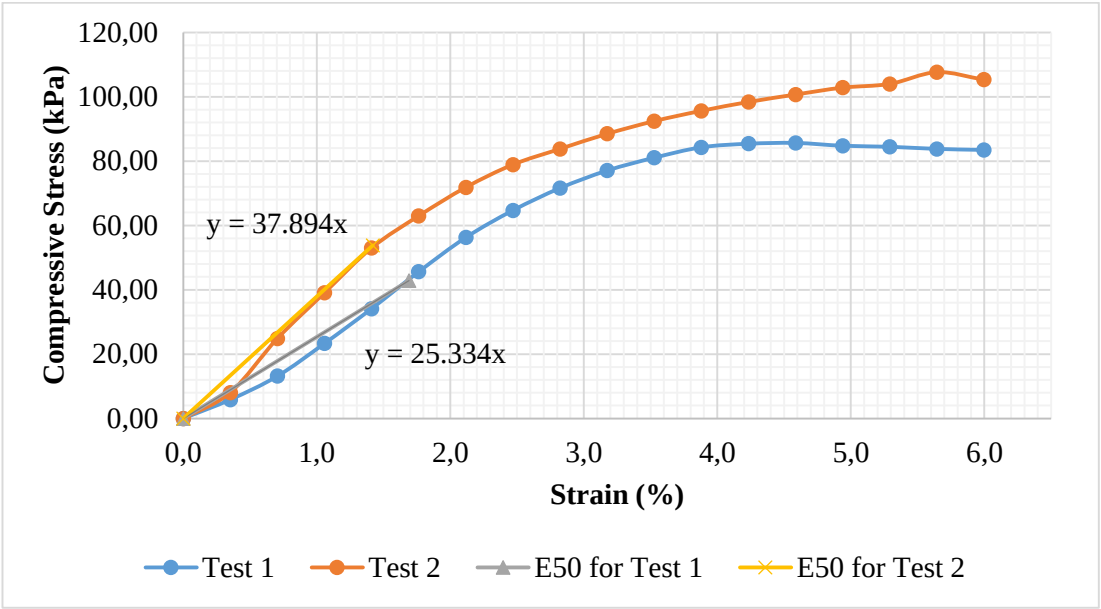

Figure 4.45. Unconfined compression test result for 25% of swell on Sample E

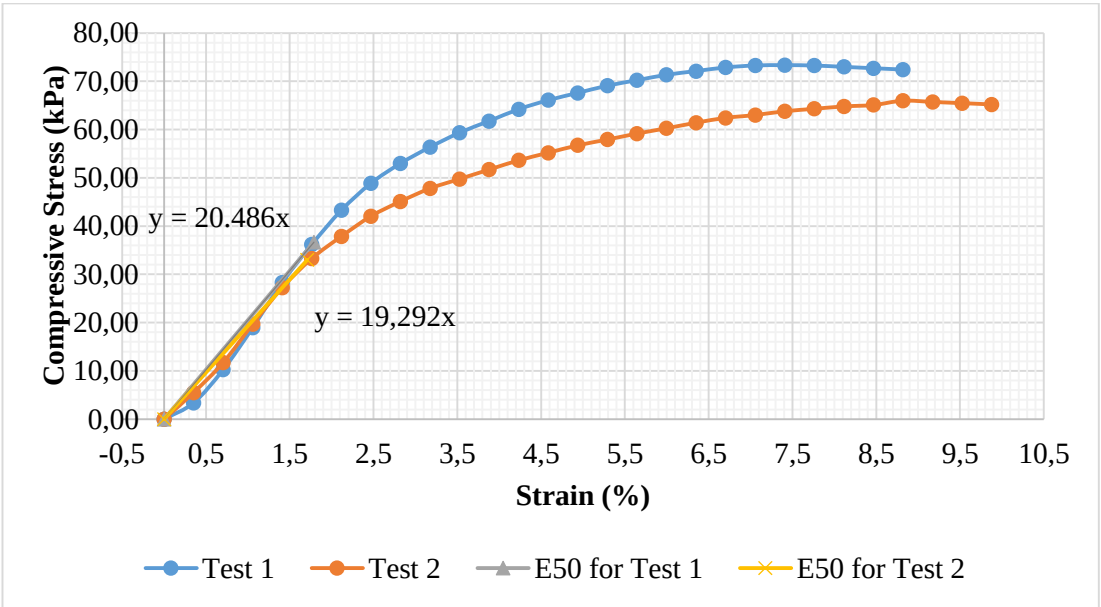

Figure 4.46. Unconfined compression test result for 50% of swell on Sample E

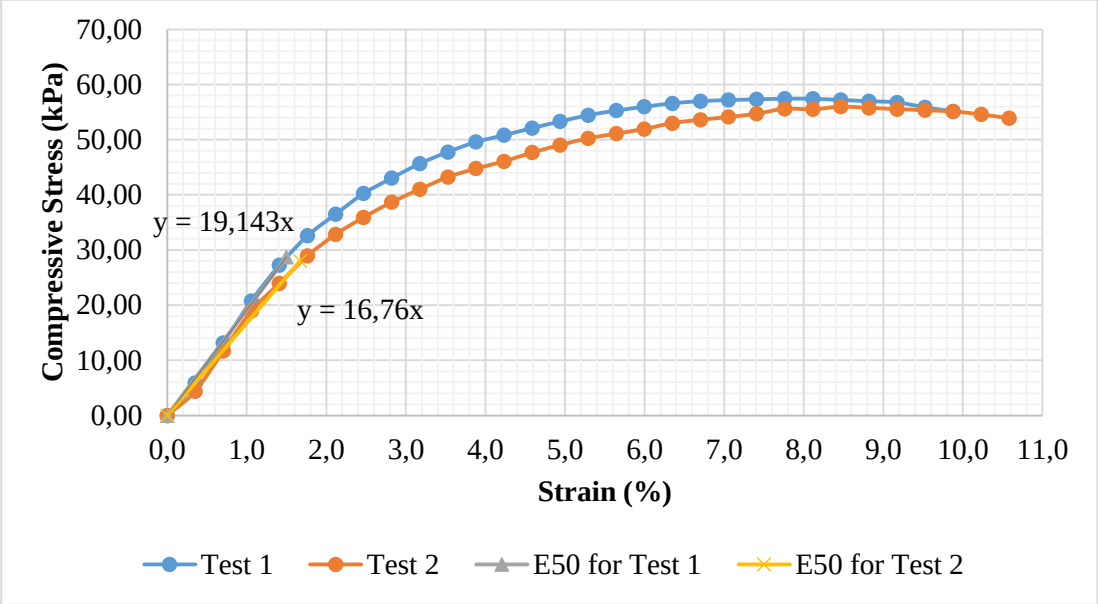

Figure 4.47. Unconfined compression test result for 75% swell

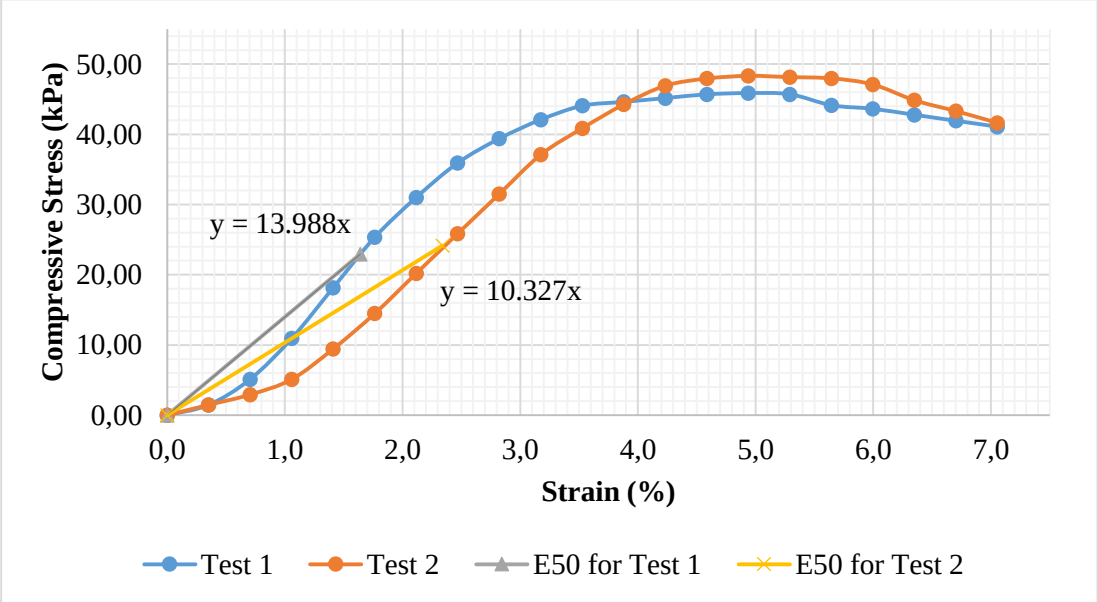

Figure 4.48. Unconfined compression test result for 100% swell

Table 4.12. Summary of unconfined compression test result for Sample E

%Swell	c_u (kPa)	Reduction in c_u* (%) $(c_{u,0\%} - c_{u,\ \text{given}\ \%})/c_{u,0\%}$	w %	Reduction in w (%) $(w_{0\%} - w_{\text{given}\ \%})/v$	E_u* (kPa)	Reduction in E_u** (%) $(E_{u,0\%} - E_{u,\ \text{given}\ \%})/E_{u,0\%}$
0	216.0	0.0	19.0	0	7355	0.0
15	66.0	69.4	26.1	37	3300	55.1
20	57.0	73.6	27.6	46	3259	55.7
25	48.3	77.6	28.4	49	3161	57.0
50	34.8	83.9	31.3	65	1990	72.9
75	28.4	86.9	34.0	79	1795	75.6
100	23.6	89.1	39.5	108	1215	83.5

Water content at which sample is prepared:w_0	=	19

*: Reduction in unconfined compressive strength was same with the one for undrained shear strength.

**: Undrained elastic modulus values were determined with secant method from stress-strain curves.

4.8. Free Swell Index Test

Free swell index test is used for determination of soil expansiveness potential. It is a quick test and so it is preferred for preliminary site investigation. In order to get an idea about expansiveness of soil samples, Free swell index test is performed in compliance with Indian Standard Methods of Test for Soils (IS:2720).

4.8.1. Test Procedure

Oven dried two samples which pass from No.40 Sieve are weighted as 10 grams (g). Then, they are poured into two glass graduated cylinder with 100 ml capacity separately. One of the cylinders is filled with distilled water while the other with kerosene up to 100 ml. After filling the cylinders, entrapped air is removed by stirring with a glass rod and slowly shaking. It is left to rest for at least 24 hours and soil specimen volume is measured. Figure 4.49 shows the resting stage. Thus, percent Free Swell Index: FSI is computed from below correlation given in Eqn 4.4:

$$FSI\ \% = \frac{Vd - Vk}{Vk} * 100 \quad \text{Eqn 4.4}$$

where

V_d= Soil specimen volume read from the graduated cylinder filled with distilled water

V_k= Soil specimen volume read from the graduated cylinder filled with kerosene/ gas oil.

As stated in the standard, in the case of existence of highly expansive soil, Sample A in this case, graduated cylinder with 250 ml capacity was used instead of 100 mm capacity cylinder.

Figure 4.49. Free swell index test at resting stage

4.8.2. Test Results

Free swell index test results were summarized and compared with each other in Figure 4.50.

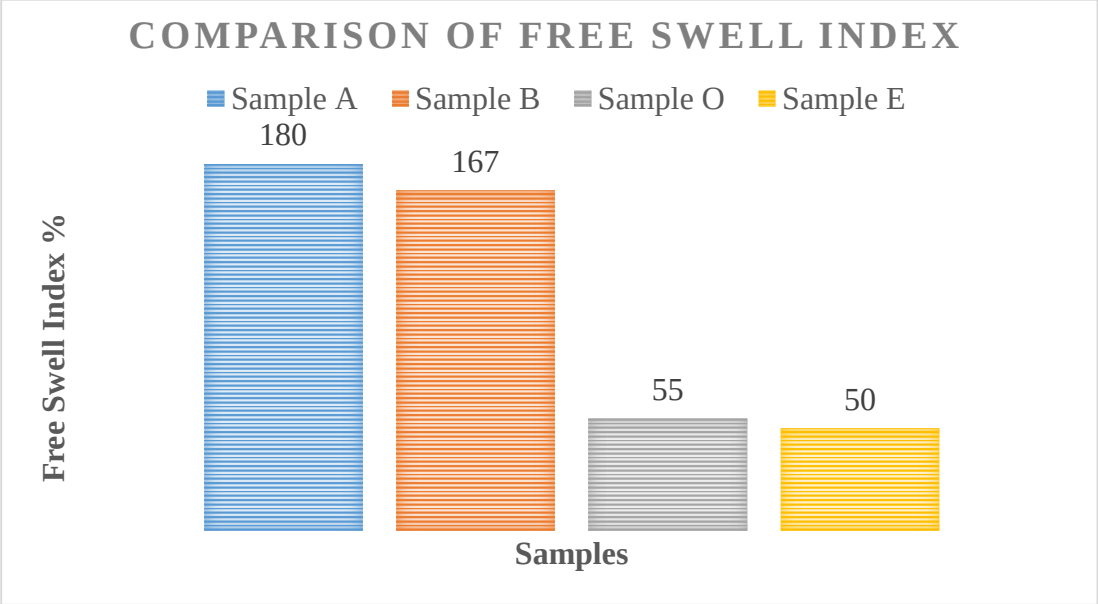

Figure 4.50. Comparison of free swell index values of samples

When values obtained from free swell index test were compared with the results obtained from swelling in molds, they gave same conclusion. Swelling potential of samples is as follows: Sample A> Sample B> Sample O> Sample E. In addition, Table 4.13 from Bureau of Indian Standards (Sridharan and K. Prakash, 2000), helps the classification of samples with respect to FSI. Based on Table 4.13, it can be said that Sample O and E have medium swelling potential whereas Sample A and B have high expansiveness.

Table 4.13. Expansivity potential of soil with respect to FSI (Sridharan and Prakash, 2000)

Degree of Expansion	**Free Swell Index %**
Low	<50
Medium	50-100
High	100-200
Very High	>200

As specified in the same article, the procedure mentioned in IS: 2720 can underestimate the swelling potential of montmorillonite and so bentonite in kaolinite rich soils. Therefore, below solution in Eqn 4.5 is suggested:

Modified Free Swell Index: $MFSI = \frac{V_d}{10}$……...……. Eqn 4.5

where

V_d= The soil specimen volume which is poured into graduated cylinder and allowed to settle down in distilled water

With the formula in Eqn 4.5, MFSI for Sample A was found as 7 and when compared with the ones in Table 4.14, Sample A was evaluated as very high swelling clay. Classification in Table 4.14 includes the use of carbon tetrachloride; however, Sivapullaiah (1987) et al. stated that kerosene or carbon tetrachloride could be used to prevent swelling of soil in free swell index test. Therefore, it was thought that classification of Sample A, in which kerosene was used, could be made according to Table 4.14.

Table 4.14. Classification of soil swelling according to MFSI (Sridharan and Prakash, 2000)

MFSI (cm^3/g)	**Sediment volume in carbon tetrachloride (cm^3/g)**	**Clay Type**	**Soil Expansivity**
<1.5	1.10-3.00	Non-swelling	Negligible
1.5-2.0	>1.1 and <MSFI	Mixture of swelling and non-swelling	Low
1.5-2.0	≤1.1	Swelling	Moderate
2.0-4.0	≤1.1	Swelling	High
>4.0	≤1.1	Swelling	Very high

4.9. Methylene Blue Test

Methylene Blue test can be done in order to determine the activity of clay can be performed according to ASTM C837 (American Society for Testing Materials) or NF P 94- 068 (The Association Fraçaise de Normalization). For this study NF P 94-068 was followed. The main principle of the test is the exchange of cations in methylene blue solution with active clay cations since cation exchange capacity is directly related to the specific surface area of clay due to anions on the clay surface. Test is very quick and gives idea about cation exchange capacity, swell potential, index properties and specific surface area. This procedure is as follows.

4.9.1. Test Procedure

10∓1 grams (g) Methylene Blue powder is mixed for 45-60 minutes (min) in 1 liter distilled water at room temperature with mixer that has 400 rpm (revolutions per minute) speed. Then, oven dried soil specimen which pass from No. 40 sieve are taken to be 30 to 60 g for clayey or excessively clayey soils and 60 to 120 g for less clayey soils. Taken soil specimens are mixed in distilled water with mixer so that they can have 0.15 sample/water ratio; for instance, 30 g specimen is mixed with 200 ml distilled water. Mixer runs for 5 min with 700 rpm speed. This speed remains constant until the end of test. A nozzle to measure 2 or 5 milliliter (ml) Methylene Blue (MB) solution is utilized from this stage of the test. 5 ml of MB solution is added to specimen-distilled water mixture and final product is mixed for about 1 to 2 min. A drop is left on No. 10 filter paper. A dark blue spot occurs on the paper. Until a light blue halo surrounding a dark blue spot is seen on the paper, MB solution of 5 ml is continued to be added to soil-water mixture. When the light blue halo, whose thickness is approximately 1 mm is observed, mixture is checked at 1 min intervals with 5 drops. If light blue halo disappears in one of the drops, then test goes on with MB solution of 2 ml by following the same procedure. Below Figure 4.51 explicitly shows the steps of Methylene Blue test:

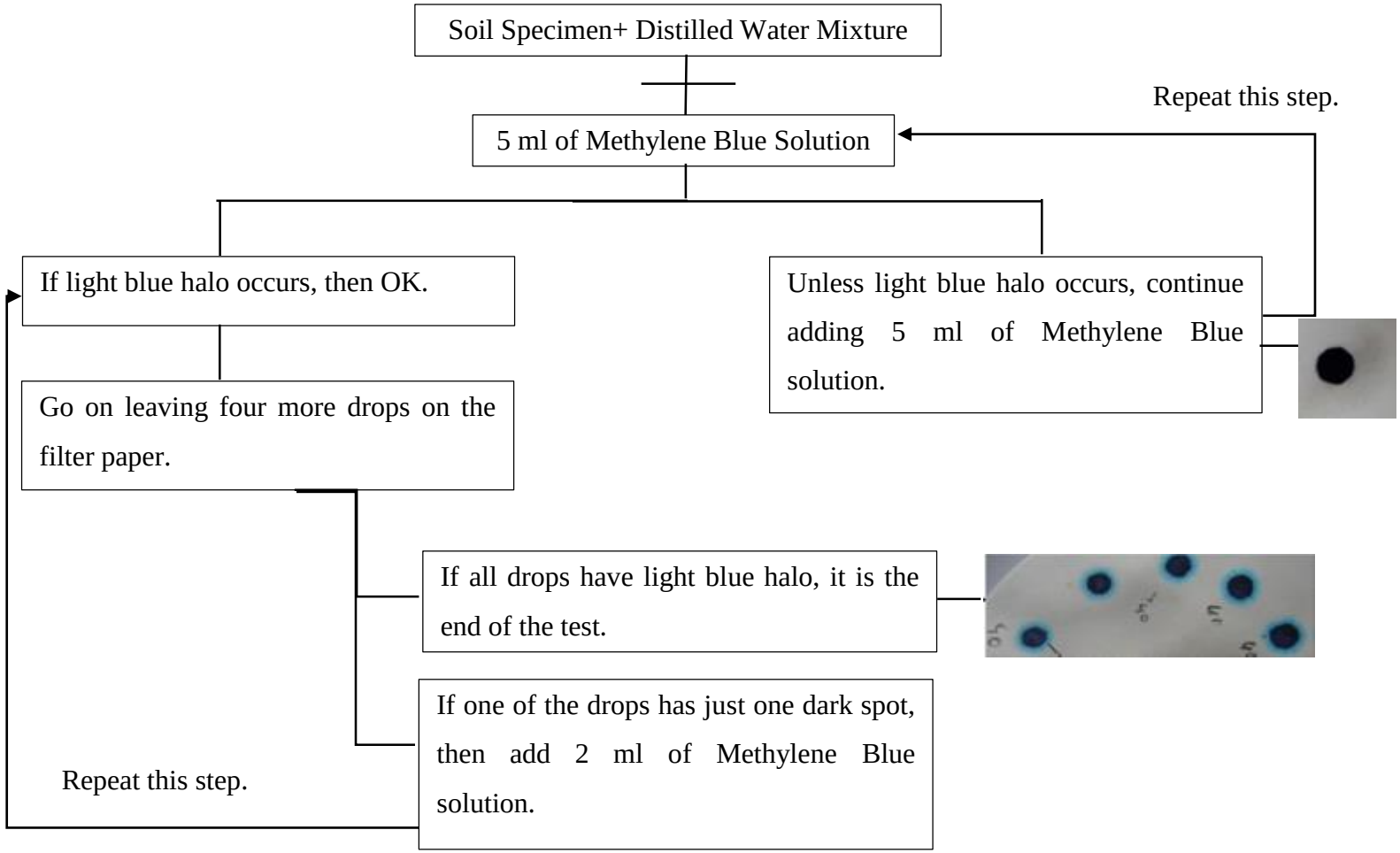

Figure 4.51. Summary of methylene blue test procedure

Once the test is finalized, Methylene Blue Value: MBV is calculated by using below formula in Eqn 4.6:

$$MBV\ (g/100\ g) = V_{cc}\ (ml) / f'(g) \quad \text{Eqn 4.6}$$

where

V_{cc}= Volume of Methylene Blue solution injected to the sample solution

f'= Sample dry weight that is determined at the beginning of the test.

4.9.2. Test Results

Methylene Blue values of samples and their comparison can be found in Figure 4.52.

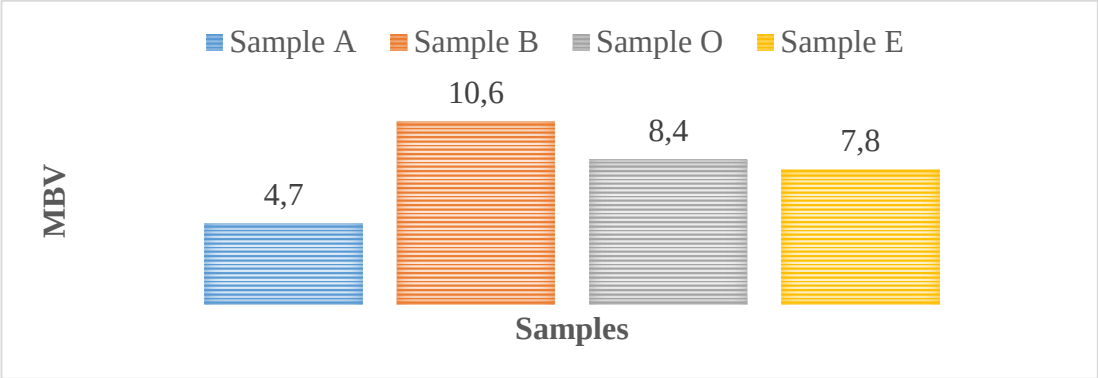

Figure 4.52. Comparison of methylene blue values of samples

According to MBV of samples, expansiveness ascending sequence is as follows: Sample B> Sample O> Sample E> Sample A. Sample A has the lowest MBV although it has the highest swelling potential according to free swell index test and tests made with molds. The reason behind this result may be due to existence of some chemicals, variability in clay minerals and fast downfall of natural soil particles. Therefore, comparison between natural and artificial soil samples does not give a realistic result.

4.10. Swell Pressure Relation with Soil Expansiveness

Swell pressure tests were performed on compacted soil specimens at water contents given in Table 4.6. Tests were made in accordance with ASTM D4546. Figure 4.53 shows the test setup. Soil specimen preparation was nearly same with the one which was explained in Figure 4.10. The differences between them was the aimed height and volume as well as the molds where specimens were compacted. Therefore, bulk weight calculations, which was given in Eqn. 4.2, were revised according to 0.0019 m height and 6.02×10^{-5} m^3 volume of consolidometer ring. Plastic rods that were used for specimen compaction in consolidometer rings are given in Figure 4.54. In addition, specimens were compacted directly into consolidometer rings.

Figure 4.53. Swell pressure test setup

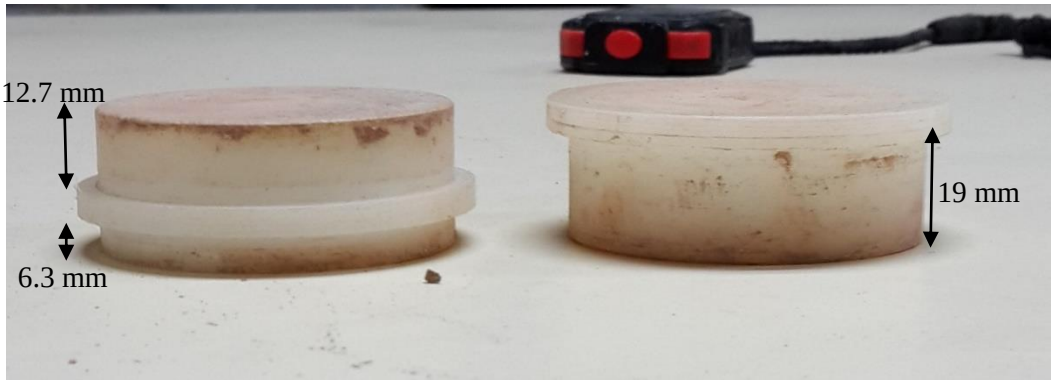

Figure 4.54. Plastic rods used for specimen compaction in swell pressure test

When Figure 4.55 which helps to compare the swell pressure values of samples was investigated, it was realized that as the swell potential of soil increased, swell pressure also increased. Actually when the definition of swelling pressure, which is the pressure necessary to keep a soil element at constant volume without any volume increase, was taken into consideration, results made sense.

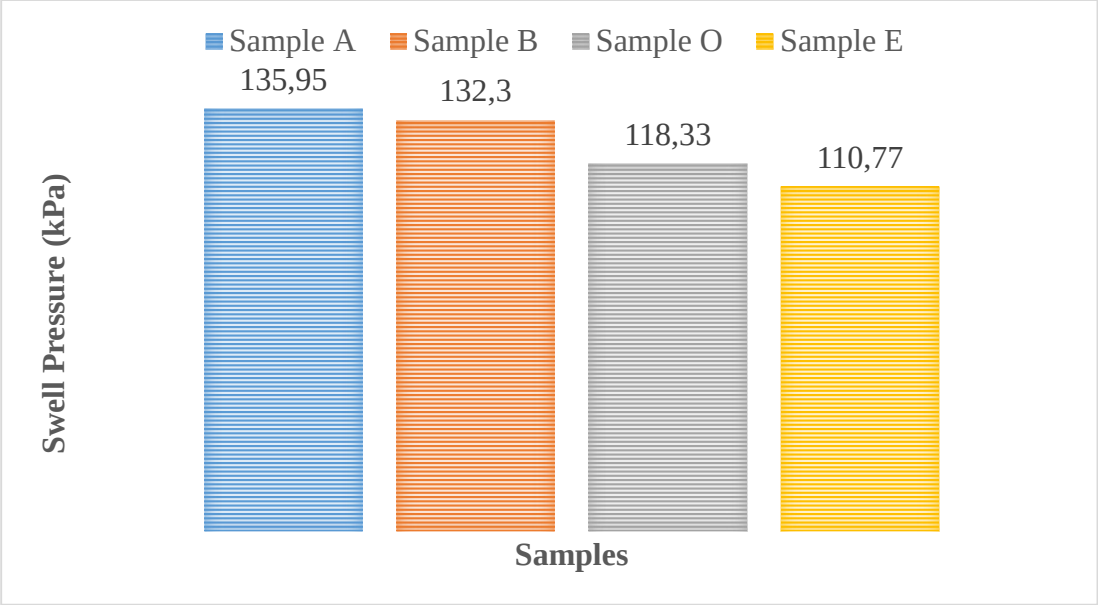

Figure 4.55. Comparison of swell pressure values of samples

4.11. Estimation of Frictional Stress

A frictional force develops between soil specimen and plastic mold during swelling in the volume constraint molds. In order to compute this frictional force and so frictional stress, it was assumed that at the time of sample movement, frictional force would be equal to the applied force to give this movement since soil specimen particles would directly transmit applied force to the lateral surface. Therefore, soil specimens were prepared as mentioned in Figure 4.10 as the first step. For the specimens that were allowed to swell to ultimate level, specimens were submerged in water and waited. When the swelling stopped, porous stones were removed. Meanwhile, this step was skipped for the specimens which would be tested for 0% of swell. Then, needed force was determined with unconfined compression test setup by applying the load to the plastic rod which was mentioned in Step 7 of Figure 4.10. At the force that gave this rod a movement was accepted as the frictional force. Figure 4.56 shows the sketch and photo of the test setup.

After frictional force was determined with this method, frictional stress: σ_f on net lateral surface area: $A_{net,side}$ due to developed frictional force: F_f was calculated by using Eqn. 4.7.

$$\sigma_f = \frac{F_f}{A_{net,side}} \quad \text{.....Eqn 4.7}$$

where

F_f= Frictional force which is equal to the applied force

$A_{net,side}$= (Lateral surface area corresponding to the swelled sample height)- (Area of perforations*154)

Area of perforation= $\Pi * d^2/ 4 = \Pi * 0.002^2/ 4 = 3.142 \times 10^{-6}$ m^2

Thus, total perforation area for 154 ones was found as 4.838×10^{-4} m^2. Table 4.15 presents calculation steps and comparison of swell pressure with formed frictional stress between mold and soil specimen at 0% and 100% of swell. As can be seen from Table 4.15, a frictional stress aroused between soil samples and mold

lateral surface, which was coincided with approximately 16.5-25% of swell pressure for 0% and 100% of swell (For the application of the frictional stress, see Appendix G).

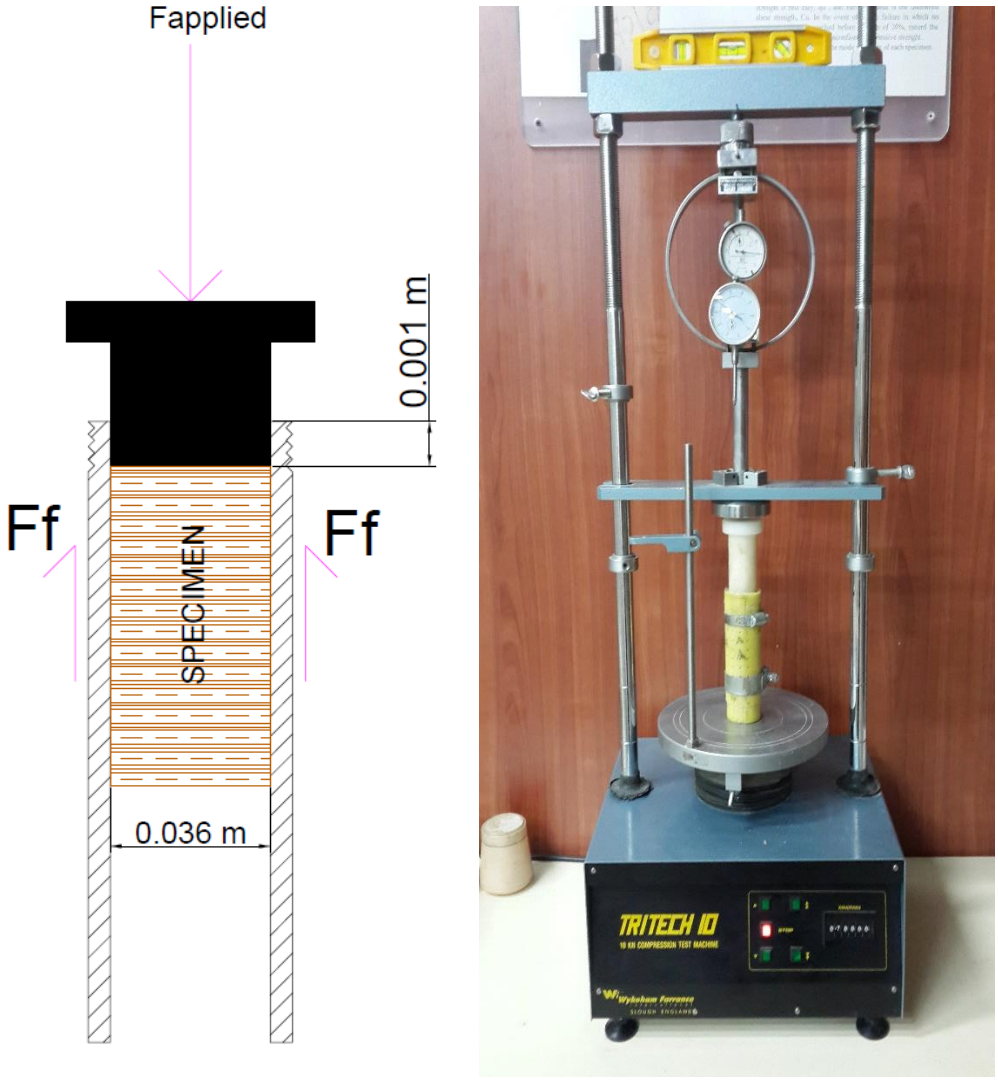

(a) (b)

Figure 4.56. (a) Sketch of test setup to determine frictional force, (b) Photo of test setup to find frictional force

Table 4.15. Calculation steps of frictional stress and comparison of frictional stress with swell pressure at 0% and 100% of swell

	100% of Swell							0% of Swell				
Sample Type	**Swelled Sample Height (m)**	**Lateral Surface Area (m^2)**	**Net Lateral Surface Area (m^2)**	**Applied Force: $F_{applied}$ (kN)**	**Frictional Stress: σ_f (kPa)**	**Swell Pressure: P_s (kPa)**	**Ratio of σ_f to P_s %**	**Net Lateral Surface Area (m^2)**	**Applied Force: $F_{applied}$ (kN)**	**Frictional Stress: σ_f (kPa)**	**Swell Pressure: Ps (kPa)**	**Ratio of σf to Ps %**
Sample A	0.088	0.0100	0.0095	0.25575	27.01	135.95	19.9	0.0077	0.2058	26.87	135.95	19.8
Sample B	0.076	0.0087	0.0082	0.2385	29.20	132.3	22.1	0.0077	0.1667	21.77	132.30	16.5
Sample O	0.075	0.0085	0.0080	0.231	28.73	118.33	24.3	0.0077	0.1603	20.93	118.33	17.7
Sample E	0.074	0.0084	0.0079	0.225375	28.41	110.77	25.6	0.0077	0.1469	19.18	110.77	17.3

CHAPTER 5

DISCUSSION OF TEST RESULTS

5.1. Relation between Unconfined Compressive Strength and % Swell

As can be seen from Figures 5.1, 5.2, 5.3 and 5.4, increase in the water contents of soil samples caused decrease in the unconfined compressive strength. Considering the swelling potential of samples, the shape of the logarithmic unconfined compressive strength versus % swell graphs for Sample A and Sample B demonstrated a smooth decrease in unconfined compressive strength values with increase in water content. On the other hand, logarithmic relation between unconfined compressive strength with % swell for Sample O and Sample E, which have lower swelling potential, showed a sudden decrease upon wetting to 10% of swell. Then, downward trend for these samples slowly continued.

Mathematical expression of unconfined compressive strength versus % swell relation for Sample A, B, O and E is also given on Figures 5.1, 5.2, 5.3 and 5.4 respectively by adding trendline in Excel software. When these relationships were analyzed with several functions such as linear, exponential and polynomial functions, it was seen that exponential function was suitable for artificial soil sample; i.e., Sample A, which has the highest swelling potential. On the other hand, the best fitted function for Sample B, Sample O and Sample E. was polynomial function. High value of coefficient of determination, R^2 was the decisive factor on the type of regression.

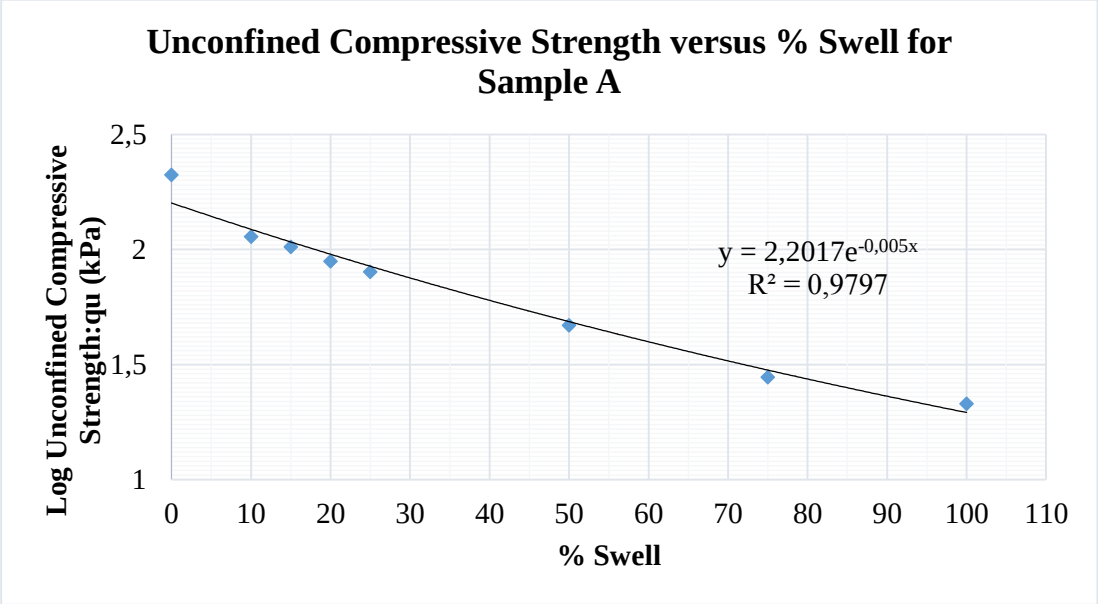

Figure 5.1. Unconfined compressive strength versus % swell for Sample A

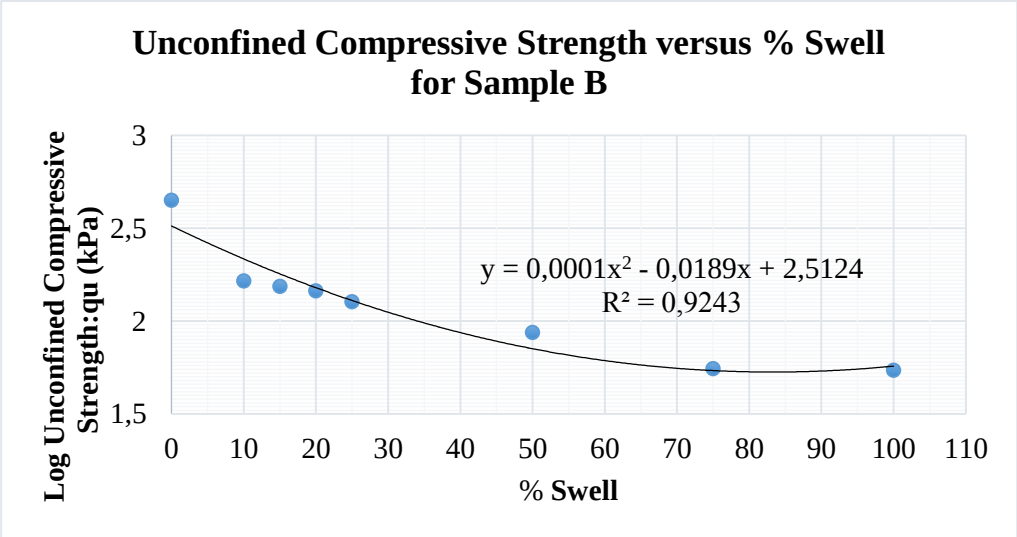

Figure 5.2. Unconfined compressive strength versus % swell for Sample B

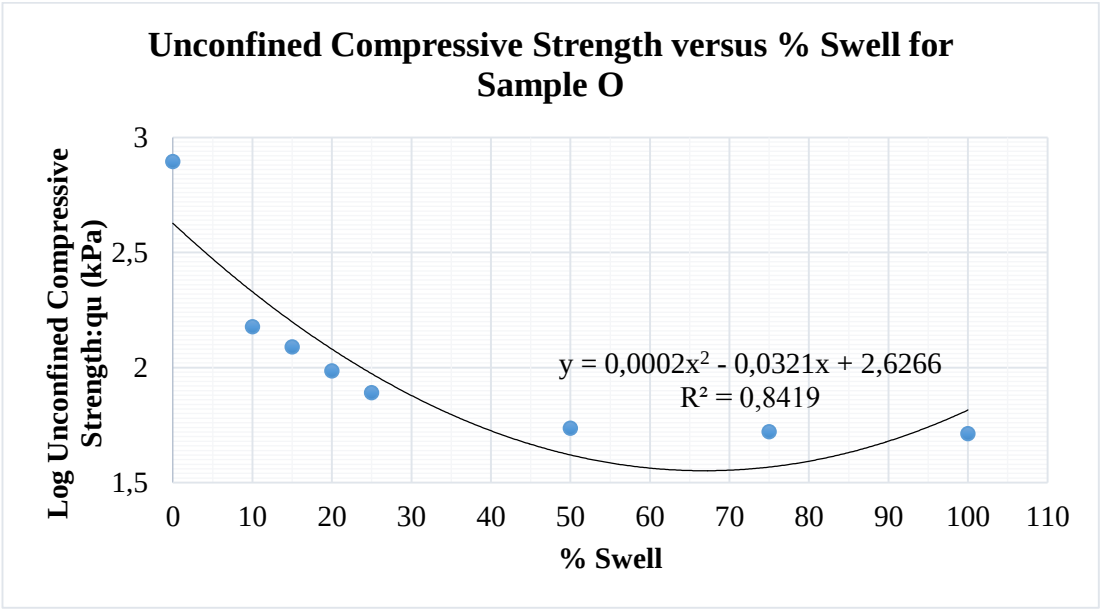

Figure 5.3. Unconfined compressive strength versus % swell for Sample O

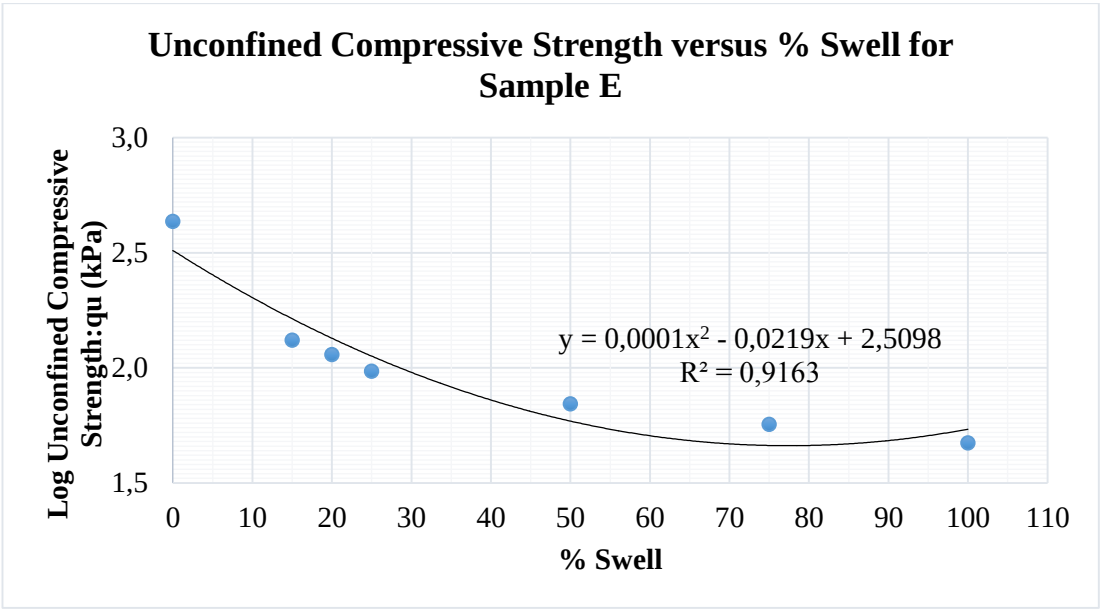

Figure 5.4. Unconfined compressive strength versus % swell for Sample E

When one general equation showing the correlation among unconfined compressive strength and % swell for all soil samples was wanted to be obtained, single variable nonlinear regression analysis at 95% confidence level was conducted. As the result of this analysis, regression equation given in Eqn. 5.1 were obtained with R^2= 0.80. Additionally, in Figures 5.5 and 5.6, validation of regression models was checked. As can be seen from Figure 5.5 experimental points were located very close to the curve got from regression equation, Eqn. 5.1. This situation can also be verified from Figure 5.6 since scatter of data points largely followed a linear trend.

$$\frac{\log q_{u \text{ at } x\% \text{ of swell}}}{\log q_{u \text{ at } 0\% \text{ swell}}} = 5.21x10^{-5}*x^2-0.008*x+0.944 \quad \text{.....Eqn 5.1}$$

where

x= Swell percent (%)

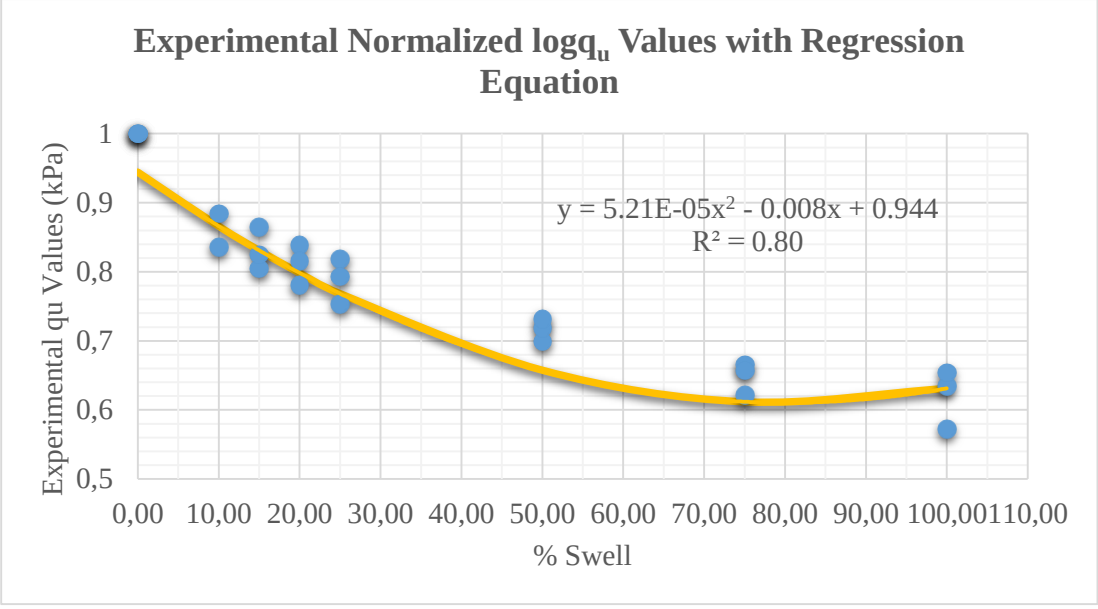

Figure 5.5. Experimental normalized logq$_u$ values with regression equation

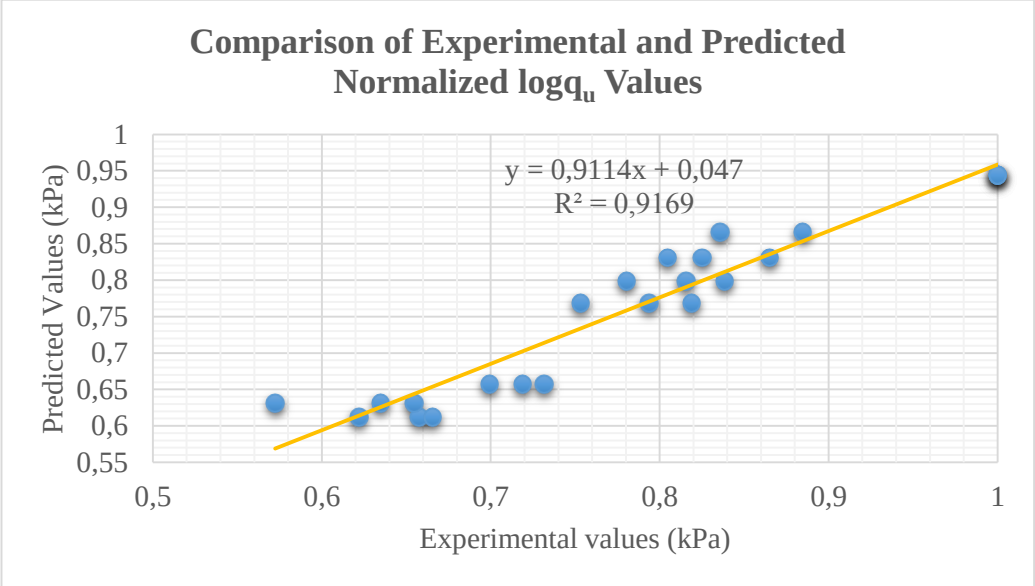

Figure 5.6. Comparison of experimental and predicted normalized logq_u values

5.2. Relation between Undrained Shear Strength and % Swell

Trend observed for unconfined compressive strength was valid for undrained shear strength since undrained shear strength is calculated by dividing the value of unconfined compressive strength to 2.

5.3. Relation between Undrained Elastic Modulus and % Swell

Undrained elastic modulus for samples also decreases with increasing water content and swelling. This relation can be examined from Figures 5.7, 5.8, 5.9 and 5.10 for each sample. Also equations for each sample were got from trendlines on Figures 5.7, 5.8, 5.9 and 5.10 in Excel.

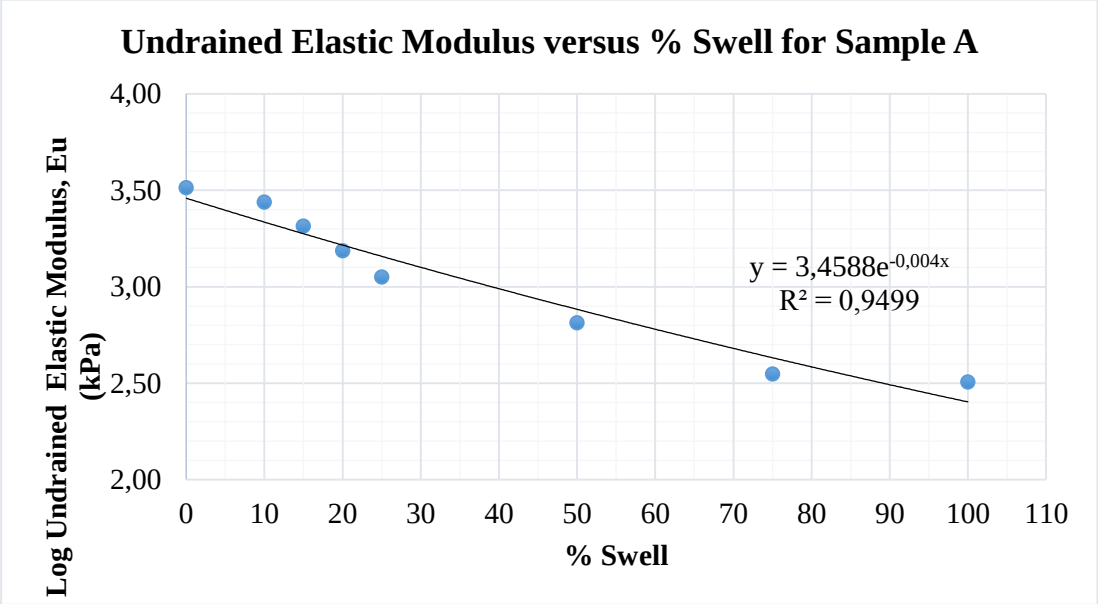

Figure 5.7. Undrained elastic modulus versus % swell for Sample A

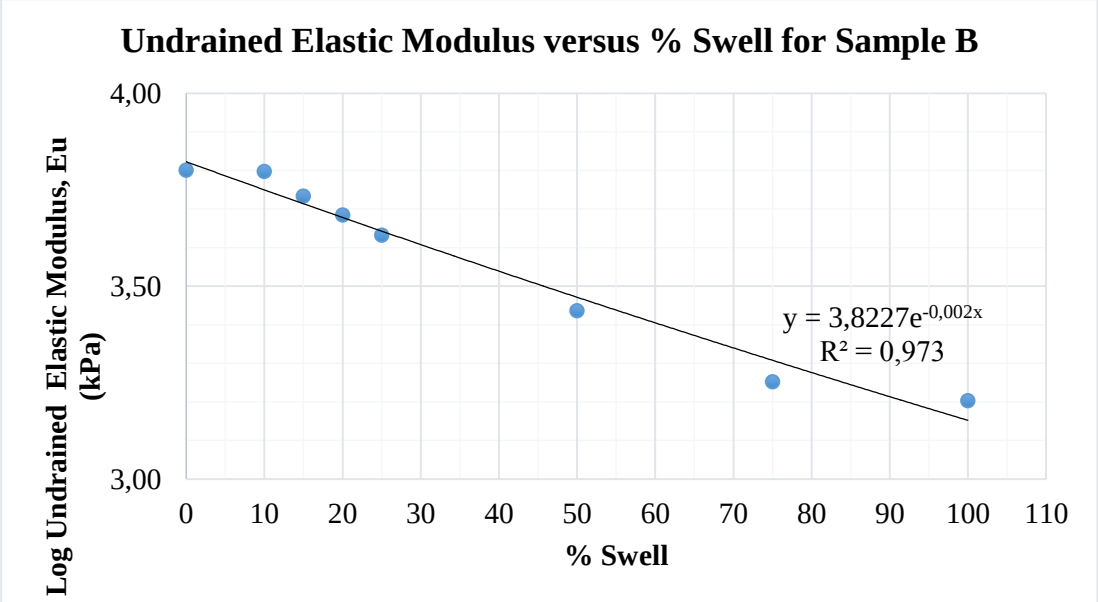

Figure 5.8. Undrained elastic modulus versus % swell for Sample B

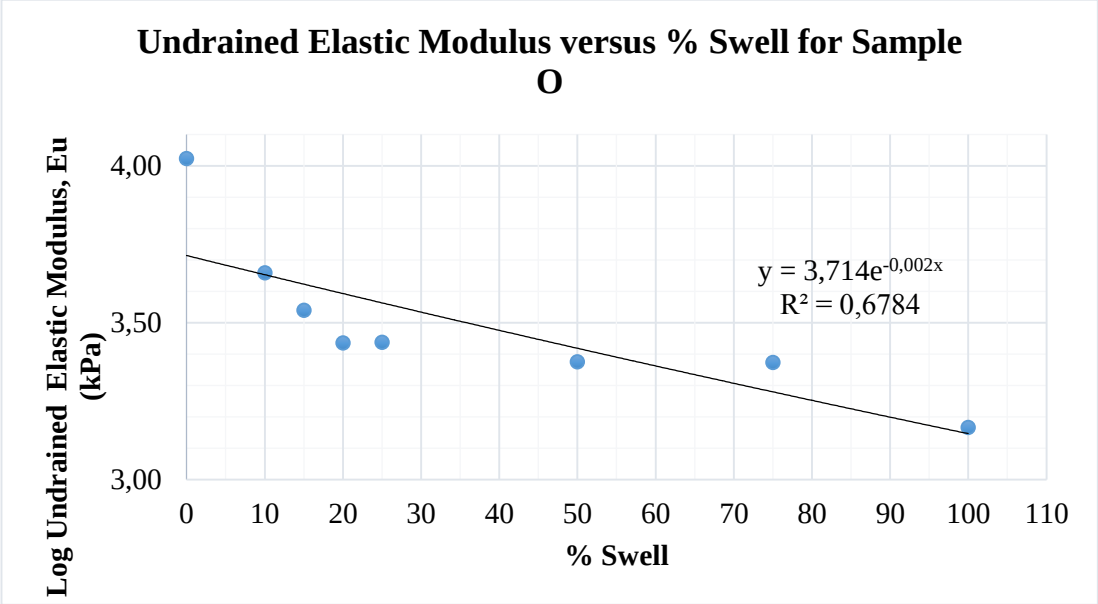

Figure 5.9. Undrained elastic modulus versus % swell for Sample O

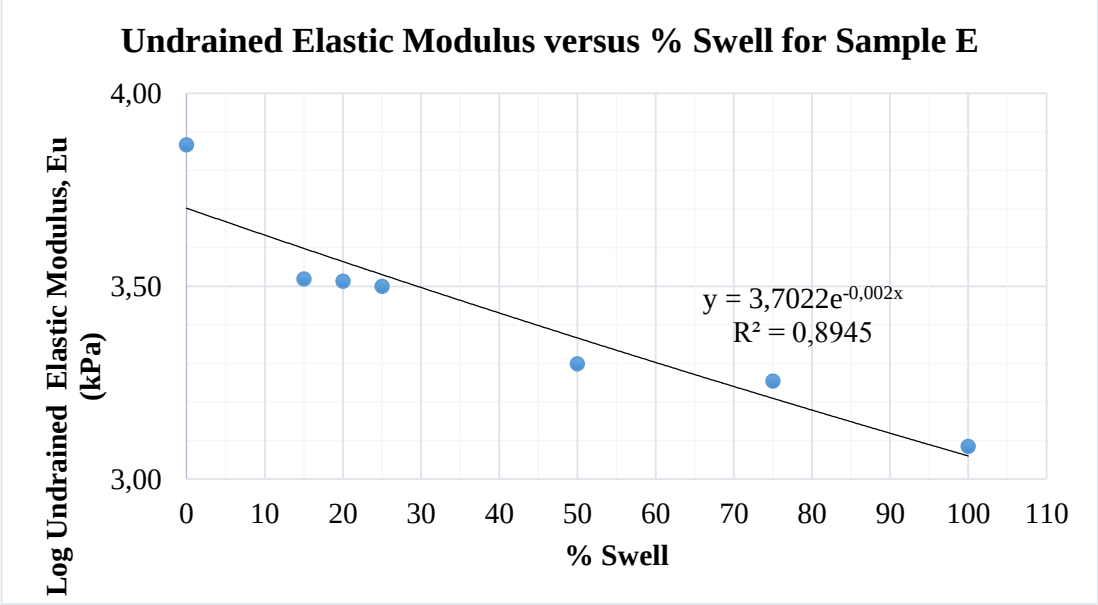

Figure 5.10. Undrained elastic modulus versus % swell for Sample E

5.4. Comparison of Undrained Elastic Modulus with Literature

Typical Young's Modulus values in MPa were summarized in Table 5.1 compiled from Kezdi (1974) and Prat et al. (1995). On the other hand, Table 5.2 shows the obtained undrained elastic modulus values with respect to swell ratio. All soil samples were evaluated as CH soil (clay of high plasticity) as the result of soil classification in Chapter 4. When Tables 5.1 and 5.2 matched each other, it was seen that all soil samples had soft to very soft modulus when vertical displacement stopped and they reached to ultimate swell. The only difference between the undrained elastic modulus values of samples was the initial states and decreases. Initial modulus of Sample A and Sample B at 0% of swell were evaluated as very soft to soft and medium respectively. However, undrained elastic modulus values of Sample O and Sample E, which have lower swelling potential, were in the range of stiff to very stiff. When Sample O and E got water and reached to 10% and 15% of swell respectively, their modulus showed a sudden decrease. From these points for Sample O and E, there was a gradual decrease.

At the end, when total decline in undrained elastic modulus values were explored, it was realized that Sample A had the most change as 90.2% with the highest swelling potential. Samples B, O and E possessed nearly the same trend with 74.7%, 86.1% and 83.5% respectively.

Table 5.1. Typical Young's Modulus values of soils in MPa (Kezdi, 1974 and Prat et al., 1995)

USCS	**Description**	**Very soft to soft**	**Medium**	**Stiff to very stiff**	**Hard**
ML	Silts with slight plasticity	2.5- 8	10- 15	15- 40	40- 80
ML, CL	Silt with low plasticity	1.5- 6	6- 10	10- 30	30- 60
CL	Clays with low-medium plasticity	0.5- 5	5- 8	8- 30	30- 70
CH	Clays with high plasticity	0.35- 4	4- 7	7- 20	20- 32
OL	Organic silts	-	0.5- 5	-	-
OH	Organic clays	-	0.5- 4	-	-

Table 5.2. Undrained elastic modulus with respect to % swell

	Undrained Elastic Modulus, E_u (MPa)			
% Swell	**Sample A**	**Sample B**	**Sample O**	**Sample E**
0	3.27	6.32	10.55	7.36
10	2.75	6.27	4.56	-
15	2.06	5.41	3.47	3.30
20	1.54	4.84	2.73	3.26
25	1.13	4.29	2.74	3.16
50	0.65	2.73	2.38	2.00
75	0.35	1.79	2.36	1.80
100	0.32	1.60	1.47	1.22

5.5. Relation between Time of Swell and % Swell

Time of swell was obtained from swell percent versus time graphs given in Chapter 4. After finding the swell percent corresponding to 100% of swell, intermediate swell steps were calculated with ratio and proportion. Then, these calculated values were matched with time on % swell versus time graphs in Chapter 4. Results were given in Figure 5.11. As can be seen from Figure 5.11, swelling times for each sample took longer with water increase. Moreover, Figure 5.11 enabled to compare the swelling times of samples with each other; thus, this case gave a chance to see the effect of expansiveness potential on swelling times at swelling steps. According to the results, it was observed that time of swell extended as the expansiveness of samples increased because Sample A needed the longest time while Sample E required the shortest time, which was coincided with the swell potential degree.

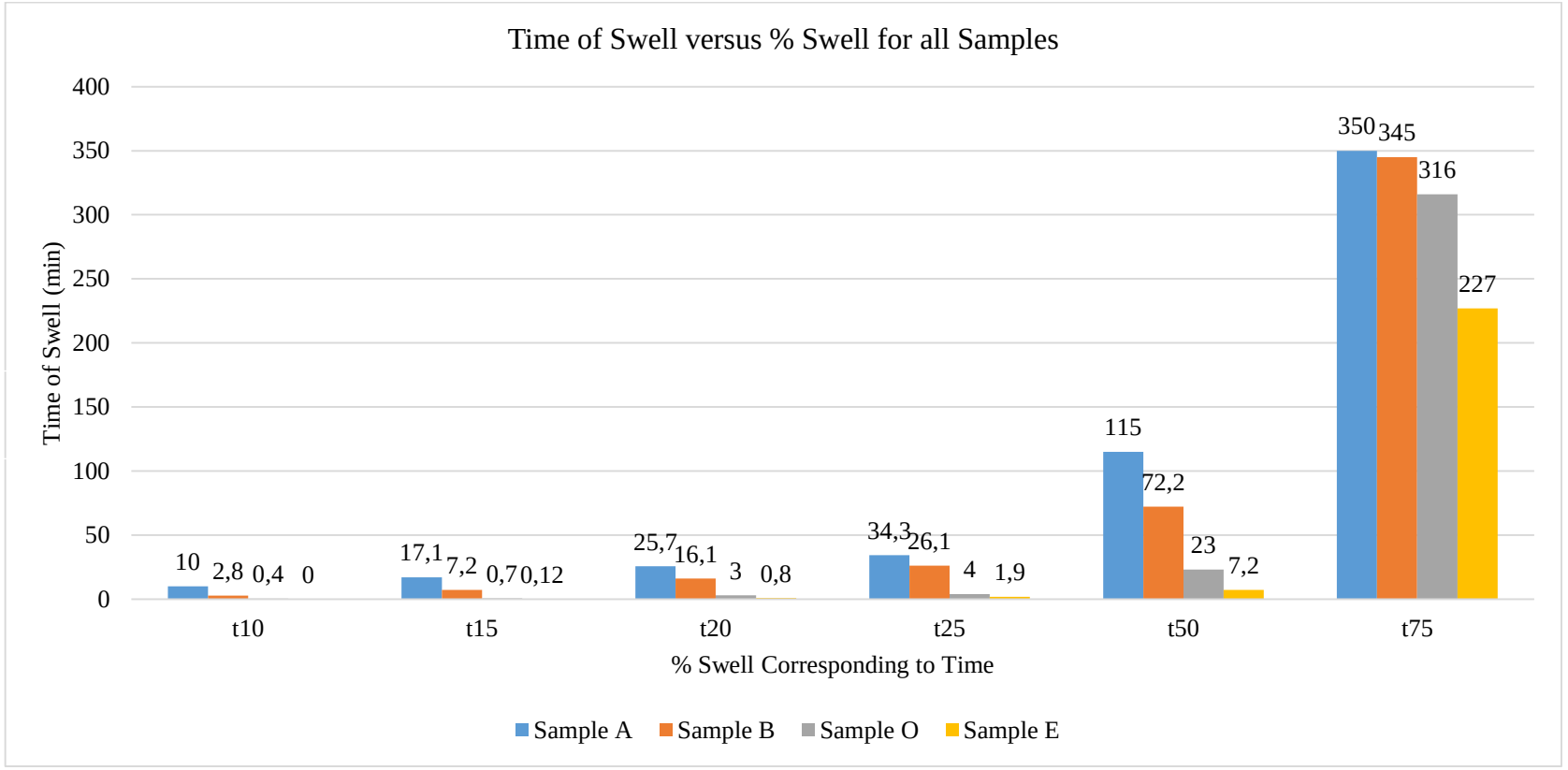

Figure 5.11: Time of swell versus % swell for all samples

5.6. Relation between Degree of Saturation and % Swell

As the samples got water and swelled, void ratio of the samples as well as degree of saturation increased. The trend of increase in degree of saturation as can be seen from Figures 5.12, 5.13, 5.14 and 5.15. In Eqn. 5.2, degree of saturation: S_r value was assumed as 1 for 100% of swell to determine final void ratio: e_f. As the second step of calculation, void ratio corresponding to swell ratio was calculated according to Eqn. 5.3. After specified void ratio values for each swell ratios, using again Eqn. 5.2, S_r values also were obtained for each swell steps.

$e*Sr=w*Gs$…….……...……...…… Eqn 5.2

$$e_{x\ \%\ of\ swell}=\frac{e_f\text{-Strain at x\% of swell}}{\text{Strain at x\% of swell+1}}$$……...……...…… Eqn 5.3

where

e= Void ratio

w= Water content

G_s= Specific gravity

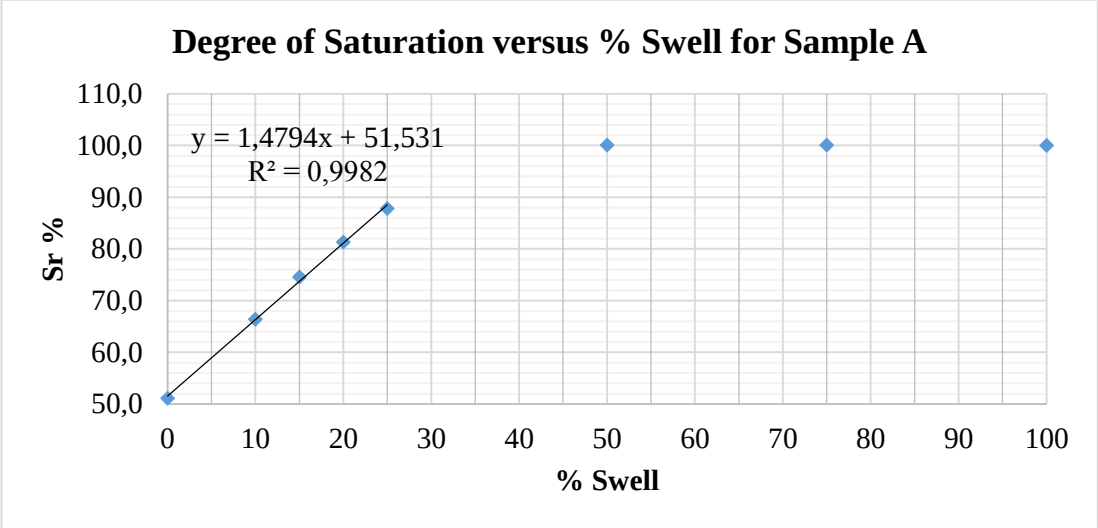

Figure 5.12. Degree of saturation versus % swell for Sample A

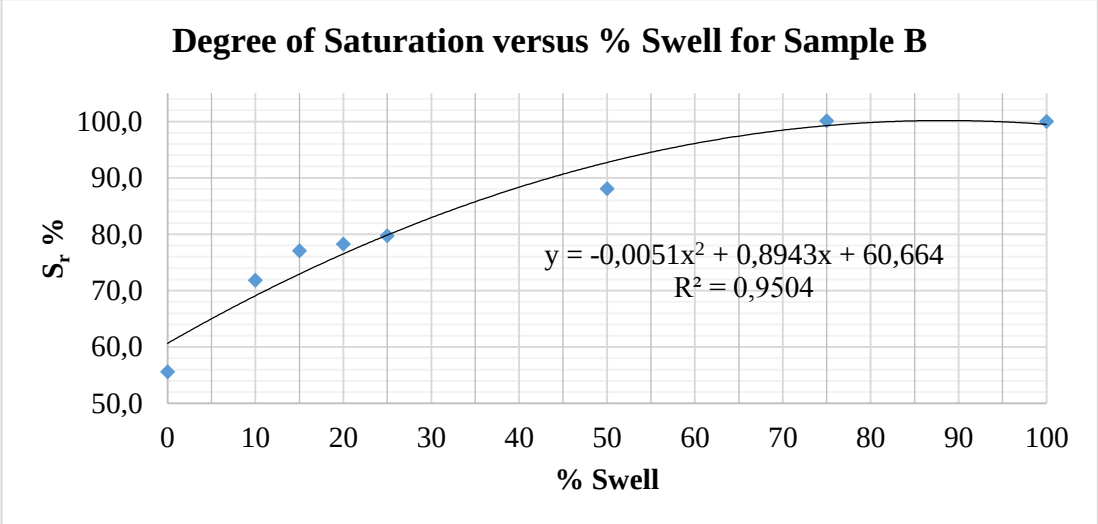

Figure 5.13. Degree of saturation versus % swell for Sample B

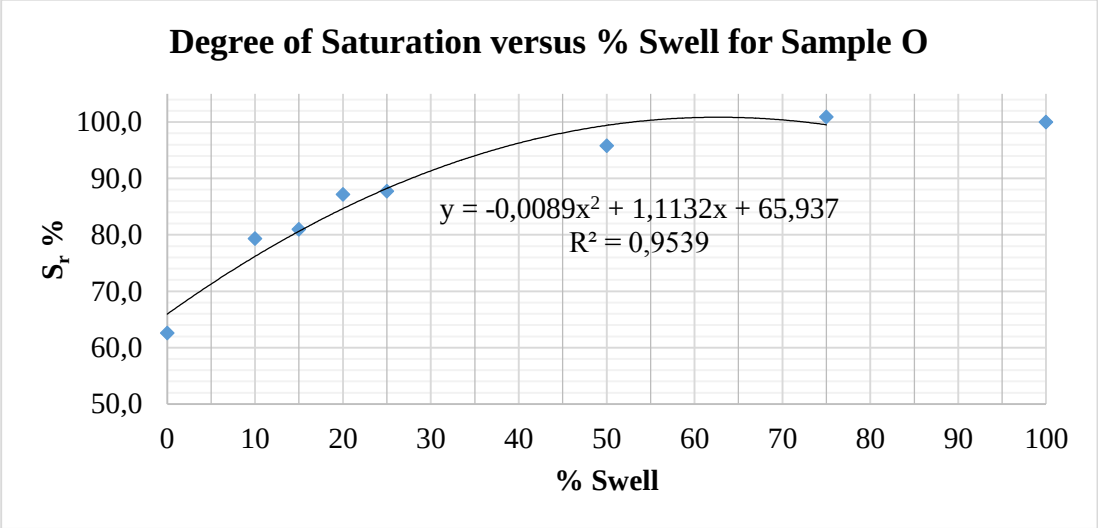

Figure 5.14. Degree of saturation versus % swell for Sample O

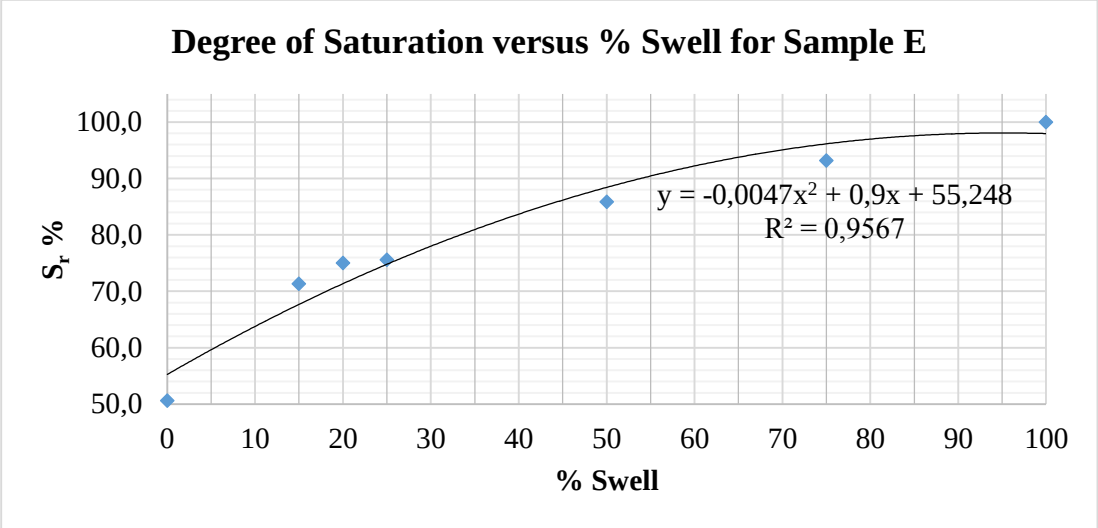

Figure 5.15. Degree of saturation versus % swell for Sample E

5.7. Relation between Liquidity Index and % Swell

Table 5.3 summarizes liquidity index: LI values of samples corresponding to % swell which were computed by using below Eqn 5.4:

$$LI=\frac{w-PL}{PL-LL} \quad \text{Eqn 5.4}$$

where

w= Water content in accordance with swell ratio

PL= Plastic limit obtained from Atterberg Limit Tests

LL= Liquid limit got from Atterberg Limit Tests

Table 5.3. Liquidity index values of samples with respect to % swell

	LI %			
% Swell	**Sample A**	**Sample B**	**Sample O**	**Sample E**
0	-0.08	-0.14	-0.18	-0.15
10	0.08	0.00	0.00	-
15	0.12	0.04	0.01	0.00
20	0.16	0.05	0.08	0.04
25	0.19	0.05	0.09	0.06
50	0.29	0.11	0.19	0.14
75	0.34	0.23	0.25	0.21
100	0.40	0.24	0.28	0.35

When values found in Table 5.3 were compared with the values in Table 5.4 acquired from Ranjan and Rao (2005), the fact that swelling tests for all samples were made in semi-solid state was pointed since their LI values were smaller than 0. Actually, this was the intended case in order to ensure that the samples would experience more swelling. Until Sample A swelled of 50%, it could be classified as stiff soil. For 50%, 75% and 100% swell, Sample A was in the medium stiff soil class. For natural samples; in other words, for Sample B, O and E, soil consistency description was stiff until 75% of swell. From this point, there were some differences. Sample B was still stiff when it reached 100% of swell. Sample O showed stiff properties till 75% of swell whereas consistency description of Sample E became stiff when it swelled 100%. To sum up, it could be said that all samples which were initiated testing in semi- solid state turned into plastic consistency at the end of swelling procedure.

Table 5.4. Consistency of cohesive soils according to liquidity index (Ranjan and Rao, 2005)

Consistency	**Description**	**LI**
Liquid	Liquid	>1.0
Plastic	Very soft	0.75- 1.00
	Soft	0.50- 0.75
	Medium stiff	0.25- 0.50
	Stiff	0- 0.25
Semi-solid	Very stiff or hard	< 0
Solid	Hard or very hard	< 0

5.8. Evaluation of Material Ability to Absorb Energy for the Measured Stress-Strain Values up to Peak Point

Material ability to absorb energy defines toughness. Since residual strength values were not measured for some samples in some swell steps, energy absorption ability of soil specimens was calculated from the area below the measured stress-strain curve at the ultimate peak stress and corresponding strain points. In the calculation, Trapezoidal Rule was used for measured strain and stress values up to peak point in the curves obtained from unconfined compression test. Then, absorbed energy values up to peak point were obtained by taking averages of two test results and summarized in Table 5.5 for each sample.

The fact that as the stored energy increases, material becomes ductile, is known. When Table 5.5 was examined, it was seen that all samples were ductile up to a certain swell percent, which can be 25% swell for Sample A or 15% swell for Sample O to give an example. After that swell percent, they started to become brittle. In general, it can be said that absorbed energy increases up to a point. After that point, soil specimens show brittle behavior.

Table 5.5. Absorbed energy values of soil samples up to peak points, which were obtained from stress-strain curves

	Absorbed Energy Value up to Peak Points of Stress-Strain Curves (J/m^3)			
% Swell	**Sample A**	**Sample B**	**Sample O**	**Sample E**
10	30.5	48.9	42.0	-
15	63.5	31.4	46.2	69.6
20	75.4	23.7	32.7	56.3
25	83.4	35.9	24.8	32.5
50	47.8	33.9	14.6	40.1
75	27.3	24.1	11.9	33.8
100	22.2	27.0	11.8	13.5

5.9. Estimation of Unconfined Compressive Strength

By performing several regression analysis at 95% confidence level, a predictive model was tried to be established between unconfined compressive strength, % swell and index properties of disturbed soil samples. In order to establish a predictive model, Excel was chosen. % swell and LI was determined as independent variables while q_u was taken as dependent variable. The best fitted

equation with R^2 value as 0.88 to this relation was found as the result of regression analysis and given in Eqn. 5.5. Thus, if two of three variables are known, the other one can be easily computed from Eqn. 5.5 without conducting any swelling experiment.

$$\frac{q_{u\ at\ x\%\ of\ swell}}{q_{u\ at\ 0\%\ of\ swell}} = -0.029 + 0.353*(LI) + 0.482*(LI)^2 + 0.958*e^{-0.065*x} \quad \text{.....Eqn 5.5}$$

where

q_u= Unconfined compressive strength in kPa

x= % Swell

LI= Liquidity index in decimals

In addition, experimental and predicted values of normalized q_u on Figure 5.16 showed a linear correlation.

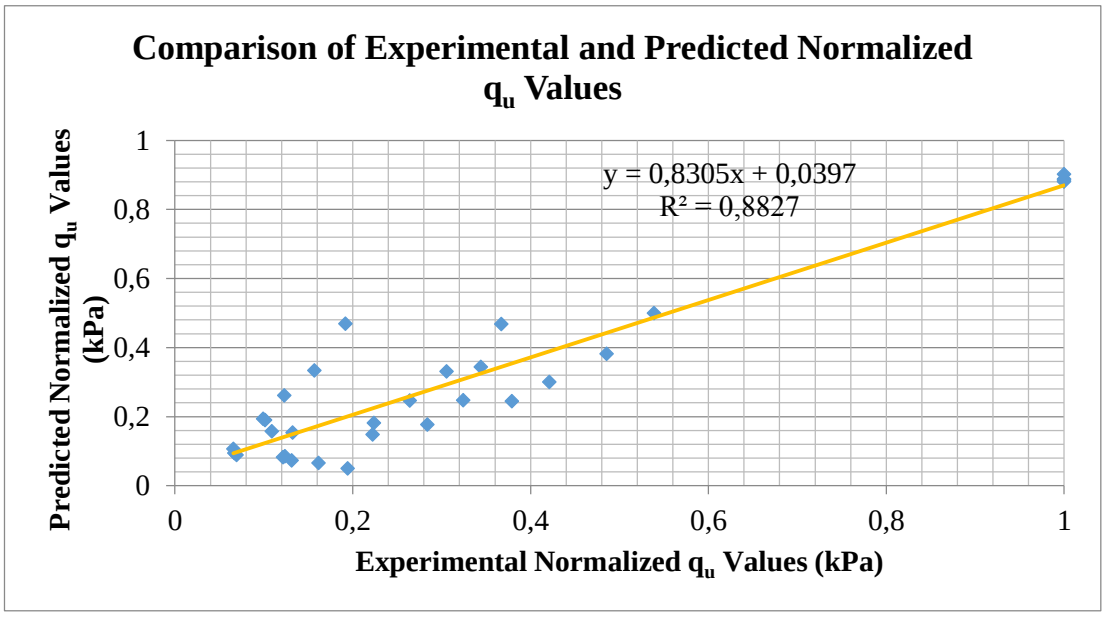

Figure 5.16. Comparison of normalized q_u values obtained from experiments and regression analysis

CHAPTER 6

CONCLUSIONS

The objective of this study was to search the effect of swelling on undrained shear strength and unconfined compressive strength of expansive soils. Three natural and one artificial samples were prepared and then swelled in designed plastic molds and sheared with unconfined compression test setup. Shearing of specimens prepared at the intended water contents without swelling was accepted as reference test. Then, they were allowed to reach ultimate swell in the molds and sheared. Thus, undrained shear strength in the intermediate steps which included 10%, 15%, 20%, 25%, 50% and 75% of ultimate swell was found. To verify the swelling potentials determined from the swell tests made in the specially designed molds, free swell index and Methylene Blue test were performed on the samples. Moreover, swell pressure and frictional stress between the specimen and the mold were determined. By taking into consideration of these experimental test results, following conclusions can be drawn:

- As expansive soil sample got water and so swelled, it lost unconfined compressive strength and undrained shear strength to a degree of about 90-% of its initial value. Decrease in unconfined compressive strength and undrained shear strength was same since undrained shear strength was found by dividing unconfined compressive strength by 2.

- Water suction capacity of soil samples was quite variable due to change in their mineral composition, existence of some chemicals or salts, variability in temperature etc. When samples reached to ultimate swell, difference in water contents with respect to initial water content became 124%, 95%, 72% and 108% for Samples A, B, O and E respectively.

- Undrained elastic modulus values were also decreased with increasing swell ratio. At 100% swell, soil samples possessed undrained elastic modulus values which were less than approximately 75-90% of their initial values.
- When Free Swell Index Test was used for quick estimation of swelling potential of soils, it was seen that FSI value was increased with increasing swelling potential.
- When Methylene Blue Test was decided to be utilized for determination of clay activity, it was observed that the obtained results of artificial and natural soil samples cannot be compared with each other. However, by taking into consideration the test results for just natural soil samples; i.e. Sample B, O and E, the fact that MBV increased as soil swelling potential got higher, was realized.
- More swelling of a sample meant larger force would be needed in order to get the vertical displacement to zero. Therefore, increase in swell potential resulted in higher swell pressure values.
- Since plastic molds prevented volumetric swelling, a frictional force and so stress developed between soil specimen and mold, which was equal to about 16.5-25% of swell pressure for 0% and 100% of swell respectively.
- It was seen that as expansiveness potential of the specimen increased, it took more time to complete the swell procedure.
- The main reason behind the swell mechanism was the water existence in interlayer spacing. Therefore, as soil took water, degree of saturation of it also increased. When Sample A reached 50% of swell, it became fully saturated. On the other hand, Sample B and O had full saturation at 75% of swell. For Sample E, which has the lowest swelling potential, fully saturation case was accomplished at the ultimate swell.
- When the results obtained from liquidity index and undrained elastic modulus were examined, existence of differences were observed. The reason of this

could be explained with the method used to calculate undrained elastic modulus and liquidity index. Undrained elastic modulus was computed by drawing secant line from the initial point to 50% of peak stress at the stress-strain curve while liquidity index was obtained from the relation between water content, liquid limit and plastic limit.

- Calculation of absorbed energy from the area under stress-strain curves up to peak point showed that soil specimens became ductile to a point as they got water. After that point, their behavior against little stress increase turned out to be brittle.

- When the relation between net bearing capacity and swell % was examined by an example in Appendix D, it was seen that once Sample A swelled until vertical displacement stopped, its net bearing capacity value decreased to approximately 90% of values at 0% swell.

- In an example problem in Appendix E, the calculation of immediate settlement values for 0% and 100% swell showed that immediate settlement values for artificial soil sample increased about 917 % of its initial value when their vertical displacement ceased.

- Factor of safety of an example slope with the expansive soil in Appendix F decreased below 1 after the soil reached 20% of swell.

- Pile length in an example swelling soil increased about 422% of its initial value when the ultimate swelling reached (Appendix G).

RECOMMENDATIONS FOR FUTURE RESEARCH

This study includes influence of swell amount on shear strength of expansive soils. For this aim, specially designed molds were used in swell procedure and swelled samples were sheared in unconfined compression test machine. These tests may be repeated on swelling clay samples from different regions of Turkey and on samples with different proportions of bentonite and kaolinite. Furthermore, mineralogy by x-ray diffraction test and chemical analysis of the test samples may be determined and correlated with MBV test.

REFERENCES

AFNOR, Mesure de la Capacite D'adsorption de Bleu de Methylene d'un sol ou d'un Materiau Rocheux, *l'Association Française de Normalisation*, NF P 94-068, 1998

Al-Rawas, A. and Goosen, M.F.A., Eds., *Expansive Soils Recent Advances in Characterization and Treatment,* Taylor and Francis Group, London, pp. 25-27, pp.375-384, 2006

Al- Mhaidib, A. and Al- Shamrani, M., Influence of Swell on Shear Strength of Expansive Soils, *Advances in Unsaturated Soil, Seepage, and Environmental Geotechnics*,pp. 160-165, 2006

ASTM, Standard Practice for Classification of Soils for Engineering Purposes (Unified Soil Classification System), *Annual Book of ASTM Standards,* D 2487- 06, Vol. 04. 08, 2011

ASTM, Standard Test Methods for Laboratory Compaction Characteristics of Soil Using Standard Effort (12400 ft- lbf/ft^3 (600 kN- m/ m^3)), *Annual Book of ASTM Standards*, D698- 07, 2007

ASTM, Standard Test Methods for Liquid Limit, Plastic Limit, and Plasticity Index of Soils, *Annual Book of ASTM Standards,* D4318- 10e1, 2010

ASTM, Standard Test Methods for One- Dimensional Swell or Settlement Potential of Cohesive Soils, *Annual Book of ASTM Standards,* D4546- 96, Vol. 04. 08, 1996

ASTM, Standard Test Method for Particle- Size Analysis of Soils, *Annual Book of ASTM Standards,* D 422- 63, 2007

ASTM, Standard Test Method for Particle- Size Distribution (Gradation) of Soils Using Sieve Analysis, *Annual Book of ASTM Standards*, D6913- 04, 2009

ASTM, Standard Test Method for Shrinkage Factors of Soils by the Mercury Method, *Annual Book of ASTM Standards,* D- 427- 98, Vol. 04.02, 1998

ASTM, Standard Test Methods for Specific Gravity of Soil Solids by Water Pycnometer, *Annual Book of ASTM Standards,* D854- 14, 2014

ASTM, Standard Test Methods for Unconfined Compressive Strength of Cohesive Soils, *Annual Book of ASTM Standards,* D2166/ D2166M- 13, 2013

Bao, C., Gong, B., & Zhan, L., Properties of Unsaturated Soils and Slope Stability of Expansive Soils. *In Proc., 2nd Int. Conf. on Unsaturated Soils (UNSAT 98),* pp. 71–98, 1998

Barshad, I., Adsorptive and Swelling Properties of Clay- Water System, *Clays and Clay Minerals,* Vol. 1, Issue. 1, pp. 70-77, 1949

Bergaya, F., Theng, B. K. G. and Lagaly, G., Eds., *Developments in Clay Science: Handbook of Clay Science, 1st Ed.,* Elsevier, Amsterdam, pp. 1-16, 2006

Birand, A., Ergun, U. and Erol, O., *CE366 Foundation Engineering 1,* METU Press, Ankara, 2011

Bishop, A. W. The Principle of Effective Stress, *Teknisk Ukeblad,* Vol.106, No.39, pp.859-863,1959

Blogs of the European Geosciences Union, http://blogs.egu.eu/, last visited on November 2015

Briaud, J. L., Introduction to Soil Moduli, *Geotechnical News,* BiTech Publisherd Ltd., Richmond, Canada, 2001

Chen, F. H., *Foundations on Expansive Soils Developments in Geotechnical Engineering, 12th Ed.,* Elsevier Scientific Publishing Company, Amsterdam, pp. 1-10, 1975

Chen, Y. J., Lin, S. S., Chang, H. W. and Marcos, M. C., Evaulation of Side Resistance Capacity for Drilled Shafts, *Journal of Marine Science and Technology*, Vol. 19, No. 2, pp. 201-221, 2011

Craig, R. F., *Craig's Soil Mechanics, 7th Ed.*, Spon Press, London, pp. 4-5, 2004

Das, B. M., *Advanced Soil Mechanics, 3rd Ed.*, Taylor and Francis Group, New York, USA, pp. 7-17, 2008

Domitrovic, D. and Kovacevic, Z.B., The Relationship between Swelling and Shear Strength Properties of Bentonites, *Proceedings of the 18th International Conference on Soil Mechanics and Geotechnical Engineering,* Paris, 2013

Eslharief, E. M., Foundations in Expansive Soils, Sudan Experience, *Conference of Graduate Studies and Scientific Research,* University of Khartoum, 2010

Fredlund, D. G. and Morgenstern, N. R., Stress State Variables for Unsaturated Soils, *Journal of Geotechnical Division, ASCE,* Vol.103, No. GT5, pp.447-466, 1977

Gardiner, D. T. and Miller, R. W., *Soils in our Environment, 8th Ed*., Prentice- Hall Publishers, Upper Saddle River, NY, 1998

Grim, R.E., *Clay Mineralogy, 2nd Ed.*, McGraw Hill, New York, pp.596, 1968

Grim, R. E., *Properties of Clay,* Authority of the State of Illinois, Urbana, 1939

Guggenheim, S., Adams, J.M., Bain, D.C., Bergaya, F., Brigatti, F., Brigatti, M.F., Drits, V.A., Formoso, M.L.L., Galan, E., Kogure, T. and Stanjek, H., Summary of Recommendations of Nomenclature Committees Relevant to Clay Mineralogy, Report of the Association Internationale Pour L'etude des Argiles (AIPEA)

Holtz, R. D. and Kovacs, W. D, *Introduction to Geotechnical Engineering,* Prentice-Hall, 1981

Inter- Organization Programme for the Sound Management of Chemicals, Environmental Health Criteria 231: Bentonite, Kaolin and Selected Clay Minerals, *World Health Organization,* Geneva, 2005

IS, Method of Test for Soils Part XL Determination of Free Swell Index of Soils, *Bureau of Indian Standards,* 2720, Part XL, 2002

Ishibashi, E. I. and Hazarika, H., *Soil Mechanics Fundamentals and Applications, 2nd Ed.*, CRC Press, 2015

Khalili, N. and Khabbaz, M. H., A Unique Relationship for the Determination of Shear Strength of Unsaturated Soils, *Geotechnique,* Vol. 48, No. 5, pp.681-687, 1998

Karube, D., Kato, S., Hamada, K. and Honda, M., The Relationship between the Mechanical Behavior and the State of Pore Water in Soil", *Journal of JSCE,* Vol.535, pp.83-92, 1996

Lambe, T. W. and Whitman, R. V., *Soil Mechanics,* John Wiley and Sons, USA, pp. 40-51, 1969

Lal, R., Ed., *Encyclopedia of Soil Science*, Vol.1., Taylor and Francis Group, USA, pp. 277-278, 2006

Lee, Y., Stress- Strain- Time Relationship of Queenston Shale, *Doctor of Philosophy Thesis*, The University of Western Ontario, Canada, 554 pages, 1988

Mitchell, J.K., *Fundamentals of Soil Behavior, 2nd Ed.*, John Wiley and Sons, 1993

Murray, H.H., *Applied Clay Mineralogy Occurences, Processing and Application of Kaolins, Bentonites, Palygorskite- Sepiılite and Common Clays, 1st Ed.,* Elsevier, Amsterdam, pp. 1-19, 2007

Nelson, J. D. and Miller, J. M., *Expansive Soils Problems and Practice in Foundation and Pavement Engineering*, John Wiley and Sons Inc., USA, pp. 8-12, 1992

New Mexico Tech Institute of Mining and Technology, www.nmt.edu, last visited on May 2015

Nicholson, P. G., *Soil Improvement and Ground Modification Methods*, Elsevier, USA, pp. 77-78, 2015

Nomenclature Committee 2006, *Clays and Clay Minerals*, Vol. 54, pp. 761-772, 2006

NovoPILE User's Manual, http://help.novotechsoftware.com, last visited on February 2016

Öberg, A. L. and Sällfors, G. A Rational Approach to the Determination of the Shear Strength Parameters of Unsaturated Soils, *Proceedings of First International Conference on Unsaturated Soils*, Paris, Vol.1, pp.151-158, 1995

Patel, A. D., Stamatakis, E., Davis, E. and Friedheim, J., *High Performance Water Based Drilling Fluids and Method of Used*, Houston, 2007

Ranjan, G. and Rao, A.S.R., *Basic and Applied Soil Mechanics, 2nd Ed*., New Age International Ltd., New Delhi, pp. 41, 2005

Reeves, G. M., Sims, I. and Cripps, Eds., J. C., *Clay Materials Used in Construction*, The Geological Society, London, pp. 20-23, 2006

Rowe, R. K., Ed., *Geotechnical and Geoenvironmental Engineering Handbook*, Vol. 1, Springer Science+ Business Media, New York, pp. 162-163, 2001

Sivapullaiah, P., Sitharam, T. and Subba, R. K., Modified Free Swell Index for Clays, *Geotechnical Testing Journal*, Vol. 10, Issue 2, pp. 80-85, 1987

Skempton, A. W. and Macdonald, D. H., The Allowable Settlement of Buildings, *Proceedings of the Institution of Civil Engineers*, Vol. 5, No. 6, pp. 727- 768, 1956

Sridharan, A. and Prakash, K., Classification Procedures for Expansive Soils, *Proceedings of the Institution of Civil Engineers- Geotechnical Engineering*, Vol. 143, pp. 235-240, 2000

Soil Expedition, http://soilnews.feedsynews.com, last visited on October 2015

Tekinsoy, M. ., Kayadelen, C., Keskin, M., and Söylemez, M., An Equation for Predicting Shear Strength Envelope with respect to Matric Suction. *Computers and Geotechnics*, 31(7), 589–593, 2004

Terzaghi, K., Erdbaumechanik auf Bodenphsikalischer Grundlage, 1925

Terzaghi, K., Peck, R.B. and Mesri, G., *Soil Mechanics in Engineering Practice, 3rd Ed.*, John Wiley and Sons Inc., USA, pp. 9-10, 1996

Tilgen, H. P., Relationship between Suction and Shear Strength Parameters of Compacted METU Campus Clay, *M.S. Thesis*, METU, Turkey, 120 pages, 2003

The European Geosciences Union Blogs, http://blogs.egu.eu/, last visited on October 2015

Türköz, M. and Tosun, H., The Use of Methylene Blue Test for Predicting Swell Parameters of Natural Clay Soils, *Scientific Research and Essays*, Vol. 6, No. 8, pp.1780-1792, 2011

University of Idaho Soil 205-90, General Soils for Distance Students Lecture Notes, http://www.uidaho.edu/, last visited on October 2015

University of Pennsylvania, http://calculus.seas.upenn.edu/, last visited on November 2015

NAVDOCKS DM-7, Soil Mechanics, Foundation and Earth Structures, *U.S. Department of the Navy Design Manual*, 1962

Wang, L., Long, W. and Gao, S., Effect of Moisture Content, Void Ratio and Compacted Sand Content on the Shear Strength of Remolded Unsaturated Clay, *The Electronic Journal of Geotechnical Engineering*, Vol. 19, Bundle Q, pp. 4413-4426, 2014

Weaver, C. E. and Pollard, L. D., *Developments in Sedimentology 15: The Chemistry of Clay Minerals*, Amsterdam, pp. 1-106, 1973

Wilbourn, K., Index Properties and Strength of Artificial Soil Using the Harvard Miniature Method, *Report*, University of Houston, USA, 2007

Wyoming Multi-Hazard Mitigation Plan, http://hls.wyo.gov/, last visited on December 2015

APPENDIX A

PROPERTIES OF MATERIAL USED TO MAKING MOLDS

Material characteristics of molds in which soil samples swelled were given in Table A.1.

Table A.1. Material properties of molds

Physical Properties	Metric
Density	1.15 g/cc
Water Absorption at Saturation	7.0 %
Mechanical Properties	
Hardness, Shore D	84
Tensile Strength, Ultimate	83.4 MPa
Elongation at Break	>= 20 %
Tensile Modulus	4.00 GPa
Compressive Strength	93.2 MPa
Compressive Modulus	2.70 GPa
Izod Impact, Notched (ISO)	5.60 kJ/m^2
Charpy Impact Unnotched	NB

Table A.1. (continued)

Coefficient of Friction	0.39
K Factor (Wear Factor)	0.44
K (wear) Factor	$500x10^4$ mm^3/N-M
Electrical Properties	
Volume Resistivity	>= 1.00e+14 ohm-cm
Surface Resistance	>= 1.00e+13 ohm
Dielectric Constant	3.7
Dielectric Strength	25.0 kV/mm
Thermal Properties	
CTE, linear	80.0 µm/m- ^{0}C
Melting Point	220 ^{0}C
Maximum Service Temperature, Air	110 ^{0}C

APPENDIX B

TYPICAL PHOTOS OF SPECIMENS AT FAILURE

Figure B.1. Photo of 15% of swell test for Specimen A at the failure

Figure B.2. Photo of reference test for Specimen B at the failure

Figure B.3. Photo of reference test for Specimen O at the failure

Figure B.4. Photo of 20% of swell test for Specimen E at the failure

APPENDIX C

CALCULATION OF UNDRAINED SHEAR STRENGTH

Calculation of undrained shear strength for Sample B at 0 % swell; i.e., at reference test, was given below as an example:

After strain and load dial gauge readings were recorded during unconfined compression test, initial cross sectional area: A_0 was calculated as 0.001092 m^2 using Eqn. C.1 for all tests at all steps.

$$A_0=\frac{\pi*D^2}{4} \quad \text{.....Eqn. C.1}$$

where

D= Initial sample diameter

Proving ring constant: C_p and initial sample height: H_0 were taken as 0.075 and 0.072 m respectively at the computations. Used proving ring determined C_p value. Table C.1 summarized the calculation steps from this point. After strain and compressive stress values were obtained, which were marked in Table C.1 with blue color, peak point was determined. Half of this peak point gave undrained shear strength value. Meanwhile, necessary unit conversions were made.

Table C.1. Calculation steps of undrained shear strength for Sample B at 0% of swell

Strain Dial Reading: δ_1	**Strain: $\varepsilon=\delta_1/H_0$**	**Corrected Area: $A=A_0/(1-\varepsilon)$ (m^2)**	**Proving Ring Dial:δ_2**	**Axial Load: $P=\delta_2*C_p$ (kg)**	**Compressive Stress: $\sigma= P/A$ (kPa)**
0.00	0.000	0.00109	0.00	0.00	0.00
10.00	0.004	0.00110	9.00	0.68	6.16
20.00	0.007	0.00110	29.50	2.21	20.11
30.00	0.011	0.00110	62.00	4.65	42.12
40.00	0.014	0.00111	119.00	8.93	80.56
50.00	0.018	0.00111	184.00	13.80	124.11
60.00	0.021	0.00112	237.00	17.78	159.28
70.00	0.025	0.00112	269.00	20.18	180.13
80.00	0.028	0.00112	275.20	20.64	183.61
90.00	0.032	0.00113	262.00	19.65	174.16
100.00	0.036	0.00113	240.00	18.00	158.95

APPENDIX D

INFLUENCE OF SWELL RATIO ON NET ULTIMATE BEARING CAPACITY

In order to see the effect of swelling at different ratios on bearing capacity, a square foundation whose depth was 1 m and dimensions were 1x1 m were taken into consideration. Foundation existence was assumed on soil from which Sample A was taken.

Skempton (1951) stated that net ultimate bearing capacity of clays: q_{nf} is computed by using below Eqn D.1 (Birand et al., 2011).

$q_{nf}=c_u*N_c$……...…….…….... Eqn D.1

where

c_u= Undrained shear strength of soil

N_c= Dimensionless bearing capacity factor taken from Skempton's Chart given in Figure D.1.

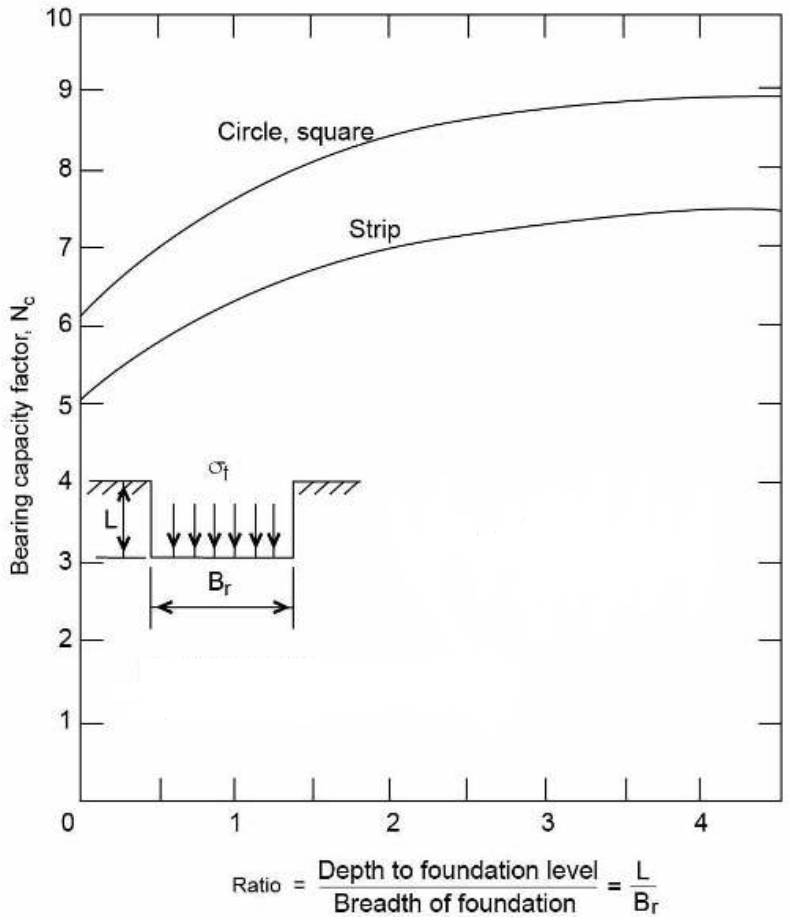

Figure D.1. Bearing capacity factors for foundations in clay (Φ= 0) (After Skempton, 1951)

Since $L/B_r = 1/1 = 1 \Longrightarrow N_c = 7.83$ was found from Figure D.1.

Decrease in bearing capacity is given in Table D.1 for Sample A. When Table D.1 was examined, it was seen that soil specimen lost their net bearing capacity up to 90% of its initial value. Also, Figures D.2 shows the relation between net ultimate bearing capacity and % swell with the mathematical expression on it for Samples A.

Table D.1. Change in net foundation pressure with variation of swell ratio for Sample A

% Swell	c_u of Sample A (kPa)	q_{nf} on Sample A(kPa)	Decrease in q_{nf} %
0	105.5	826.1	0
10	56.8	444.7	46
15	51.3	401.7	51
20	44.5	348.4	58
25	40	313.2	62
50	23.5	184.0	78
75	14	109.6	87
100	10.7	83.8	90

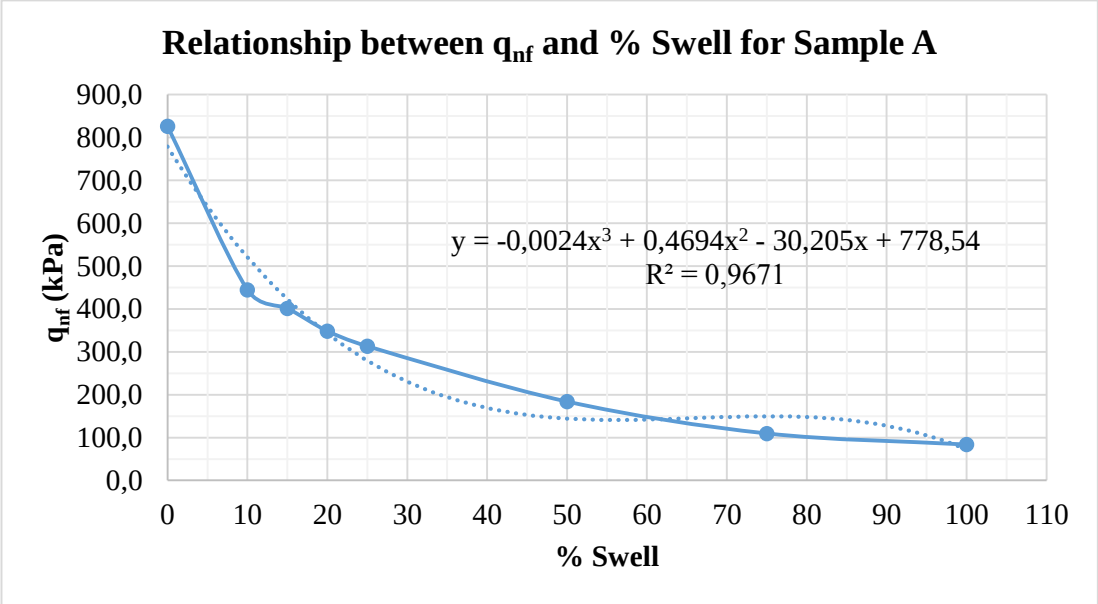

Figure D.2. Relation between q_{nf} and % swell for Sample A

APPENDIX E

INFLUENCE OF SWELL RATIO ON IMMEDIATE SETTLEMENT

Again, in order to see the effect of swelling at different ratios on immediate settlement, a square foundation whose depth was 1 m and dimensions were 1x1 m were taken into consideration. Foundation existence was assumed on soil from which Sample A was taken.

In order to see the change in immediate settlement, by assuming soil was fully saturated, the formula, which was specified by Schleicher (1926), given in Eqn E.1 was utilized (Birand et al., 2011):

$$S_i = \frac{q_n * B}{E_u} * (1-\nu^2) * I_s \quad \text{..... Eqn E.1}$$

where

S_i= Immediate settlement determined using Elastic Theory

q_n= Net foundation pressure

B= Width of the foundation

E_u= Undrained elastic modulus

I_s= Shape factor

ν = Poisson's ratio

From Table E.1, I_s value was selected as 0.95 as average for square foundation. Moreover, ν value was taken as 0.5 for undrained clays. Net foundation

pressure and width of the foundation were assumed as 30 kPa and 1 m respectively as in the case of bearing capacity calculation. Then, immediate settlement calculations with varying undrained elastic modulus values due to distinct swelling ratios are given in Table E.2. When Table E.2 is investigated, it is seen that immediate settlement reaches to such a large value of 66.6 mm for Sample A. This is not a surprising result due to high swelling potential of it. Skempton and Mcdonald (1956) proposed 45 mm as limiting value for maximum total settlement in clay. Total settlement is found by summing immediate, consolidation and secondary settlement effects. When Sample A reaches to ultimate swell at which vertical displacement ceased, it exceeds this limiting value with just immediate settlement value of 66.6 mm. This prevents a safe foundation design since settlement criteria is not satisfied.

Moreover, Figure E.1 indicates increase in immediate settlement with swelling for Samples A. An equation for Sample A was obtained on Figure E.1 by adding trendline in Excel.

Table E.1. Values of I_s (Birand et al., 2011)

Foundation Property	**Center**	**Corner**	**Average**
Square	1.12	0.56	0.95
Rectangle, L/B=2	1.52	0.76	1.30
Rectangle, L/B=5	2.10	1.05	1.83
Circle	1.00	0.64	0.85

Table E.2. Change in immediate settlement with variation of swell ratio for Sample A

% Swell	E_u for Sample A (kPa)	S_i for Sample A (mm)
0	3265	6.5
10	2748	7.8
15	2060	10.4
20	1535	13.9
25	1126	19.0
50	651	32.8
75	353	60.6
100	321	66.6

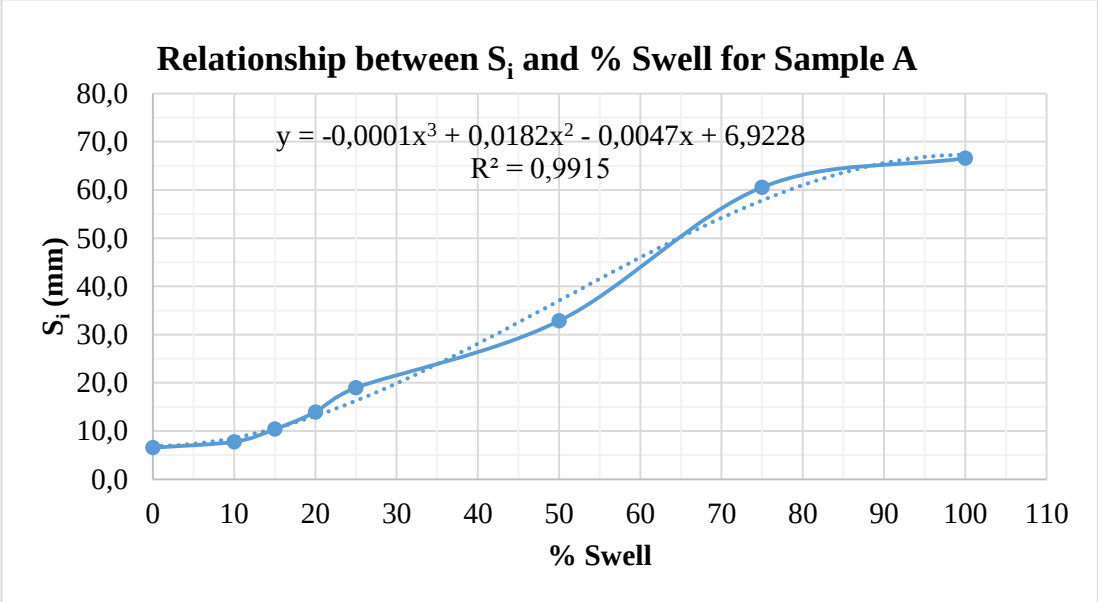

Figure E.1. Relation between S_i and % swell for Sample A

APPENDIX F

INFLUENCE OF SWELL RATIO ON SLOPE STABILITY

In order to see the effects of swelling on slope stability of expansive clay, slope whose height and angle was assumed as 10 m and 54^0 respectively. Slope of a soil was considered from which Sample A was taken.

Change in factor of safety against sliding was search according to Eqn. F.1 (Taylor, 1948):

$$FS = \frac{c_u}{N_s * \gamma * H} \quad \text{.....Eqn. F.1}$$

where

c_u= Undrained shear strength

N_s= Stability coefficient depending on slope angle

γ= Unit weight of soil sample

H= Slope height

Unit weight of soil sample was computed from G_s in Table 4.3 as 25.9 kN/m^3. Additionally, N_s value was determined as 0.183 from Figure E.1 for Φ_u= 0 and slope angle as 54^0. Table F.1 shows the calculation steps. Figure F.2 presents the change in FS versus % swell with the mathematical correlation on it. As can be seen from Table F.1, after 20% of swell, FS value is even under 1.

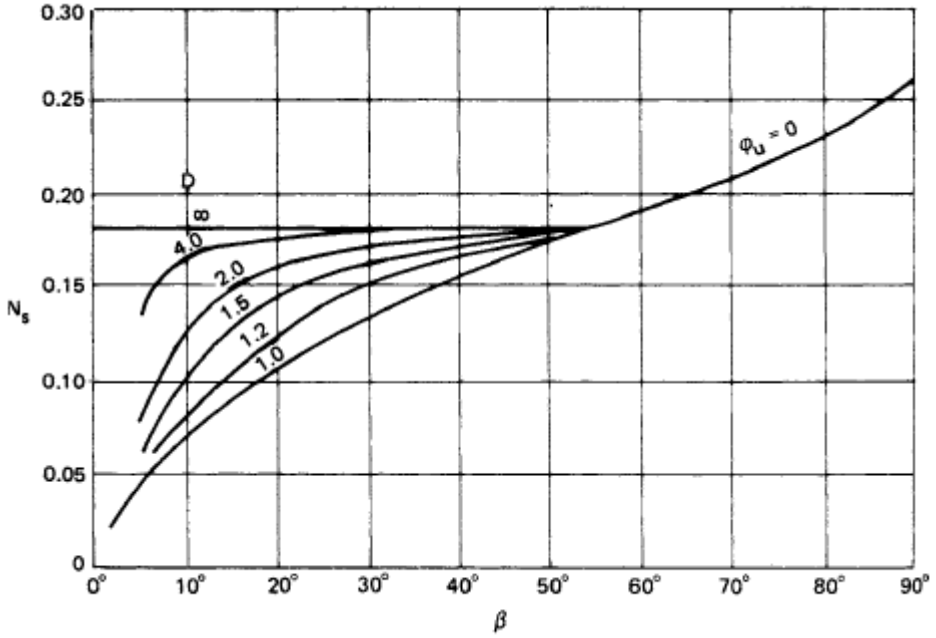

Figure F.1. Taylor's stability chart for Φ_u= 0 conditions (1948)

Table F.1. Change in FS against sliding with variation of swell ratio for Sample A

% Swell	**c_u of Sample A (kPa)**	**$FS_{against\ sliding}$**
0	105.5	2.23
10	56.8	1.20
15	51.3	1.08
20	44.5	0.94
25	40	0.84
50	23.5	0.50
75	14	0.30
100	10.7	0.23

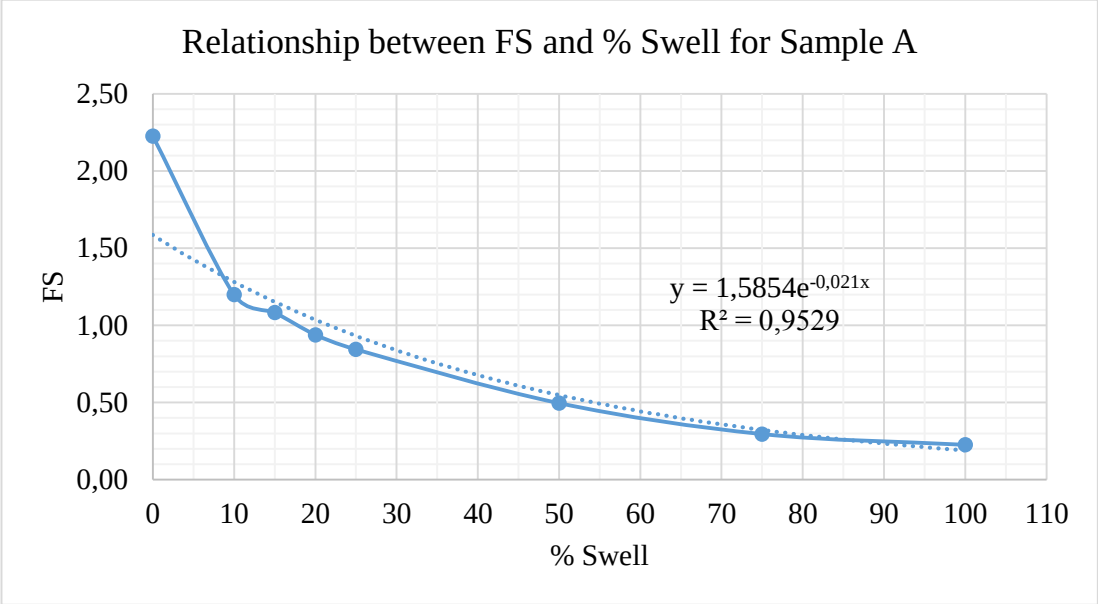

Figure F.2. Relation between FS and % swell for Sample A

APPENDIX G

INFLUENCE OF SWELL RATIO ON PILE LENGTH

In order to see the effects of swelling on length of pile foundation, calculations were performed based on the uplift and resisting forces given in Figure G.1 (Elsharief, 2010).

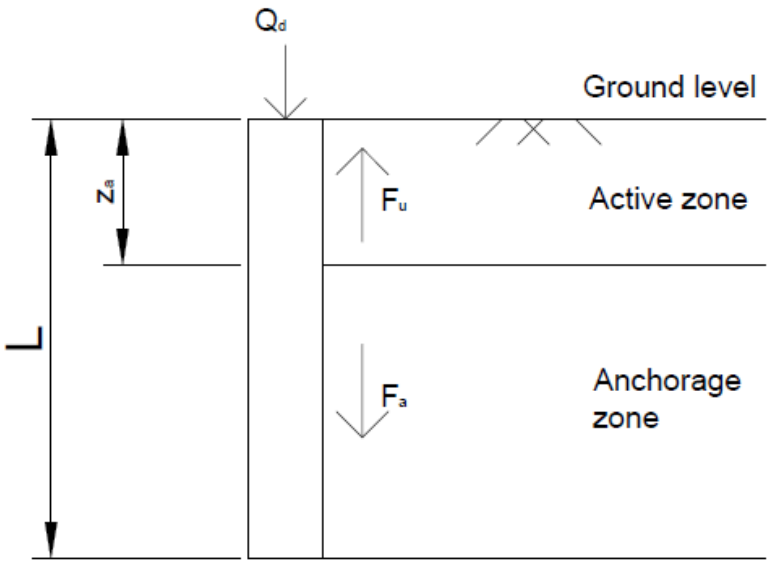

Figure G.1. Forces acting on a pile in swelling soil

Uplift force within the active zone: F_u (Chen, 1975) is calculated with Eqn. G.1.

$F_u = \pi * d_p * Z_a * \beta * P_s$ ..... Eqn. G.1

where

Z_a= Depth of active zone, which was assumed as 2 m

β= Uplift factor, which was given in Table 4.15 as approximately 0.2 for both 0% and 100% of swell

d_p= Pile diameter

P_s= Swell pressure

On the other side, resisting forces:W_f along the anchorage zone is computed with Eqn. G.2.

$W_f = F_a + Q_d = \pi * d * \alpha * c_u * (L - Z_a) + Q_d$ ..... Eqn. G.2

where

α= Adhesion factor, which is found from the equation ($\alpha = 0.30 + 0.17 * \frac{c_u}{P_a}$ where P_a= 101.3 kPa) given by Chen (2011)

c_u= Undrained shear strength of the soil

L= Pile length

Q_d= Allowable load from the superstructure, which was assumed as 10 kN

Since $Fu \leq W$ for a safe pile design $\Longrightarrow$ Eqn. G.1 and Eqn. G.2 are equated and it is given in Eqn. G.3.

$0.4 * P_s = \alpha * c_u * (L-2) + 10$ ..... Eqn. G.3

Then, calculations were performed for Sample A and presented in Table G.1. If Table G.1 was examined, as the soil swelled, needed pile length increased.

Table G.1. Change in L with variation of swell ratio for Sample A

% Swell	c_u of Sample A (kPa)	Water Content:w (%)	Adhesion factor: α	A* c_u (kPa)	L from Eqn. G.3 (m)
0	105.5	23.9	0.477	50.329	2.88
10	56.8	33.8	0.395	22.454	3.98
15	51.3	36.7	0.386	19.806	4.24
20	44.5	39.1	0.375	16.673	4.66
25	40	41.1	0.367	14.685	5.02
50	23.5	46.8	0.339	7.977	7.56
75	14	50.2	0.323	4.529	11.80
100	10.7	53.8	0.318	3.402	15.04